Full waveform inversion of supershot-gathered data for optimization of turnaround time in seismic reflection survey

Ehsan Jamali Hondori

2016

KYOTO UNIVERSITY

FULL WAVEFORM INVERSION OF SUPERSHOT-GATHERED DATA FOR OPTIMIZATION OF TURNAROUND TIME IN SEISMIC REFLECTION SURVEY

A Thesis

By

Ehsan Jamali Hondori

Department of Civil and Earth Resources Engineering

Submitted in partial fulfillment of the requirements

for the degree of

Doctor of Philosophy in Geophysics

2016

ABSTRACT

Two major problems occur in practice when simultaneous sources are used in the seismic full waveform inversion (FWI). First, simulating the data which are generated from different shot points but recorded at the same receiver locations produces a crosstalk noise which degrades the FWI resulting models. In order to minimize the crosstalk between simultaneous sources, random phase encodings are assigned to the individual sources to keep track and minimize the interference between different shots. However, the level of success in this method depends on the optimal selection of the simultaneous sources arrangement and careful evaluation of different shot assembling strategies is necessary to achieve the best possible result.

The second problem is that initial underground seismic velocity estimation in the case of a greenfield development is a challenging work which restricts the successful application of the full waveform inversion. Even in the brownfield case, where some velocity models are already available, the success of FWI depends on several factors including bandwidth of the seismic data, quality of the initial models, etc. Since any greenfield seismic project does not have a priori information on seismic velocities, the successful application of FWI encounters serious problems. On the other hand, application of the FWI in a brownfield situation with some level of known velocities makes it possible to achieve reliable high resolution velocity models. It should be noted that despite availability of approximate velocity models in the case of a brownfield dataset, the original greenfield data may have not been processed using full waveform inversion method. The available velocity models have limited spatial resolution and FWI models are extremely desirable.

Moreover, the acquired data are generally observed from a seismic source with a band-limited rather than wide-band signature. Indeed, all of the current works addressing FWI using random phase encoded simultaneous sources assume that the observed data includes very low frequency components. This unrealistic assumption is easily violated when the band-limited nature of the seismic data is taken into account.

In this research I develop a robust full waveform inversion code using random phase encoded simultaneous sources for the efficient high resolution subsurface modeling. In order to suppress the crosstalk noise, I evaluate the effect of different supershot gather formation strategies including close, random, and full configurations of individual shots. The close configuration which assembles the neighboring shots into supershot gathers proves to be the most effective strategy for the crosstalk noise suppression. The computation time for acoustic FWI can be reduced dramatically, while obtaining the velocity models as accurate as conventional FWI using sequential sources.

In order to handle the problem of FWI in the brownfield case, I propose that the missing low frequency part of the velocity model can be extracted from well logs, as a source of full-band data, to fill the gap in the band-limited seismic data. Geological constraints which are provided by accurate picking of horizons and well log interpolation help to apply a constrained acoustic impedance inversion. I will use a known density model to convert the resulting acoustic impedance section to velocity model. Finally I will perform a time to depth conversion to build an interval velocity model and use it as initial model for simultaneous sources FWI of the band-limited data.

I also suggest a method for FWI initial model building when there is no well log data available. Basically, velocity models resulting from data processing tasks should be able to provide a long wavelength component of the correct model, if the dip complexities are handled properly. I will show that dip move-out (DMO) correction can relax the dip complexities by modifying the apparent velocities for the subsurface structures. A velocity analysis after DMO correction will provide an accurate RMS velocity field which is converted to interval velocity in depth to make the initial velocity model for band-limited FWI. In fact, DMO correction and velocity analysis are as effective as geological constraints for supplying the low spatial frequency component of the velocity model. Although alternative methods like migration velocity analysis (MVA) or differential semblance optimization (DSO) are capable of building initial models for FWI, DMO correction can achieve reliable velocity models with a much cheaper cost.

In order to achieve the objectives of the thesis, I developed a MATLAB package for full waveform inversion using random phase encoded simultaneous sources and validated the performance and accuracy of the results using Marmousi2 model. Several examples of acoustic FWI and a crosstalk analysis showed that high resolution velocity models could be obtained using FWI with random phase encoded simultaneous sources. Also examples of band-limited FWI showed the validity of the new initial models for solving the current problems in the brownfield seismic cases.

ACKNOWLEDGMENTS

I would like to express my special appreciation and thanks to my advisor Professor Hitoshi Mikada, I would like to thank you for encouraging my research and for allowing me to grow as a research scientist. Your advice on both research as well as on my career have been priceless. I would like to thank referees of my thesis for their kind comments which helped me to improve the contents of the thesis. Also, I would like to thank the members of geophysics laboratory at Kyoto University, especially Ms. Shiori Kamei for her kind helps and supports and also for preparing the required paper works during my research. A special thanks to my family who always supported me by their kind helps. Last but not the least, I would like to thank my beloved wife Somayeh who always was my support in the hard moments.

Table of Contents

LIST OF TABLES

LIST OF FIGURES

Chapter I

Chapter II

Chapter III

Chapter IV

CHAPTER I: INTRODUCTION TO FULL WAVEFORM INVERSION OF SUPERSHOT-GATHERED SEISMIC DATA

1.1 Review

Studying the interior of the earth using geophysical methods provides an accurate tool for the characterization of the subsurface materials, which is required either for natural resources exploration or risk analysis of hazards due to the dynamic behavior of the earth. Seismic survey has been widely used for several decades as the most common and fundamental geophysical technique. The method is based on observation of seismic energy, which is generated using active or passive sources and recorded by receivers on the land or in the sea. The acquired data is then processed to eventually build models for the elastic properties of the earth, which are later interpreted by the geologists.

The time and cost of seismic data acquisition using active sources extremely depend on the number of sources. Obviously, a longer time is needed to complete the survey in an area with a larger number of shot points and more financial resources are required for such a survey. In order to reduce the data acquisition time, simultaneous seismic sources have received considerable attention and several works have been conducted using this data acquisition technology (Beasley et al., 1998; Stefani et al., 2007; Howe et al., 2008). In principle, the simultaneous sources methodology is very simple. The sources are dithered in time relative to one another to enable data separation using a sparse inversion technique. Once separated, the data can be processed conventionally, and will benefit naturally from the improved spatial sampling (Beasley et al., 2012). In fact, two or more seismic sources at different shot locations are excited with a small random time delay to acquire data more efficiently.

Simultaneous sources surveys have been already used to efficiently reduce the operation time and cost in the seismic data acquisition projects. Due to the similarity between data acquisition and the required wave propagation simulations in the imaging problems like reverse time migration (RTM) or full waveform inversion (FWI), simultaneous sources have the potential to be used in the seismic imaging methods too. Generally, forward modeling is the most computationally intensive part of RTM and FWI which requires waveform simulation from all the shots in the survey with the computation time directly depending on the number of sources. In an analogy with data acquisition, simultaneous seismic sources have been used to reduce the calculation time of the waveform simulation (Romero et al., 2000; Krebs et al. 2009; Boonyasiriwat and Schuster, 2010; Anagaw and Sacchi, 2014). In a very similar way to simultaneous shooting in data acquisition, two or more seismic sources are excited simultaneously. The only difference is that instead of separating simulated data of simultaneous sources, the observed data from conventional acquisition are assembled into supershot gathers to match the observed and simulated waveforms correctly.

1.2 Current Challenges in FWI Using Simultaneous Sources

Two major problems occur in practice when simultaneous sources are used in the seismic full waveform inversion. First, simulating the data which are generated from different shot points but recorded at the same receiver locations produces a crosstalk noise which degrades the FWI resulting models. Second, initial underground seismic velocity estimation in the case of a greenfield development is a challenging work which restricts

the successful application of the full waveform inversion. Even in the brownfield projects where some velocity models are already available, the success of FWI depends on several factors including bandwidth of the seismic data, quality of the initial models, etc.

1.2.1 Crosstalk Noise Suppression

Random phase encoding technique could be implemented to suppress the crosstalk noise resulting from interference between the individual sources assembled into a supershot gather (Ben-Hadj-Ali et al., 2011). However, the level of success in this method depends on the optimal selection of the simultaneous sources arrangement and careful evaluation of different shot assembling strategies is necessary to achieve the best possible result. An example of FWI using random phase encoded simultaneous sources is presented by Boonyasiriwat and Schuster (2010), who used dynamic random phase encodings for the FWI in time domain. They could relatively improve the quality of the FWI results compared to a previous work by Krebs et al. (2009), using dual randomization of source locations and source polarities for the shots assembling in a supershot gather. However, the resolution of the velocity models they could obtain is clearly lower than what one can expect from FWI. **Figure 1.1** shows a cross section and depth slice of their 3D velocity model. Although large-scale features of the model could be slightly improved compared to the method of Krebs et al. (2009), the detailed structures could not be recovered with enough resolution. Moreover, by comparing their true model and FWI result it is obvious that a large amount of crosstalk noise remained in the FWI model, especially in the shallow part. One major reason could be inappropriate shot assembling strategy which

they used for supershot gather formation. Another principal reason for the low resolution results in their work could be related to poor initial velocity model.

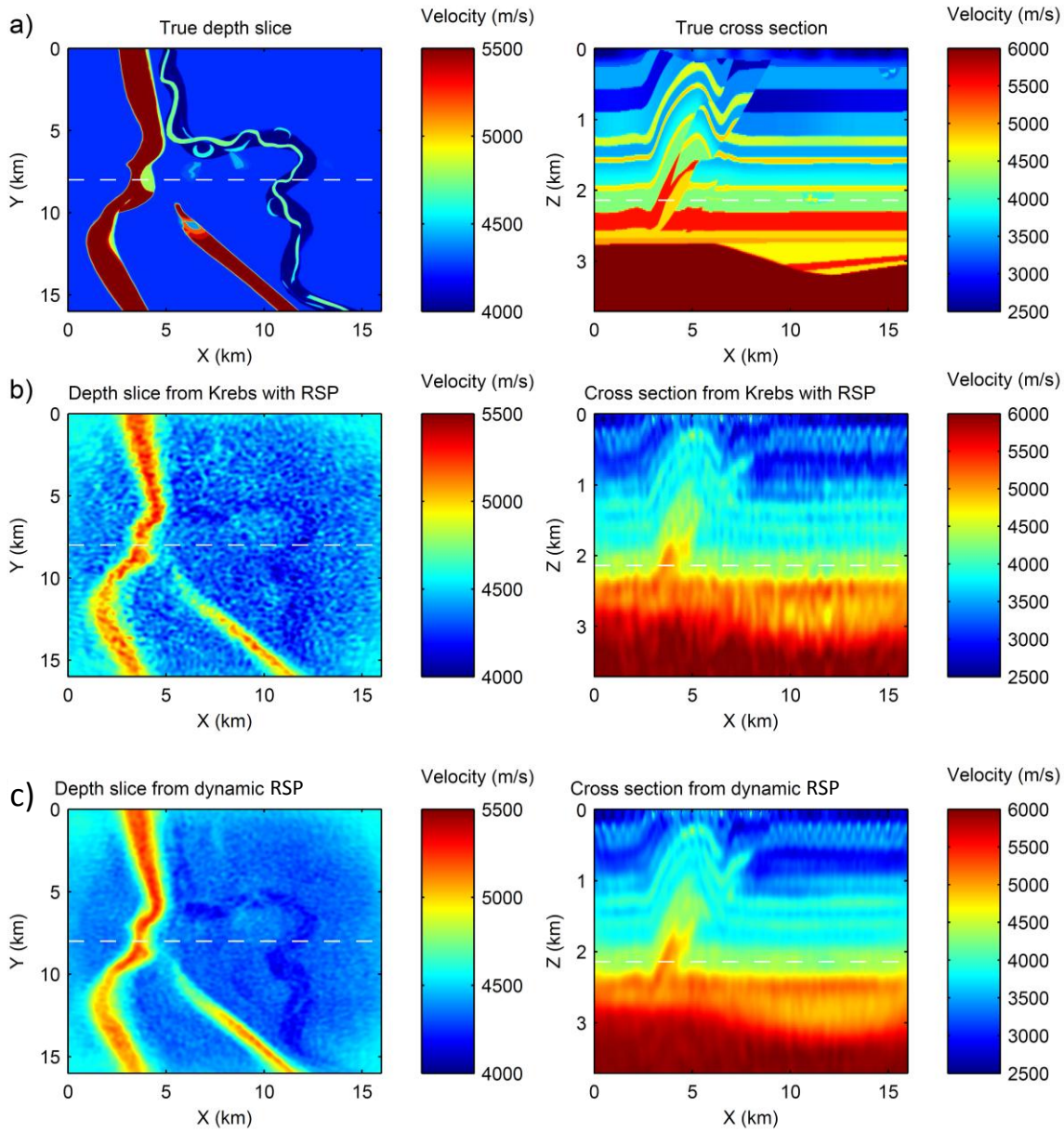

Figure 1.1 FWI results obtained by random source polarity (RSP) in the work conducted by Boonyasiriwat and Schuster (2010); (a) true velocity model , (b) velocity model resulting from method of Krebs et al. (2009), and (c) slightly improved velocity model by dynamic dual randomization of source polarity and source locations (Figure borrowed from Boonyasiriwat and Schuster, 2010).

1.2.2 Simultaneous Sources FWI in the Brownfield Situation

Since any greenfield seismic project does not have a priori information on seismic velocities, the successful application of FWI encounters serious problems. On the other hand, application of the FWI in a brownfield situation with some level of known velocities makes it possible to achieve reliable high resolution velocity models. It should be noted that despite availability of approximate velocity models in the case of a brownfield dataset, the original greenfield data may have not been processed using full waveform inversion method. As a result, the available velocity models have limited spatial resolution and high resolution FWI models are extremely desirable. Moreover, the acquired data are generally observed from a seismic source with a band-limited rather than wide-band signature. Indeed, all of the current works addressing FWI using random phase encoded simultaneous sources assume that the observed data includes very low frequency components. This unrealistic assumption is easily violated when the band-limited nature of the seismic data is taken into account. Due to the limitations in data acquisition technology, the frequencies lower than a certain limit (≈5 Hz) are not practically observable in the seismic data.

Anagaw and Sacchi (2014) present a series of different frequency selection strategies to achieve the best possible model through full waveform inversion using simultaneous sources in frequency domain. However, they consider the starting frequency to be as low as 2.93 Hz, which is below the lowest observable frequency. The absence of low frequencies in the observed data is a crucial problem for full waveform inversion which strictly relies on these low frequencies to build the low wavenumber component of the model.

As **Figure 1.2** illustrates, full waveform inversion is essentially a data fitting problem. The left panel in this figure shows a wrong fitting which tries to match two different samples from observed and calculated data in a high frequency situation. This problem, which is called *cycle skipping*, leads the local optimization algorithm to reach a local, rather than global minimum of the misfit function. On the other hand, the right panel in **Figure 1.2** shows correct fitting between observed and calculated data in the low frequency case, in which FWI is able to successfully reach the global solution. Due to the band-limited nature of the seismic data, the cycle skipping problem remains an open issue for the successful application of FWI even in the brownfield cases.

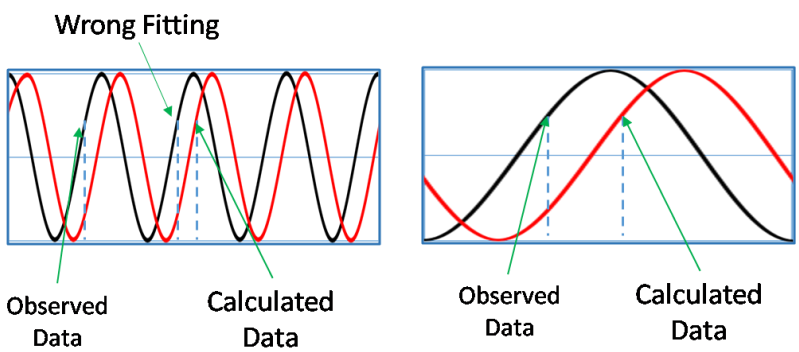

Figure 1.2 Starting FWI from high frequencies leads to cycle skipping because of wrong fitting (left), but low frequencies assure the correct fitting and convergence of FWI algorithm (right).

Claerbout (1985) gives an insight on the level of reliability of information which could be obtained from seismic reflection surveys. As **Figure 1.3** illustrates, estimated velocity from conventional seismic processing represents the low spatial frequency part of the true velocity within the range of 0-2 Hz and reflectivity represents the high frequency part of true velocity within the range of 10-100 Hz. The information gap shown in this figure explains the reason why cycle skipping problem happens, when FWI is initialized from an inaccurate initial model. In fact, the reflection data can cover only the higher spatial frequency part of the velocity spectrum and a considerable part of lower frequency area is unavailable. It is necessary to provide the missing part of the model using innovative methods or from other sources of information. Cooke and Schneider (1983) used *geological constraints* extracted from well logs to improve acoustic impedance inversion by importing low frequency component of the model from well data. Ferguson and Margrave (1996) used well logs to improve the impedance section from recursive inversion and could achieve reliable results. Similarly, geological constraints can provide the low spatial frequency component of the model for the FWI problem.

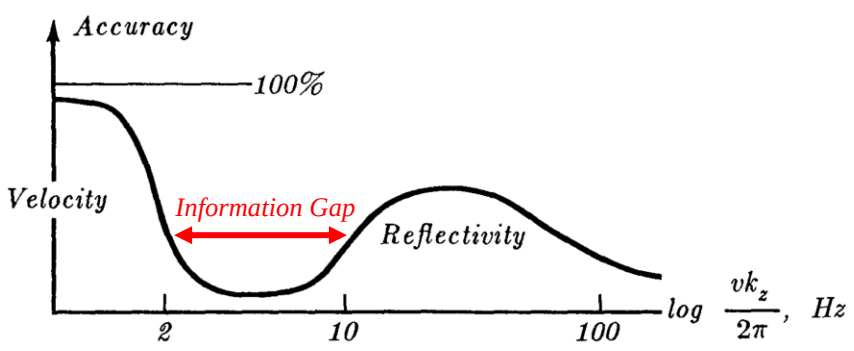

Figure 1.3 Reliability limits of the information obtained from seismic reflection survey (figure borrowed from Claerbout, 1985).

1.3 Objectives of the Thesis

1.3.1 Developing a Robust FWI Code Using Random Phase Encoded Simultaneous Sources

First of all, I shall develop a robust full waveform inversion code using random phase encoded simultaneous source for the efficient high resolution subsurface modeling. In order to suppress the crosstalk noise, I will evaluate the effect of different supershot formation strategies. Three geometrical configurations will be considered for supershot gather formation including close, random, and full configurations of individual shot gathers. I will show that the close configuration is the most effective strategy for the crosstalk noise suppression in the FWI using random phase encoded simultaneous sources. Having developed the FWI code and tested the shot assembling configurations, I shall focus on the FWI application using random phase encoded simultaneous sources in the brownfield situation.

1.3.2 Extracting and Implementing Geological Constraints for Low Frequency Compensation in Brownfield Situation

I propose that the missing low frequency part of the velocity model can be extracted from well logs, as a source of full-band data, in order to fill the gap in the band-limited seismic data. Since well logs are an accurate source of rock physics information it is possible to borrow this information to build a reliable initial velocity model for FWI. However, the

well log data is valid only in the vicinity of the well location and it is necessary to expand this information over all survey area. Conventional seismic data processing normally provides a reliable migrated section which implicitly includes the reflectivity. I will perform an accurate interpretation on the seismic section to build a table of geological horizons. Then I will use these interpreted horizons for a guided interpolation of the low-pass filtered acoustic impedance values extracted from well logs. I use the interpolated values to perform a geologically constrained acoustic impedance inversion of seismic reflectivity section. This results in an accurate acoustic impedance section which is built by inverting seismic section with geological constraints from well logs. I will use a known density model to convert this acoustic impedance section to velocity model. Finally I will perform a time to depth conversion to build an interval velocity model and use it as initial model for FWI. What I propose is to gather all the available information, not only from seismic data but also from well logs and interpretation results, to build a reliable velocity model by bridging between seismic and geological information for the band-limited FWI in the brownfield situation.

1.3.3 Dip Move-out Correction and Velocity Analysis for Filling the Missing Low Frequencies

I also propose a solution for the FWI initial model building problem when there is no well log data available for the brownfield case. Although FWI is not able to fill the low frequency gap in the velocity model just by band-limited waveform fitting, it is possible to fill this gap by advanced velocity analysis methods. The main reason for the limited

reliability of velocity in **Figure 1.3** is the complexity of the subsurface structures which dramatically restricts the accuracy of stacking velocities resulting from apparent velocity analysis. In order to improve the reliability level of the velocity models derived from seismic data processing, more sophisticated velocity analysis methods which can deal with subsurface complexities should be used. Wave equation migration velocity analysis (WEMVA) and differential semblance optimization (DSO) are among the velocity model building methods which can produce reliable initial models for FWI (Li, 2013). However, the cost of these algorithms could be considerably high, due to several rounds of migration on pre-stack data. Moreover, there are few industrial packages which have already accommodated these tools. On the other hand, dip move-out (DMO) correction can relax the dip complexities prior to velocity analysis in a much cheaper way. Since DMO correction works as a *partial pre-stack migration*, it can resolve the ambiguities in the structure and assure a reliable velocity analysis job. I will use DMO correction to pick accurate RMS velocities on the dip corrected Marmousi2 data set, and convert the RMS velocities in time to interval velocities in depth to build the low spatial frequency velocity model for FWI initialization.

1.4 Agenda

The principal goal of this thesis is to perform full waveform inversion on supershot-gathered band-limited seismic data and improve the efficiency and accuracy of the method. In order to do so, I shall develop a robust full waveform inversion code for FWI using random phase encoded simultaneous sources in Chapter II. I will describe the

theoretical background and also algorithm in this chapter followed by several examples from Marmousi2 complex model to validate the FWI code, which I developed in MATLAB with parallel processing capabilities. This chapter builds the required foundation of full waveform inversion using simultaneous sources and prepares the FWI engine for the next chapters.

I shall present sparse spikes reflectivity inversion in Chapter III, to develop the required reflectivity section for geologically constrained acoustic impedance inversion for initial velocity model building. Indeed, the reflectivity section resulting from this chapter will help to bridge between low spatial frequency model from well logs and band-limited data from seismic reflection survey to achieve reliable results by FWI code developed in chapter II.

Chapter IV focuses on the FWI initial model building using two methods; first one to be horizon-guided well log interpolation with constrained acoustic impedance inversion, and the second one to be velocity analysis on DMO corrected seismic data. I will show that by efficiently using the products of conventional seismic data processing routines in the brownfield situation, reliable velocity models could be obtained and these initial models assure to achieve accurate FWI results using random phase encoded supershots with optimized turnaround time for seismic survey.

CHAPTER II: FULL WAVEFORM INVERSION USING RANDOM PHASE ENCODED SIMULTANEOUS SEISMIC SOURCES

2.1 Introduction

An important issue of the FWI application is its computational burden in terms of processing time and cost. This problem could be tackled by blending individual shot gathers into supershot gathers which are simulated using simultaneous seismic sources during waveform forward modeling and residual back-propagation for gradient calculation. This technique should ideally result in a speedup of inversion with a factor of number of shots assembled in a supershot. A drawback is the crosstalk noise which appears in the inversion results due to interference of different shots in a supershot gather. In fact, while calculating the gradient using supershot gathers, modeled wavefields from one source are correlated with back-propagated residuals from receivers associated with different sources. As a result, footprint of the crosstalk noise degrades the inversion results and several iterations are required to minimize the effect of the crosstalk noise. Random phase encoding method has been introduced as a tool to minimize the crosstalk noise in the subsurface models resulting from full waveform inversion using simultaneous sources (Romero et al., 2000; Krebs et al. 2009; Boonyasiriwat and Schuster, 2010; Ben-Hadj-Ali et al., 2011).

Although some of the recent works showed a desirable speed-up in FWI computation time by using simultaneous sources, still the band-limited nature of seismic data keeps these applications far from realistic cases. Moreover, the resolution expected from FWI could not be obtained using some of these methods (Krebs et al. 2009; Boonyasiriwat and Schuster, 2010). For the efficient suppression of crosstalk noise, source encodings should be assigned to the individual shot gathers before assembling them into supershot gathers.

However, different phase encoding functions may achieve different levels of success. Also, spatial configuration of the individual shot gathers which are assigned into a supershot gather can affect the FWI result.

In this chapter, I shall develop the FWI engine which can efficiently reduce the computation time using simultaneous sources. Also, I shall evaluate different strategies for assembling sequential shots into supershot gathers to select the best combination for computational efficiency and model accuracy. I will examine three different spatial configurations for supershot formation; close configuration (CC), random configuration (RC), and full configuration (FC). In the close configuration a number of neighboring shots will be assembled into one supershot gather, while in the random configuration individual shots are selected from random shot locations in the survey to form the supershot gather. Full configuration takes all the shots in the survey and assembles them into one supershot gather. Through a crosstalk analysis, I will show that the close configuration achieves the highest level of efficiency and model accuracy compared to the other configurations. In the following sections, I will briefly describe the frequency domain waveform forward problem, the inverse problem, and the mathematical equations for calculating gradient using sequential sources and phase encoded simultaneous sources. Then, I shall explain the phase encoding in frequency domain and the strategies to select individual shot gathers for assembling into supershot gathers. A series of examples using Marmousi2 model will validate the developed algorithm and FWI code for further usage in the next chapters.

2.2 The Forward Problem

Different forward modeling methods have been developed in order to generate the synthetic seismic waveforms, either in time or frequency domain (Virieux, 1986; Levander, 1988; Graves, 1996; Operto et al., 2007; Robertsson et al., 2007). The method of choice for acoustic waveform modeling in this thesis is based on optimal finite difference operators in frequency domain, as introduced by Jo et al. (1996). The general compact matrix form of wave equation in frequency domain is shown as

$$\mathbf{Au} = \mathbf{s} \tag{2.1}$$

where, **A** is the complex-valued impedance matrix, **u** is the seismic wavefield and **s** is the source term. Under the acoustic assumption **u** represents pressure field, while in the elastic case **u** represents horizontal and vertical displacements (or particle velocities). The linear system of equations (2.1) is generally solved by decomposition of the impedance matrix at different frequencies. The seismic waveforms for multiple sources in the right hand side term could be efficiently calculated, once matrix decomposition is completed (Pratt et al., 1998). The computational demand of the forward modeling depends not only on the dimensions of impedance matrix **A** at the decomposition phase, but also on the number of the sources in the right hand side term. The purpose of using simultaneous sources method is to reduce the number of effective sources in the right hand side term by combining individual shots into supershots which are excited simultaneously.

2.3 The Inverse Problem

Full waveform inversion problem is considered as an inverse problem in which the misfit between observed data from seismic experiment and calculated data from wave propagation simulation is minimized. Theoretical development of the seismic waveform inversion problem dates back to the early works by Lailly (1983) and Tarantola (1984), who recast the pre-stack migration imaging method of Claerbout (1971) as a local optimization problem which minimizes the least squares misfit between observed and simulated data. An initial model is iteratively updated by calculating a model perturbation in the opposite direction of the gradient of misfit functional. The misfit itself is generally defined as the least squares norm of the residual waveforms and the gradient is efficiently calculated using adjoint state method as described by Askan (2006) and Plessix (2006). In order to increase the convergence rate of the local optimization algorithm, the gradient is preconditioned with the inverse of the Hessian matrix (Pratt et al., 1998). Vigh and Starr (2008) introduced a parabola fitting method to calculate the step length for updating the model parameter. A detailed mathematical expression of gradient and Hessian calculations could be found in Pratt et al. (1998). Although the FWI method was computationally demanding at the beginning, some applications were reported (Gauthier et al., 1986). The computational burden of full waveform inversion became relatively affordable with advances in the high performance computer resources and development of efficient forward modeling techniques, including finite element methods (Marfurt, 1984; Min et al., 2003), finite difference methods (Virieux, 1986; Jo et al., 1996), and finite volume methods (Brossier et al., 2008). Recent applications of acoustic FWI (Hicks and Pratt, 2001; Ravaut et al., 2004; Gao et al., 2006; Operto et al., 2006; Bleibinhaus et

al., 2007) and elastic FWI (Gelis et al., 2007; Brossier et al., 2009) proved the potential of the method to be applied on large datasets. A detailed review of full waveform inversion with applications to different types of data has been presented by Virieux and Operto (2009).

Since the number of model parameters in the inverse problem is too large, the use of global optimization methods is not feasible and local optimization algorithms are used. The misfit functional is generally defined as the least squares norm of residual wavefield as

$$E(p) = \frac{1}{2}\sum_{i=1}^{N_s} \Delta\mathbf{d}_i^t \Delta\mathbf{d}_i^* \tag{2.2}$$

where, $\Delta\mathbf{d}$ is the residual wavefield resulting from subtraction of observed and modeled data, and superscripts t and * denote transpose and complex conjugate, respectively. The model parameter is shown by p and the summation is over all sources. The simple misfit function represented in equation (2.2) ignores any incorporation of *a priori* statistical information, preconditioning, or weighting terms on the observed or modelled data. A more detailed form of misfit functional could be found in literature (Virieux and Operto, 2009; Pratt, 1998). Due to the local optimization algorithm used for FWI, it is assumed that the minimum of the misfit function is in the vicinity of the initial model. Considering

the Born approximation, it is reasonable to define the updated model parameter as the summation of the starting model and a model perturbation term as

$$p_{k+1} = p_k + \Delta p \tag{2.3}$$

where, k is the iteration number. The model perturbation term Δp is searched in the direction of the steepest descent of the misfit function. The gradient at each iteration could be efficiently calculated using adjoint state method as described by Askan (2006) and Plessix (2006). In frequency domain, the gradient is calculated for every single frequency as

$$\mathbf{g}_{k,p} = \sum_{i=1}^{N_s} \mathbf{u}_i^t \frac{\partial \mathbf{A}^t}{\partial p} \mathbf{A}^{-1} \Delta \mathbf{d}_i^* = \sum_{i=1}^{N_s} \mathbf{u}_i^t \frac{\partial \mathbf{A}^t}{\partial p} \mathbf{r}_i^* \tag{2.4}$$

where, $\mathbf{u}$ is the modeled wavefield, $\mathbf{A}$ is the impedance matrix, $\Delta\mathbf{d}$ is the residual wavefield, p is the model parameter, k is the iteration number, and the summation is over all sources. The adjoint wavefield which is calculated by back-propagation of the residuals from each source is shown by $\mathbf{r}_i$. In order to increase the convergence rate of the local optimization algorithm, the gradient is preconditioned with the inverse of the Hessian (Pratt et al., 1998) to finally update the model parameter as

$$p_{k+1} = p_k - \alpha \mathbf{H}^{-1} \mathbf{g}_{k,p} \tag{2.5}$$

where, **H** is the Hessian matrix and α is the step length calculated using a parabola fitting line search method (Vigh and Starr, 2008). Calculating exact Hessian could be computationally expensive and even approximate Hessian requires a large number of forward modeling. As a result, it is desirable to use diagonal of the approximate Hessian which was introduced by Shin et al. (2001) as pseudo Hessian. The pseudo Hessian could be efficiently calculated using the same virtual sources used in the adjoint state method and computation cost is dramatically reduced. However, pseudo Hessian has weak illumination to recover the deeper parts of the model and additional improvements are necessary (Choi et al., 2008; Oh and Min, 2012). One of the effective modifications to the original pseudo Hessian has been introduced by Oh and Min (2012), where they included an auxiliary matrix into the original pseudo Hessian matrix to enhance the deep parts of the updated model. This improved pseudo Hessian is used in the frequency domain full waveform inversion code developed for the purpose of this thesis.

2.4 Simultaneous Shooting and Phase Encoding Method

Full Waveform Inversion requires several runs of iterative local optimization algorithm to achieve satisfactory results. The number of forward modeling per iteration for gradient calculation linearly depends on the number of seismic sources in the survey. When the

modeling expands over a large area with numerous shot gathers in the observed data, the computational cost of FWI could be prohibitive and robust algorithms should be designed to overcome this problem. One of the solutions to reduce the calculation cost and time is to assemble a number of shot records to form a supershot gather. This will reduce the number of effective sources in the forward modeling stages required for FWI. In the frequency domain, monochromatic sources could be assembled as

$$\bar{\mathbf{s}} = \sum_{i=1}^{N_s} a_i \mathbf{s}_i \tag{2.6}$$

where $\bar{\mathbf{s}}$ is the monochromatic supershot and random phase encodings are selected such that $|a_i|=1$ (Ben-Hadj-Ali et al., 2011). This leaves the amplitude of the sources same as to the original, but modifies the phase of each source randomly. The modeled wavefields using assembled simultaneous sources generate a supershot gather as

$$\bar{\mathbf{u}} = \sum_{i=1}^{N_s} a_i \mathbf{u}_i \tag{2.7}$$

where, $\bar{\mathbf{u}}$ is the monochromatic modeled wavefield which is simulated by exciting assembled sources simultaneously to form the supershot gather. The adjoint wavefields could be calculated for the simultaneous sources similarly

$$\overline{\mathbf{r}^*} = \sum_{i=1}^{N_s} a_i^* \mathbf{r}_i^* \tag{2.8}$$

The conjugate of a_i results from the fact that the source of the back-propagation is the conjugated residual wavefield. Substituting equations (2.7) and (2.8) in to equation (2.4) results in the monochromatic gradient of misfit function for the simultaneous sources as

$$\bar{\mathbf{g}}_{k,p} = \sum_{i=1}^{N_s} \mathbf{u}_i^t \frac{\partial \mathbf{A}^t}{\partial p} \mathbf{r}_i^* + \sum_{i=1}^{N_s} \sum_{\substack{j=1 \\ j \neq i}}^{N_s} a_i a_j^* \mathbf{u}_i^t \frac{\partial \mathbf{A}^t}{\partial p} \mathbf{r}_j^* \tag{2.9}$$

The first term in equation (2.9) is the same as conventional gradient calculated for individual sources, however, the second term corresponds to the interference between incident wavefield from one shot and back-propagated residuals from the other shots. This term degrades the imaging results and therefore is considered to be noise, called crosstalk noise. Random phase encoding should work in such a way that multiplication

result of a_i and a_j produces incoherent crosstalk noise and the summation in the second term of equation (2.9) is suppressed.

2.5 Random Phase Encoding in Frequency Domain

Phase encoding of the simultaneous sources could be applied either in time domain FWI (Krebs et al., 2009; Boonyasiriwat and Schuster, 2010) or in frequency domain FWI (Ben-Hadj-Ali et al., 2011; Anagaw and Sacchi, 2014). Boonyasiriwat and Schuster (2010) used randomized polarities for each individual shot to be stacked in a supershot gather for time domain FWI. Moreover, they selected shots randomly from different locations in the survey area for supershot gather formation. Phase encoding in frequency domain could be simply performed by multiplying a complex term to each individual source as

$$\begin{cases} a_i = \exp(\ell \phi_i), \\ \ell = \sqrt{-1} \end{cases} \tag{2.10}$$

where, ϕ_i is the amount of random phase shift to be applied on each individual shot. This was used by Ben-Hadj-Ali et al. (2011) to efficiently suppress crosstalk noise for different configurations of shot assembling geometries and inversion frequencies. Anagaw and Sacchi (2014) investigated the effect of frequency selection strategies for

full waveform inversion using simultaneous seismic sources. They showed that the crosstalk noise effect could be different over different frequency ranges and an optimized FWI scheme could be defined based on the inversion of frequency groups with slightly overlapping ranges.

Here, I use a random phase encoding function based on random polarity for the shot gathers to be assembled in a supershot gather. This is a special case of random phase encoding when the amount of random phase shift is either $\phi_i = 0$ or $\phi_i = \pi$. The same phase encodings were used by Boonyasiriwat and Schuster (2010) for time domain full waveform inversion and here I implement it in frequency domain. As suggested by Anagaw and Sacchi (2014), I use frequency groups of individual values with slightly overlapping bands to efficiently minimize the crosstalk effect in full waveform inversion.

2.6 Spatial Configuration Strategies for Simultaneous Sources

Different shot assembling geometries could be examined for the optimum combination of random phase encoding and shot selection. Ben-Hadj-Ali et al. (2011) used two partial configurations of closely located and distantly located sources, and a full configuration of all sources in one supershot gather to evaluate random phase encoding effect on FWI results. They noticed that the partial close configuration, which assembles neighboring shots into one supershot gather, provides the most reliable results for FWI using random phase encoded simultaneous sources. On the other hand, Boonyasiriwat and Schuster (2010) used random distribution of sources to minimize the crosstalk noise. I will use three different strategies in order to combine individual sources into supershots; Close

Configuration (CC), Random Configuration (RC), and Full Configuration (FC). This will provide the chance to compare the effect of shot selection on FWI results.

Figure 2.1 shows each configuration strategy for a survey line including 20 seismic sources. In each configuration, the individual sources which are displayed by the same color are assembled into a supershot. In close configuration (CC), the survey area is divided to equal spatial segments and all the sources in one segment are assembled in one supershot. In this strategy the distance between individual sources inside a supershot remains minimum. The advantage of this configuration is that an average shot to receiver offset could be calculated based on the center of the segment cluster, and then this average offset could be applied in the gradient calculation stage in the form of a weighting matrix to enhance the effect of far-offset data in FWI. Weighting matrix **W** is calculated using the squared average offset values as below

$$\mathbf{W} = \left(average \quad offset \right)^2 \tag{2.11}$$

When FWI is performed using sequential sources, the average offset is the same as shot to receiver offset, while when simultaneous sources are used for FWI this average offset is calculated from the central point in the spatial segment of close configuration. Brossier et al. (2009) suggested that a quadratic offset dependent weighting matrix can improve the deeper part of the model by enhancing contribution of the long-offset data in FWI.

Random configuration (RC) follows a random selection of sources from the entire survey area to create supershots. This method was used by Boonyasiriwat and Schuster (2010) to increase the incoherence of the crosstalk noise in different iterations. Full configuration (FC) assembles all the shots of the survey into only one supershot. The effect of random phase encoding in crosstalk noise reduction will be checked for these strategies for an optimum combination of spatial geometries and number of simultaneous sources.

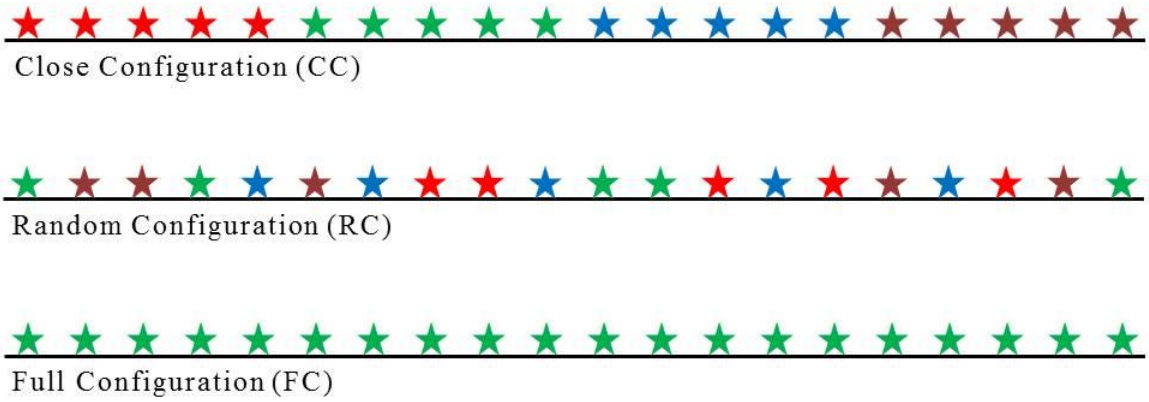

Figure 2.1 Different spatial configurations for shot assembling, sources with same color are assembled in one supershot.

2.7 Algorithm of Frequency Domain FWI Using Random Phase Encoded Simultaneous Sources

In order to mitigate the nonlinearity of the FWI problem, it is preferred to start the FWI iterations from lower frequencies through a multiscale scheme. A number of discrete frequencies selected based on the method introduced by Sirgue and Pratt (2004), are arranged in different frequency groups from lower to higher values. The frequencies inside each group are inverted simultaneously and the results of FWI from each frequency group are used as initial model for the next frequency group. The hierarchical process of multiscale FWI helps to recover the background low wavenumber component of the model in the early stages of the FWI and substantially reduce the nonlinearity of the problem. The flowchart of the frequency domain full waveform inversion algorithm used in this thesis is shown in **Figure 2.2**.

The random phase encodings are generated at every iteration to reduce the crosstalk noise from iteration to iteration. The most computationally expensive part of the algorithm which is marked by blue area in the flowchart is performed in parallel to simultaneously calculate the gradient and improved pseudo Hessian for all the individual frequencies in each frequency group. Array processing and loop vectorization techniques have been used in different parts of the forward modeling, gradient, and improved pseudo Hessian calculations to efficiently use the computational resources. Step length calculation requires two more misfit evaluations to perform a parabola fitting as described by Vigh and Starr (2008). As a result, two more forward modeling per individual frequencies are needed to estimate the misfit value for the current iteration and frequency group. A parallel distribution of observed data from the individual frequencies in the current

frequency group provides the chance to perform all the required forward modeling and misfit estimations simultaneously.

Due to the important role of long offset data in full waveform inversion, an offset dependent weighting matrix is used to scale the gradient when applicable, i.e. the case of sequential sources or close configuration of simultaneous sources. When using simultaneous sources it is not possible to assign a single offset value to each receiver point, because every receiver is associated with different shots. However, in the close configuration (CC) strategy, it is possible to assign an average offset from center of supershot segment to each receiver point. Weighting matrix is simply calculated by square of the average offset for each receiver point. This weighting helps to improve the deeper parts of the model. Moreover, smoothing the gradient helps to minimize any undesired instability near shot and receiver locations. The sequential sources could be inverted using the same algorithm as a special case, when each supershot includes only one source without any encoding.

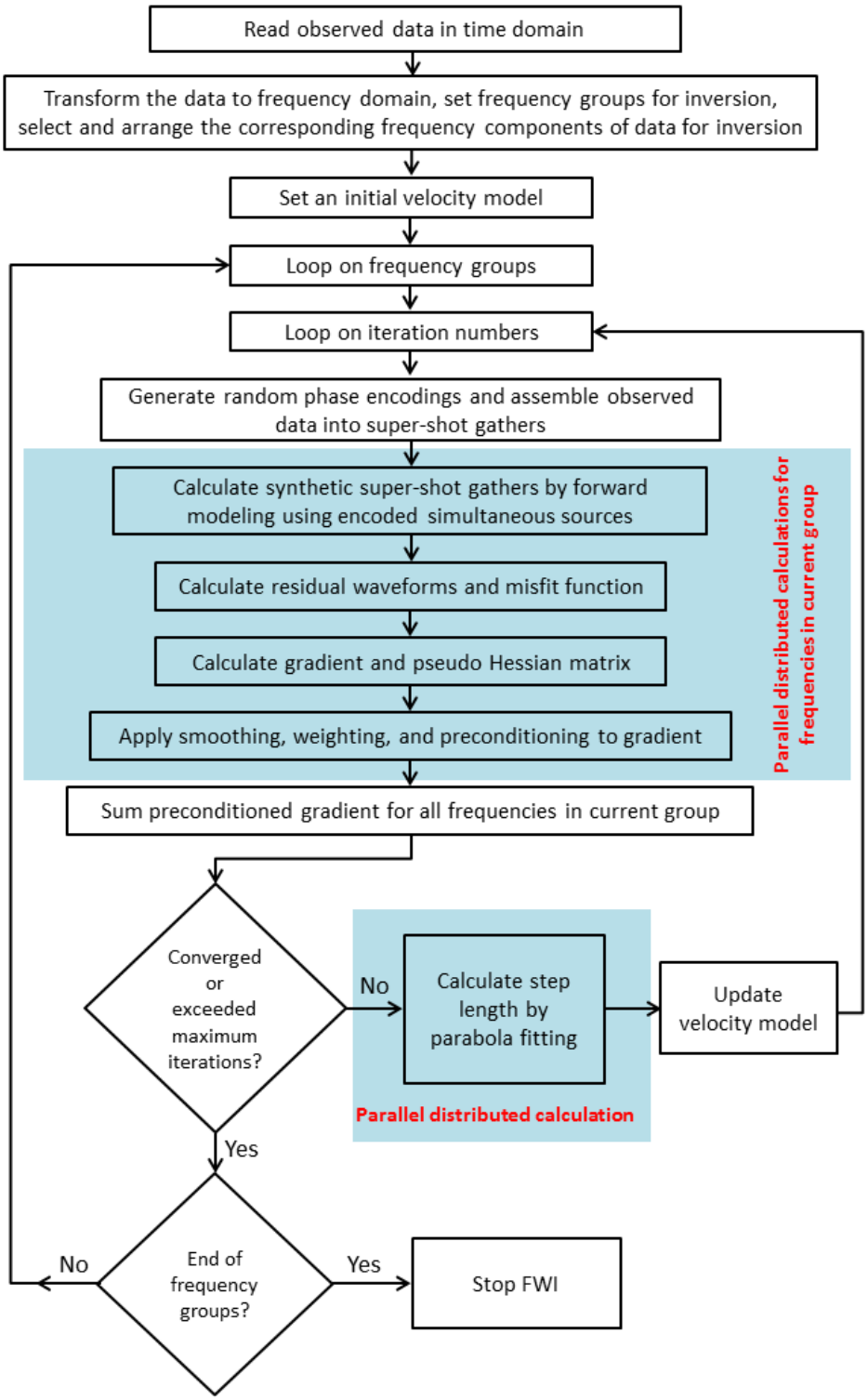

Figure 2.2 Flowchart of frequency domain full waveform inversion using encoded simultaneous sources.

2.8 Synthetic Dataset Generation Using Marmousi2 Model

A dataset of time domain shot gathers are generated using Marmousi2 model to be used for all the examples in the different chapters of the thesis. When performing full waveform inversion, the original time domain waveforms are converted to frequency domain and a few numbers of frequencies are selected based on the method introduced by Sirgue and Pratt (2004) for a frequency domain FWI. The time domain shot gathers will be used later again, in chapter III for a sparse spikes reflectivity inversion and in chapter IV for initial velocity model building. Here I shall describe the acquisition geometry and recording parameters for the dataset generation, before showing the full waveform inversion results using simultaneous sources. **Figure 2.3** shows the P wave velocity from Marmousi2 model which expands 13.5 km in horizontal and 3.25 km in vertical directions, with some minor cropping applied on the margins of the original model. A constant density of 1000kg/m^3 has been used here. The geometry for the simulation of 2D seismic line on a grid with sample intervals of 7.5m includes 450 shot locations at every 30m and 900 receiver locations at every 15m. Shot depth is assumed to be 30m and receivers are located on the surface. In order to exclude the surface related multiple reflections a perfectly matched layer (PML) boundary condition (Berenger, 1994; Drossaert and Giannopoulos, 2007) is applied on the top of the modeling area. A Ricker wavelet with dominant frequency of 15Hz is used as the source wavelet. In order to generate shot gathers in time domain, a frequency domain finite difference modeling is performed following the method of Jo et al. (1996). Then, an inverse Fourier transform converts the waveforms from frequency domain to time domain. In order to create noisy data, which is required for some of the examples, a white Gaussian random noise has

been optionally added to the time domain dataset to generate a second dataset including random noise with a signal to noise ratio of 5. A sample shot gather of noise-free and noise contaminated data is shown in **Figure 2.4**. The horizontal location of this sample shot gather is illustrated using a red star in **Figure 2.3**.

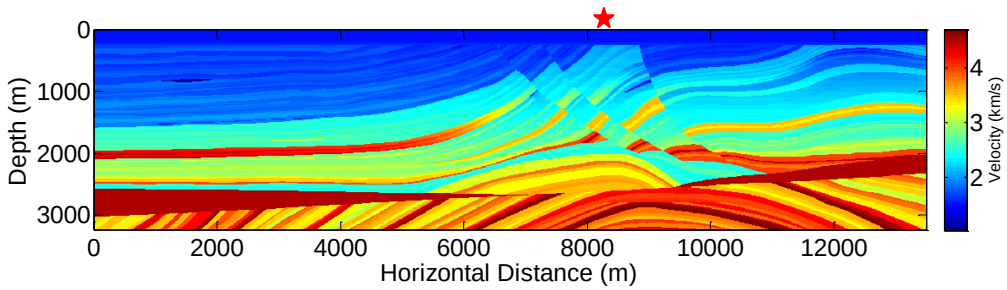

Figure 2.3 True P wave velocity of Marmousi2 model. The red star shows the source location of the sample shot gather.

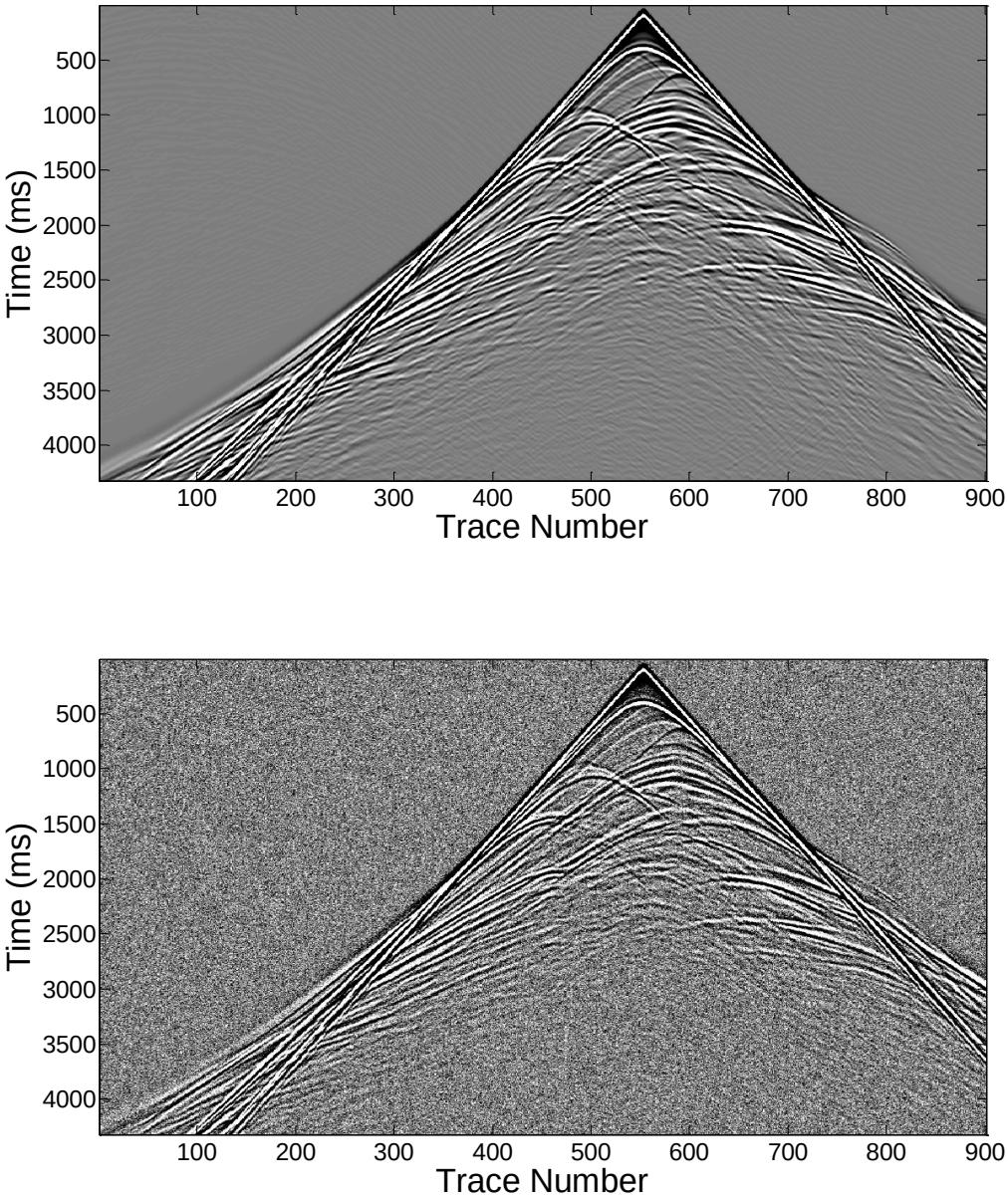

Figure 2.4 Sample shot gather of generated dataset using Marmousi2 model: noise-free case (top), and noise-contaminated data with signal to noise ratio of 5 (bottom).

2.9 FWI Results Using Marmousi2 Dataset

The generated synthetic dataset has been used through several examples in order to validate the full waveform inversion code. Time domain shot gathers have been converted to frequency domain and a number of 13 discrete frequencies have been selected based on the method suggested by Sirgue and Pratt (2004). The selected frequencies are arranged in 6 frequency groups, as shown in **Table 2.1**. Each frequency group shares the first and last individual frequencies with the previous and next groups, respectively, to make an overlap between different groups. A Gaussian filter with window size of 500m has been applied on the true velocity model to generate a smooth initial model, as shown in **Figure 2.5**, to start FWI iterations in all the examples of this chapter. It should be noted that the water column with constant depth of 210m is kept unchanged during FWI, i.e. the shallow part of the initial model includes the true water velocity and FWI will update the velocities below seafloor. However, as I will show in chapter IV, the initial model should be improved when the low frequency data are not available. In the following sections different configurations of shot assembling will be examined for the optimum selection of number of supershots and simultaneous sources.

Table 2.1 Discrete frequency values (Hz) arranged in 6 groups for FWI

group 1	group 2	group 3	group 4	group 5	group 6
2.0, 2.5, 3.0	3.0, 3.5, 4.33	4.33, 5.33, 6.5	6.5, 7.83, 9.5	9.5, 11.5, 14.0	14.0, 17.16, 20.66

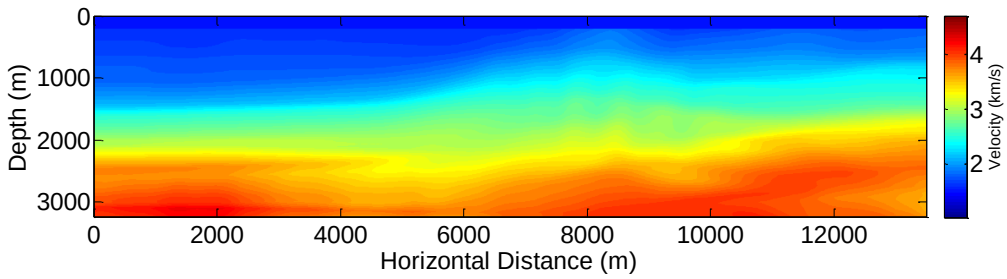

Figure 2.5 Smooth initial model created by applying a Gaussian filter on true velocity model.

2.9.1 Conventional FWI Using Sequential Sources

The first example shows the results of conventional full waveform inversion in a sequential mode. All the shot gathers are used to perform FWI using the 6 frequency groups and the smooth initial model. **Figure 2.6** shows the velocity models resulting from each frequency group. The result of each group has been used to start FWI on the next frequency group. Number of iterations for each frequency group is set to 30 and an offset dependent weighting has been used. Sequential sources are actually handled as a special case in the algorithm, when each supershot includes only one individual source with no random phase encoding. The final model is the output of frequency group 6. As the figures show, low frequencies build a rough velocity model at the early stages of FWI and the higher frequencies add more details to the subsurface structures to finally deliver a high resolution model.

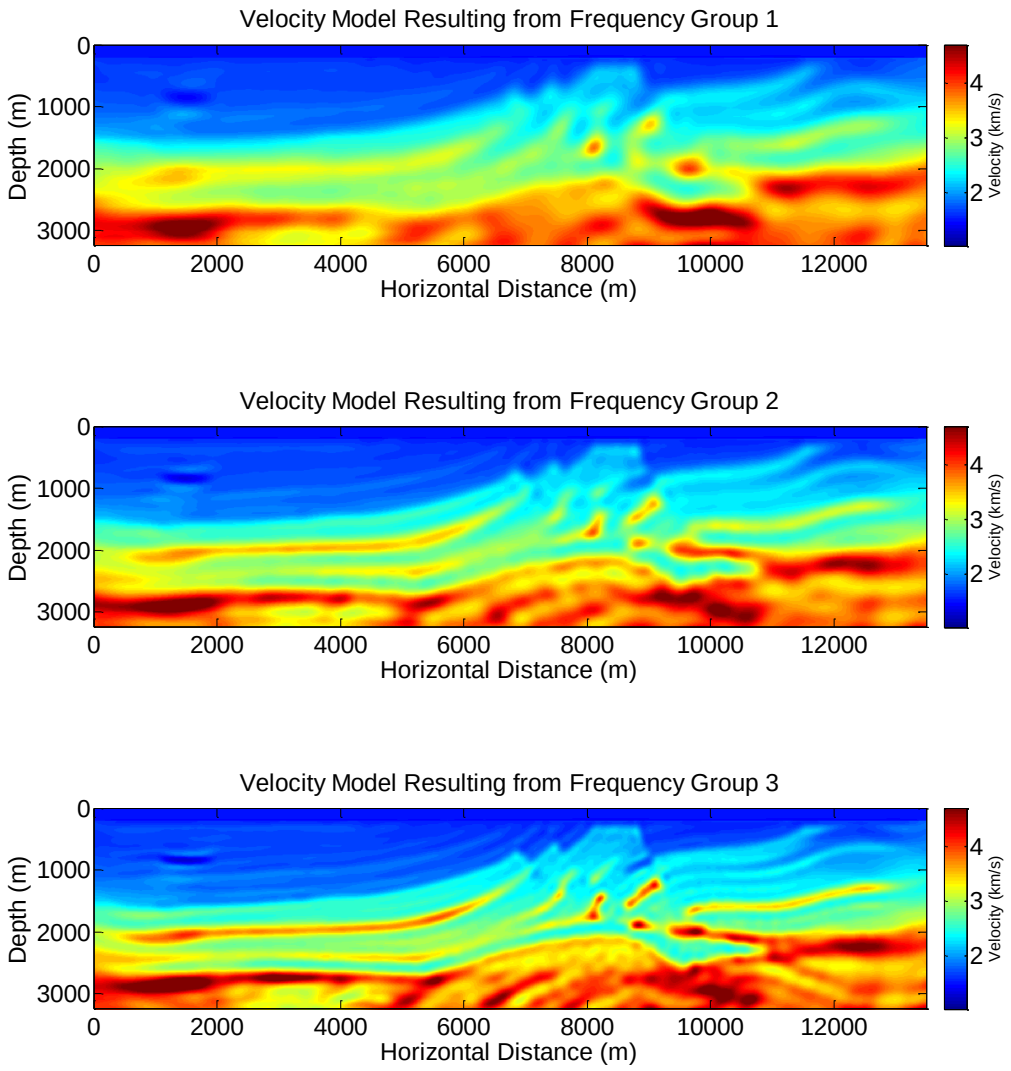

Figure 2.6 Velocity models resulting from conventional FWI using sequential sources. Each panel shows the result of FWI on a frequency group from 6 groups shown in **Table 2.1** (continue to next page).

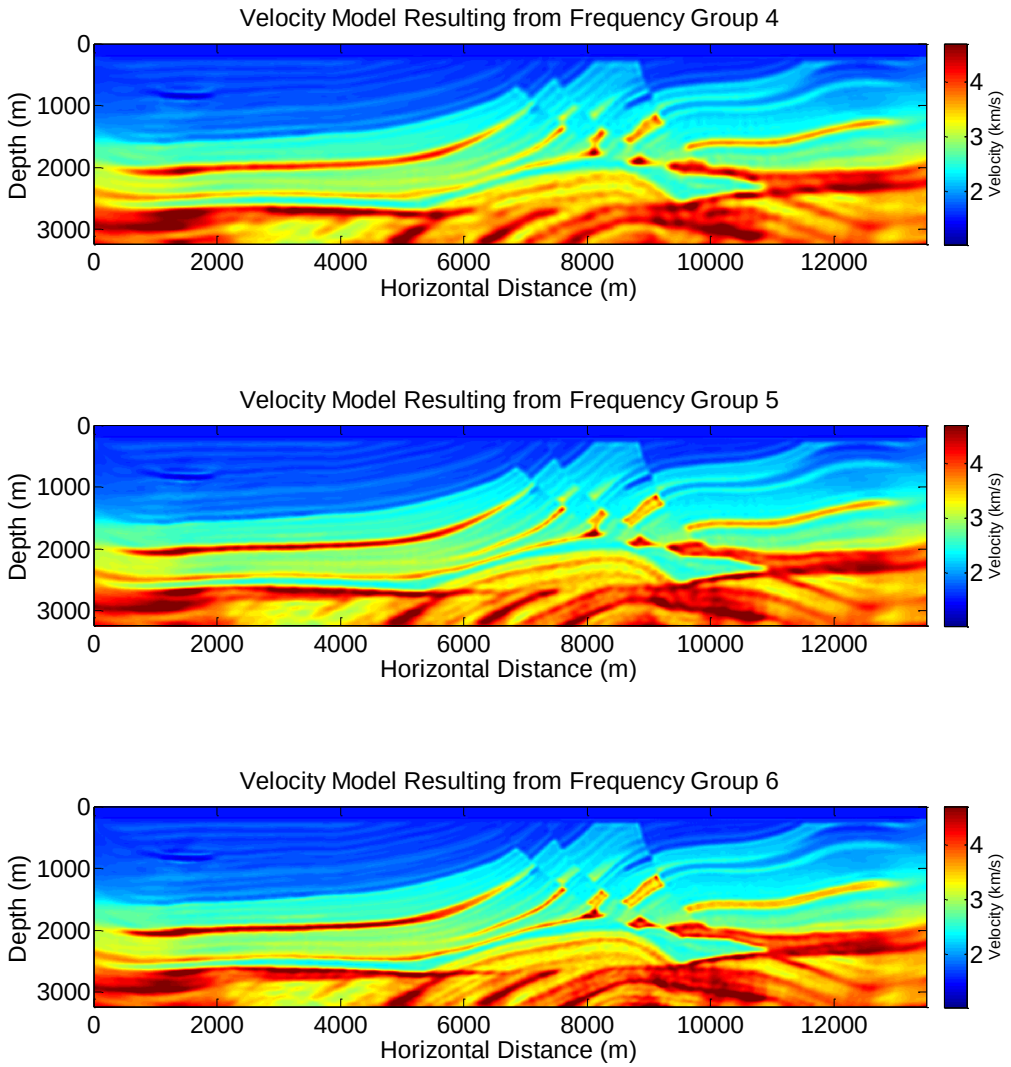

Figure 2.6 (continued from previous page) Velocity models resulting from conventional FWI using sequential sources. Each panel shows the result of FWI on a frequency group from 6 groups shown in **Table 2.1**.

Misfit values from different frequency groups are normalized by the maximum misfit value from each corresponding frequency group and are displayed in **Figure 2.7**, where the low frequency components make a significant contribution to misfit reduction and higher frequencies slightly decrease the misfit. Although the quality of the FWI results using sequential sources is comparable with the true velocity model, the computation time for achieving these results is quite high. A single iteration of FWI for each frequency group took 1602.98 s. The large finite difference grid, with 1801 horizontal and 434 vertical nodes, could be one of the main reasons of this high computational burden. Forward modeling on this grid requires an impedance matrix with dimensions of 919334 × 919334, including additional rows and columns for a PML boundary of 30 nodes on each side of the grid. However, matrix decomposition phase in forward modeling has been efficiently optimized using multithreaded and array processing techniques in a parallel mode to minimize the required time for matrix solution. The other reason for this high computation time is the large number of sources in the survey. Since gradient calculation requires forward modeling of all the seismic sources in a sequential scheme, increasing number of sources linearly increases the required processing time. Although the finite difference grid could be resampled by using a larger grid interval to reduce the impedance matrix dimensions for the sake of efficiency, full waveform inversion is intended to be applicable on large datasets and it is necessary to reduce the computational burden resulting from sequential sources. This problem will be solved using random phase encoded simultaneous sources as the next example will illustrate.

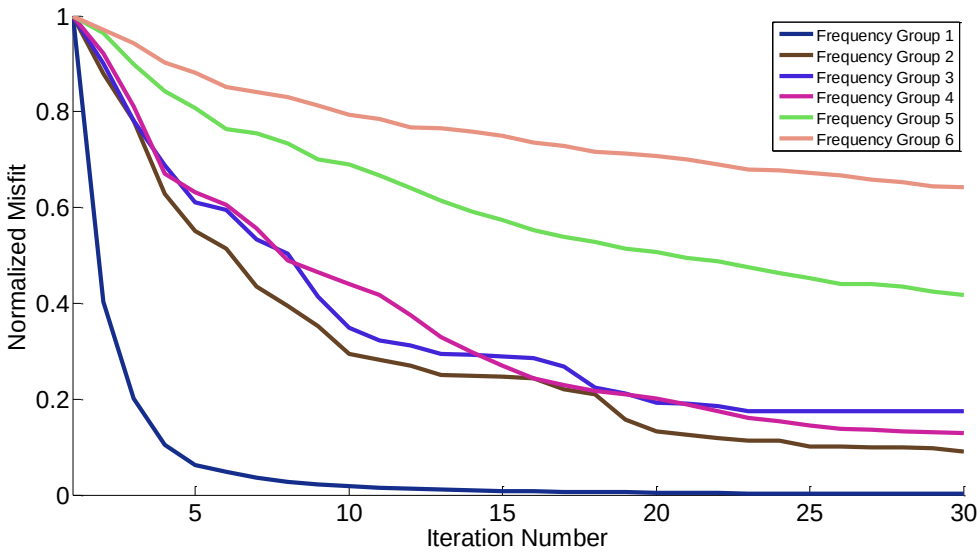

Figure 2.7 Normalized misfit values for FWI using sequential sources.

2.9.2 FWI Using Simultaneous Sources with Close Configuration

Individual sources are assembled in supershot gathers with close configuration (CC) to improve the efficiency of the full waveform inversion algorithm. In order to examine different number of simultaneous sources which could be assembled in a supershot gather with close configuration, two examples are shown in **Figure 2.8**. The first strategy assembles 9 simultaneous sources in 50 supershot gathers, and the second one takes 18 simultaneous sources into 25 supershot gathers, both with close configuration geometry. As a result, the spatial horizontal extent of one segment is 270m for the first and 540m for the second case, respectively. As the results show, both examples could achieve

acceptable velocity models which are comparable to the FWI result using sequential sources. The advantage of using simultaneous sources in decreasing computation time of FWI is approved by the new results. One iteration of FWI for each frequency group using 50 supershot gathers took 227.22 s, while it took only 135.07 s when using 25 supershot gathers. The original processing time for 450 sequential sources was 1602.98 s which shows a speed-up of 7.05 and 11.86 for FWI using 50 and 25 supershot gathers, respectively. **Table 2.2** includes the required time for each iteration of FWI using different source assembling strategies. The result of full waveform inversion using sequential sources has been also shown in **Figure 2.8,** as a reference for comparison. The normalized misfit values for FWI using two close configurations of 50 and 25 supershot gathers are shown in **Figure 2.9**, the fluctuating behavior of misfit curves are because of randomly changing the phase encodings from iteration to iteration. However, the overall trend of the misfit curves decrease by the iterations.

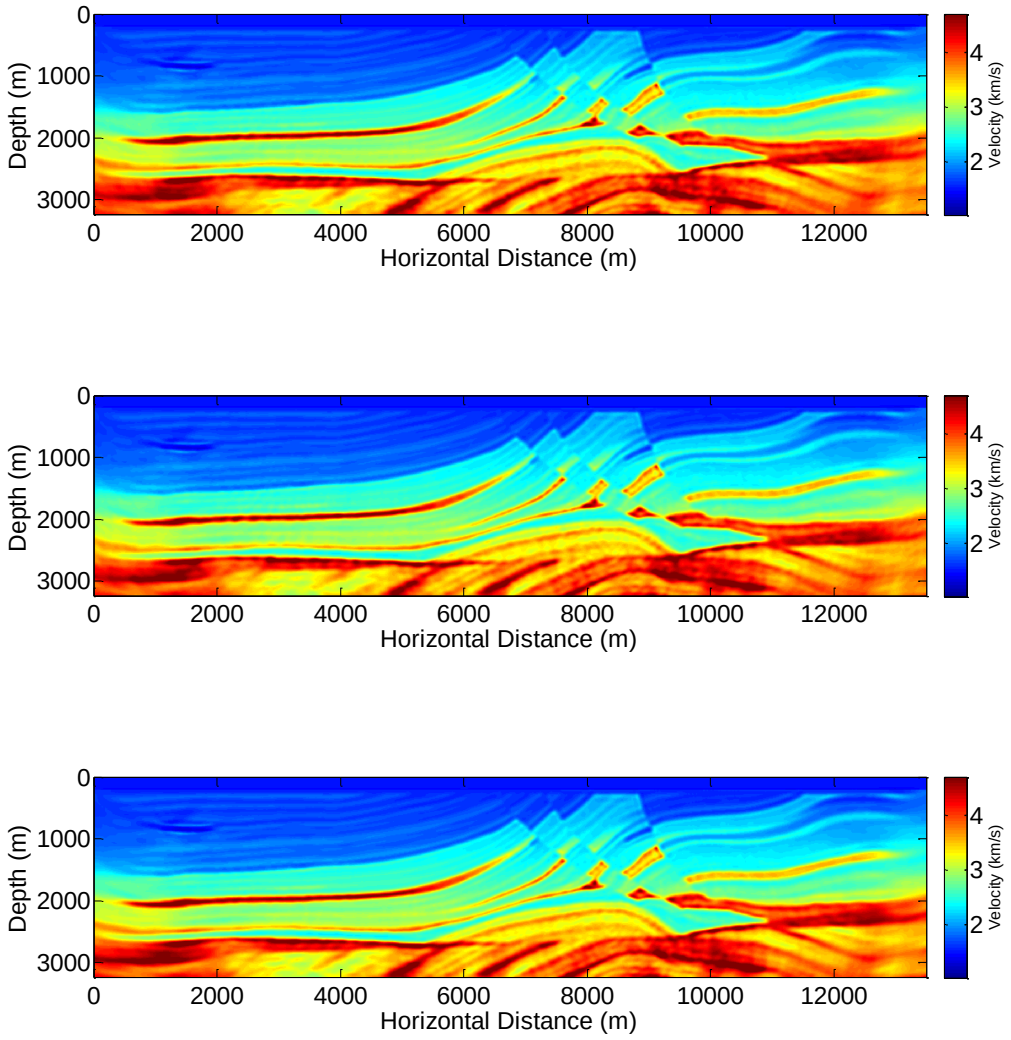

Figure 2.8 FWI results using 450 shots assembled in: 50 supershot gathers of 9 simultaneous sources with CC (top), 25 supershot gathers of 18 simultaneous sources with CC (middle), and 450 sequential sources (bottom).

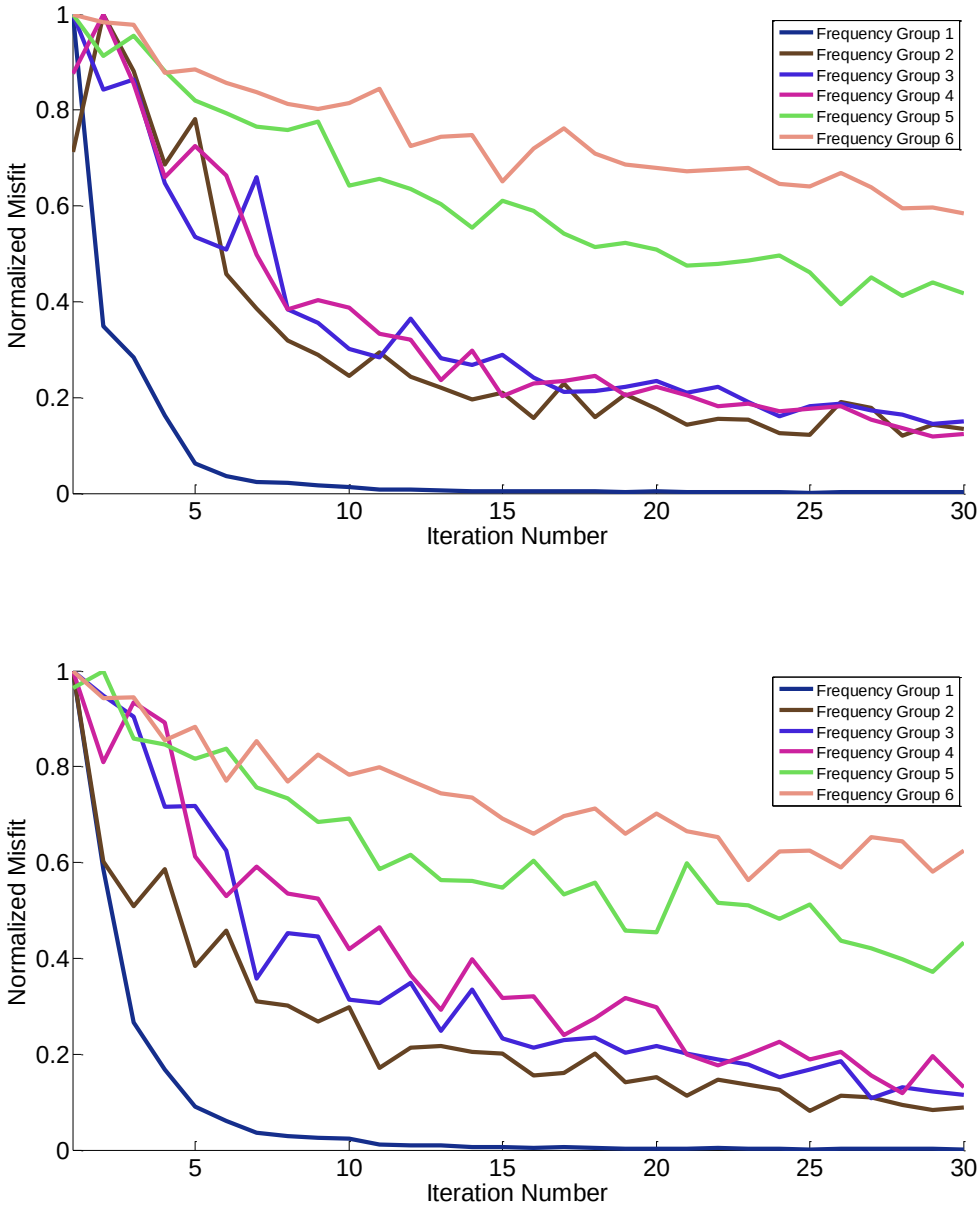

Figure 2.9 Normalized misfit values for FWI results using 450 shots assembled in: 50 supershot gathers of 9 simultaneous sources with CC (top), and 25 supershot gathers of 18 simultaneous sources with CC (bottom).

If a smaller dataset from the same survey area could produce the same results using full waveform inversion, then there would be a chance to minimize the acquisition cost and time for the future survey plans by efficiently recording a fewer number of shots. In order to check this possibility, I select every other shot from the original dataset, which results in 225 shot gathers, for another example. In fact, the original data was acquired using shot interval of 30m, but now I select shot gathers with shot interval of 60m and use them for full waveform inversion using simultaneous sources. 225 shot gathers are assembled in 25 supershot gathers, each involving 9 individual shots. Since the shot interval is now doubled, the horizontal extent of each segment in close configuration becomes 540m. **Figure 2.10** shows the results of FWI using this reduced number of shots for noise-free, and noise contaminated data with signal to noise ratio of 5. The results are very similar to the FWI results obtained by using the full dataset. It means the shot interval could be effectively increased to 60m to use only 225 sources for full waveform inversion. Since the number of supershot gathers for full waveform inversion is 25, the computation time is similar to the case of assembling 450 shots in 25 supershot gathers (**Table 2.2**). However, the required dataset is half of the original one and a survey with the reduced number of shots can produce the same results, which can reduce the acquisition cost and time for any future acquisition plans. Normalized misfit values for this example are shown in **Figure 2.11.** The effect of random noise is obvious in the misfit values as the background level of misfit is increased due to the noise appearing in the observed data.

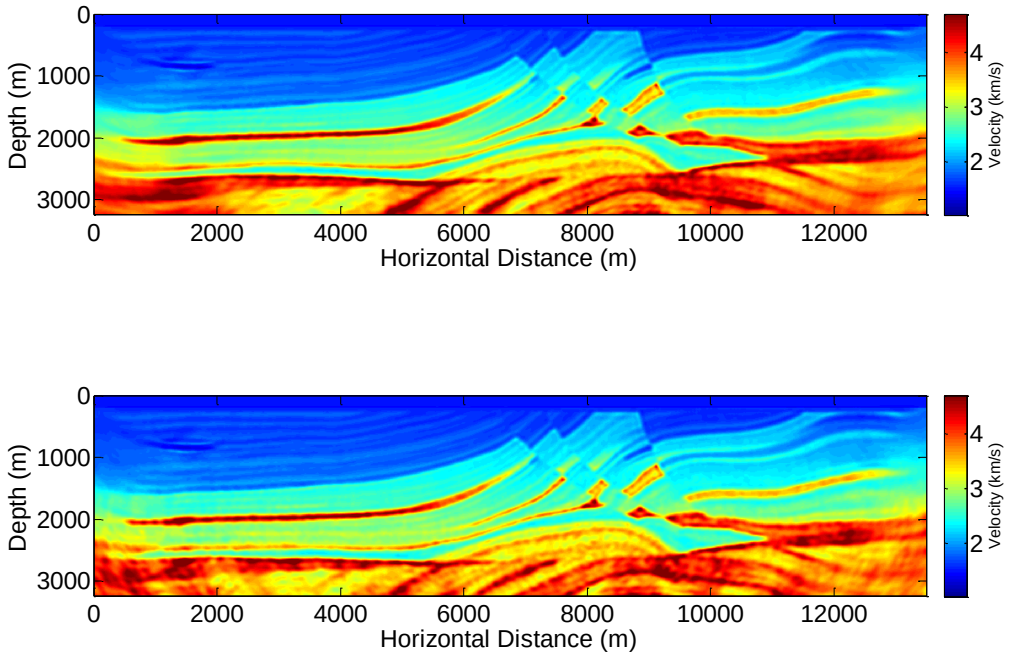

Figure 2.10 FWI results using 225 shots assembled in 25 supershot gathers of 9 simultaneous sources with CC for: noise-free input data (top), and noise contaminated input data with signal to noise ratio of 5 (bottom).

In order to evaluate the resulting velocity models, a sample shot gather has been generated using the FWI resulting models. The source location for this sample shot gather is displayed in **Figure 2.3** with the red star. Time domain shot gathers are modeled for smooth initial model and FWI resulting models and compared against input data from true velocity model, as shown in **Figure 2.12**.

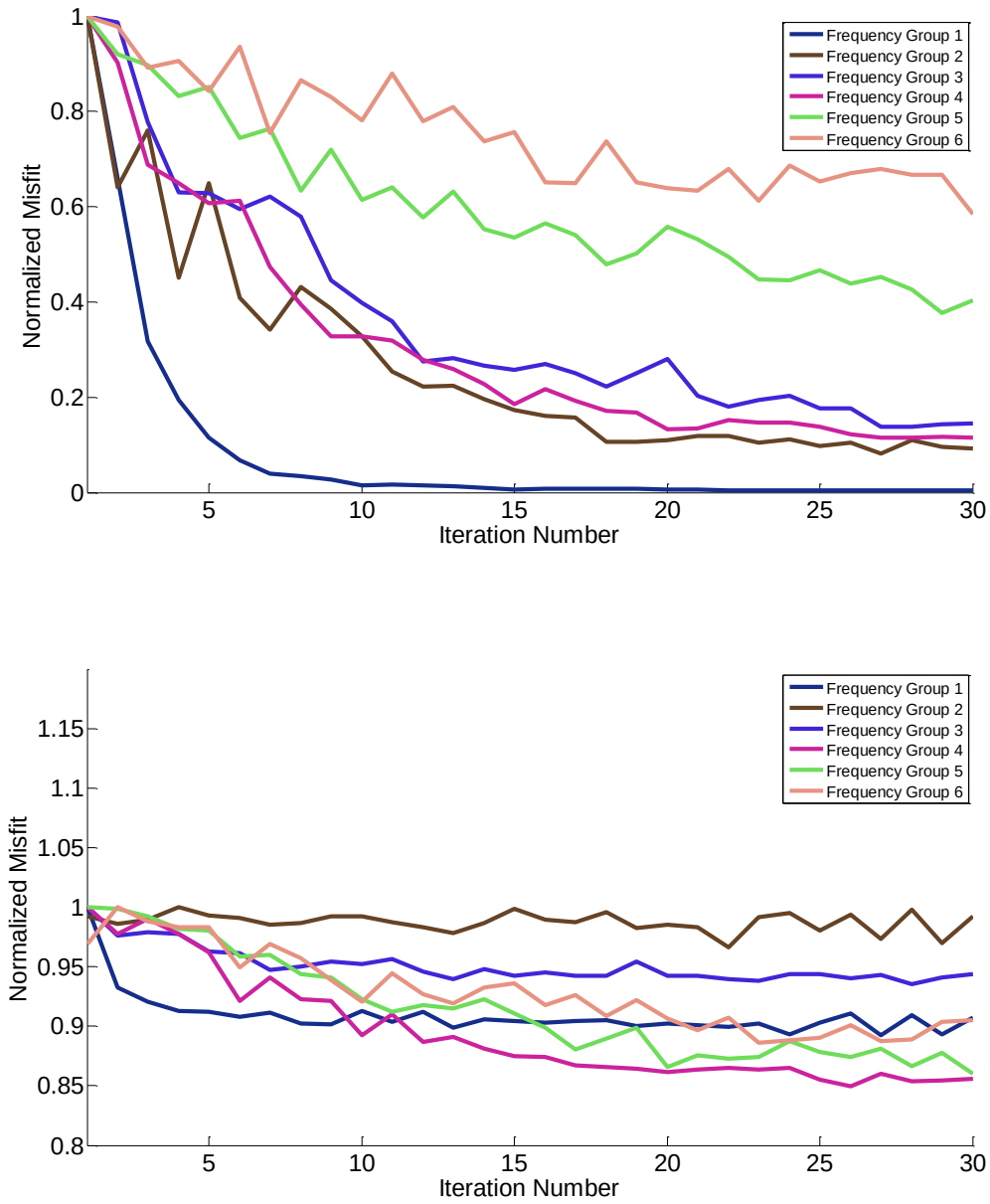

Figure 2.11 Normalized misfit values for FWI results using 225 shots assembled in 25 supershot gathers of 9 simultaneous sources with CC for : noise-free input dataset (top), and noise contaminated input dataset with signal to noise ratio of 5 (bottom).

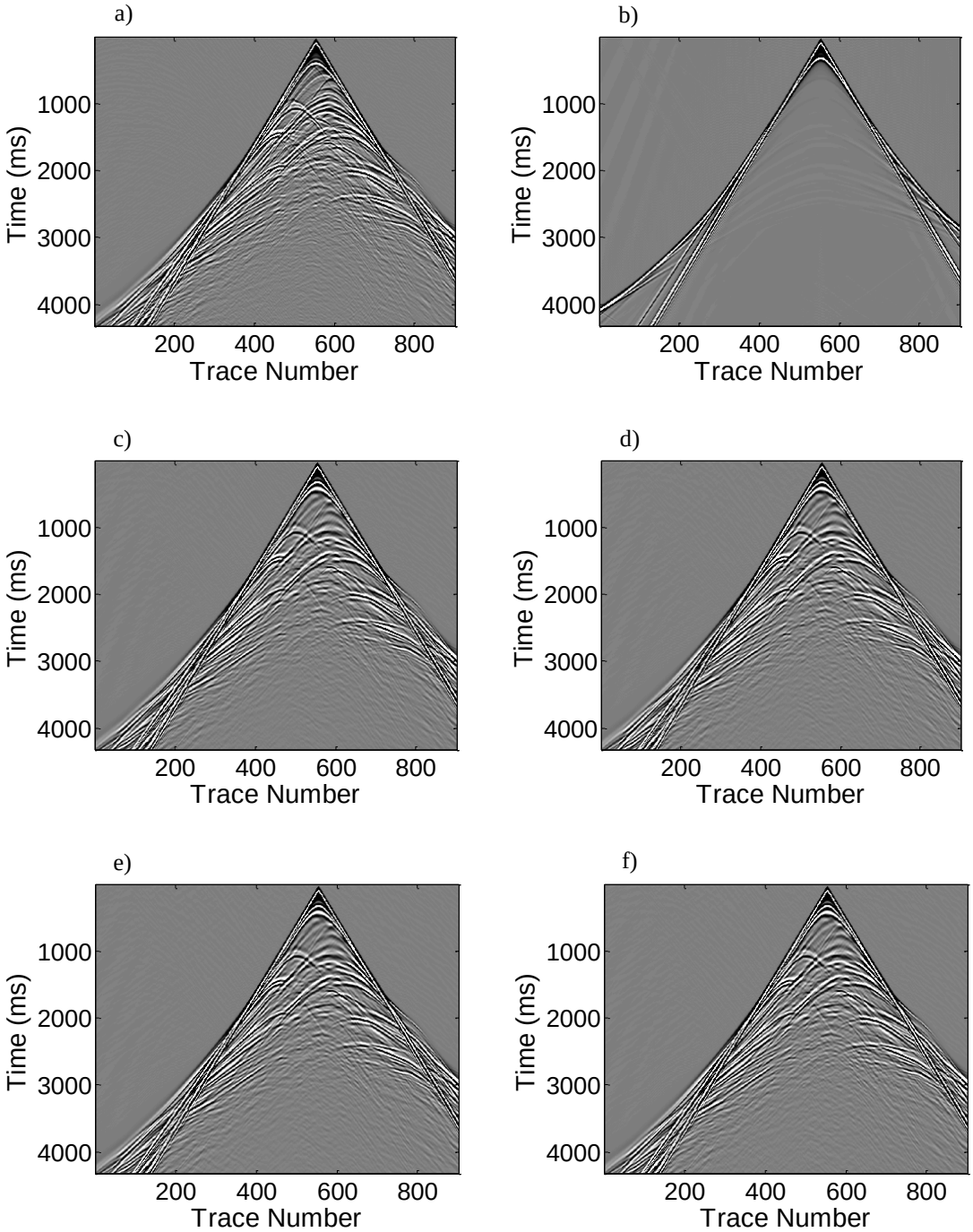

Figure 2.12 Time domain shot gathers simulated using: true model (a), smooth initial model (b), FWI result using 450 sequential sources (c), FWI result using 50 supershots of 9 simultaneous sources (d), FWI result using 25 supershots of 18 simultaneous sources (e), and FWI result using 25 supershots of 9 simultaneous sources (f).

2.9.3 FWI Using Simultaneous Sources with Random Configuration

In order to check the effect of source configuration strategy while assembling individual shots into supershot gathers, here I show the results of FWI using random configuration (RC). In this strategy, the individual sources are selected from random locations in the original geometry of the survey line and are assembled into supershots (**Figure 2.1**). The random location of the sources changes from iteration to iteration to increase the incoherence of the crosstalk noise. Random phase encodings are used, same as previous section, to suppress the crosstalk noise. Three different examples of source assembling using random configuration (RC) are shown in **Figure 2.13**. Top panel shows the FWI result using 450 shot gathers assembled in 50 supershots of 9 simultaneous sources with random configuration. Although the velocity model obtained by FWI is acceptable in shallow to medium depth range, the deeper parts show less accurate results especially on both sides of the model. It seems that randomizing source location is less effective than the first strategy, i.e. close configuration. The reason could be the offset dependent weighting which could not be applied during gradient calculation using random configuration. Since the random locations of sources does not allow for such an offset dependent weighting matrix to be used, the deeper parts of the model which are usually recovered by long-offset data will be degraded. Middle panel in **Figure 2.13** shows the FWI result using 450 shot gathers assembled in 25 supershots of 18 simultaneous sources using RC. The bottom channel shows the results using 225 supershots of 9 simultaneous sources using random configuration. Although the shallow to medium depths show reliable velocities, the deeper parts suffer from the same problem as top panel especially on the both sides on the model. However, the FWI result using 225 shot gathers

assembled in 25 supershots of 9 simultaneous sources shows a better reconstruction of the model, compared to the other two panels. Misfit values for each frequency group are normalized by the maximum value of misfit in the corresponding groups and are displayed in **Figure 2.14**.

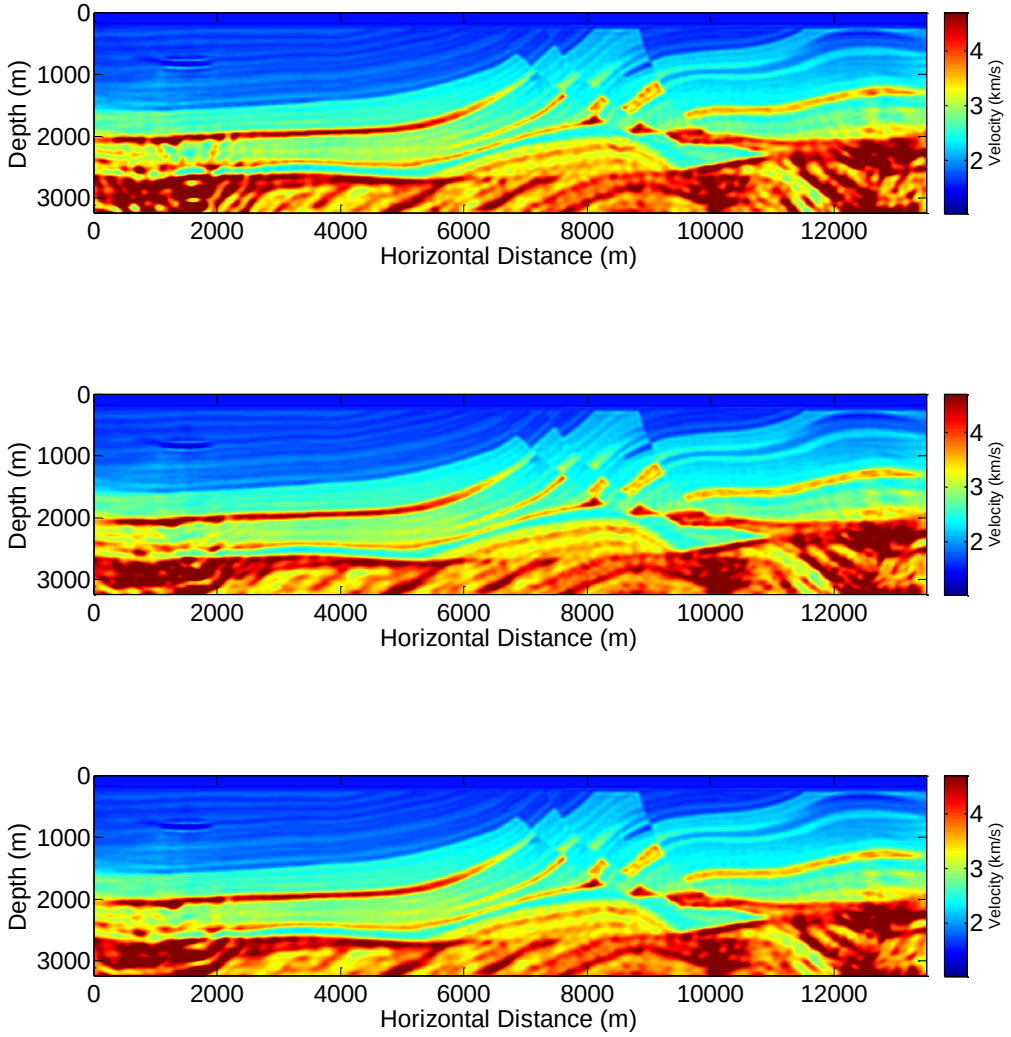

Figure 2.13 FWI results using random configuration of: 450 shots assembled in 50 supershot gathers of 9 simultaneous sources (top), 450 shots assembled in 25 supershot gathers of 18 simultaneous sources (middle), 225 shots assembled in 25 supershot gathers of 9 simultaneous sources (bottom).

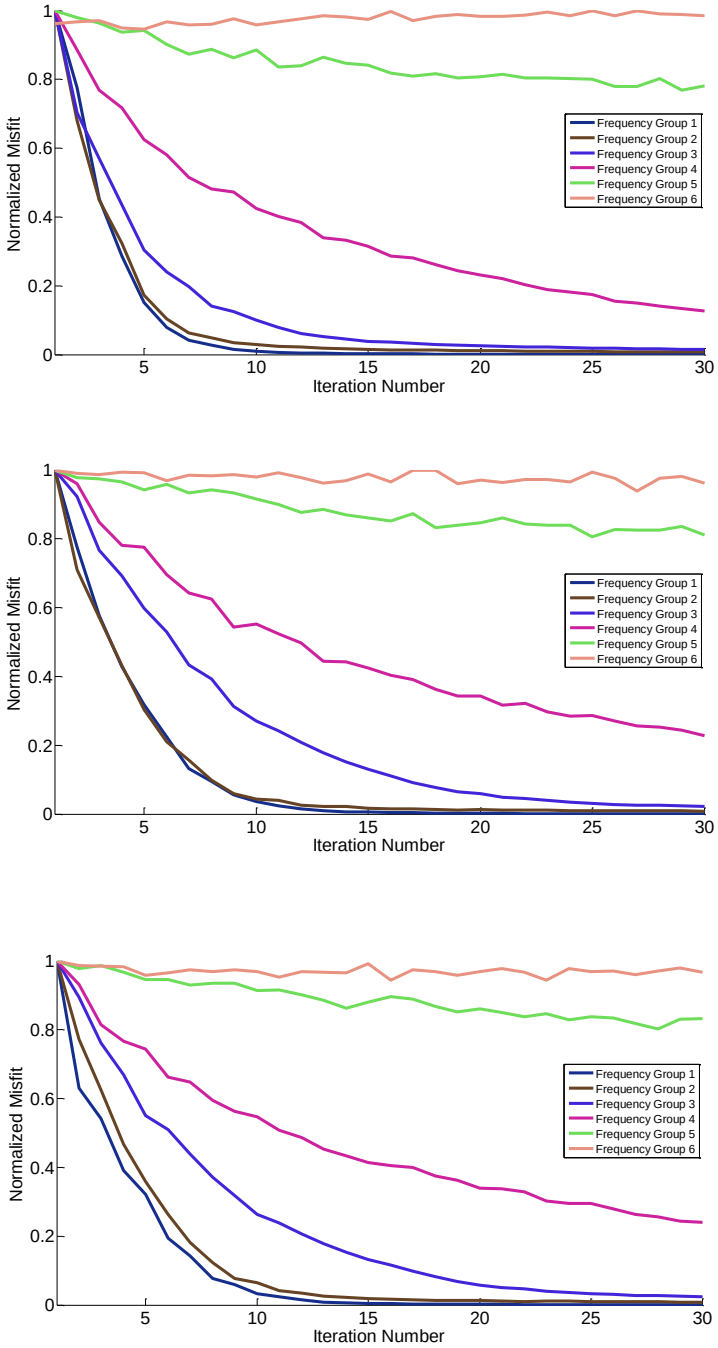

Figure 2.14 Normalized misfit values for FWI results using random configuration of: 450 shots assembled in 50 supershot gathers of 9 simultaneous sources (top), 450 shots assembled in 25 supershot gathers of 18 simultaneous sources (middle), 225 shots assembled in 25 supershot gathers of 9 simultaneous sources (bottom).

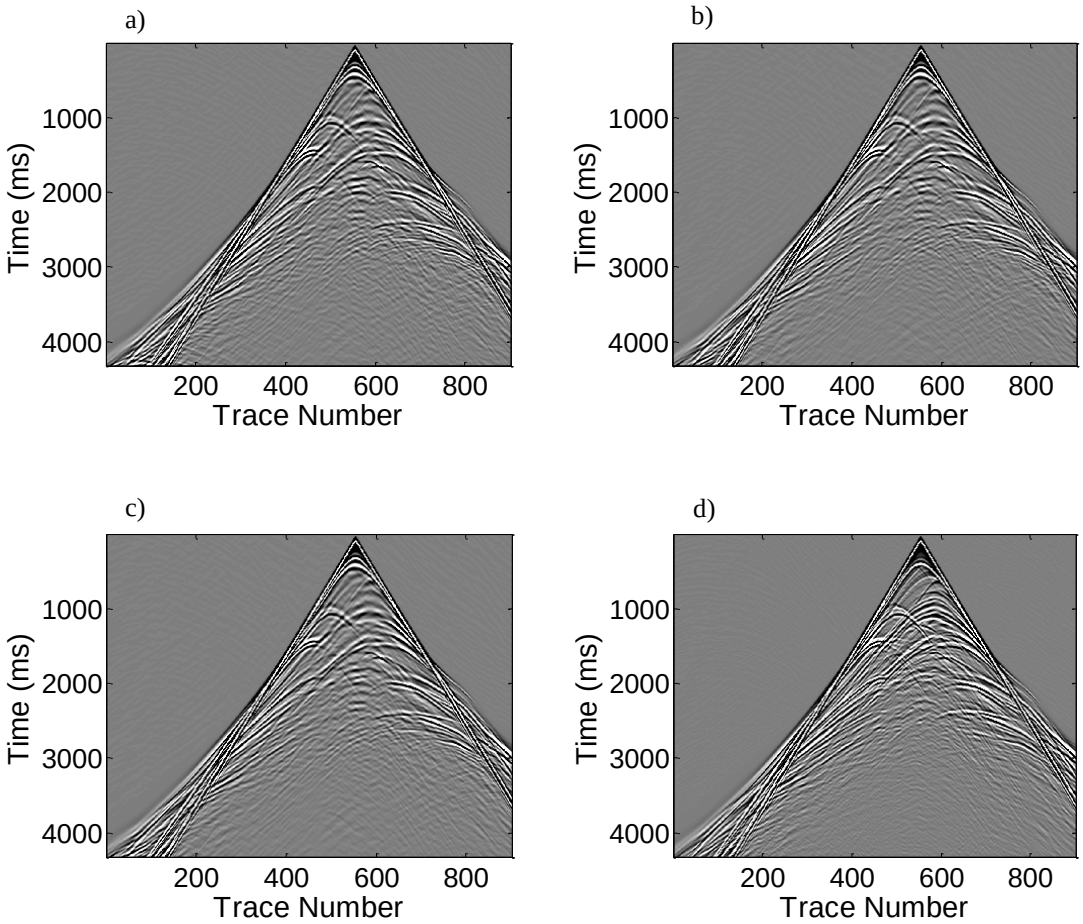

Figure 2.15 Time domain shot gathers simulated using FWI result from: 450 sources assembled in 50 supershots of 9 simultaneous sources (a), 450 sources assembled in 25 supershots of 18 simultaneous sources (b), 225 sources assembled in 25 supershots of 9 simultaneous sources (c). The observed input data from true model is shown in (d).

2.9.4 FWI Using Simultaneous Sources with Full Configuration

Full configuration (FC) of individual shots takes all the sources in the survey and assembles them in one supershot gather. This configuration has the highest level of crosstalk between different shots, because all of the receivers contribute to all the shots simultaneously. In order to reduce the crosstalk noise level random phase encodings change from iteration to iteration, same as CC and RC), but much higher number of iterations are required. **Figure 2.16** shows the result of full waveform inversion using 450 and 225 individual shot gathers assembled in supershot gathers using full configuration with 100 iterations per frequency group. As both panels show, the effect of crosstalk is evident in the deeper part of the model. Although the reduced number of 225 shots shows slightly better result, the FWI models are still poor in comparison with CC and RC strategies. Full configuration required 49.05 s and 48.56 s for each iteration of FWI using 450 and 225 sources, respectively. However, the number of iterations was increased from 30 to 100 compared to CC and RC strategies to reduce the crosstalk noise level. **Table 2.2** shows the required time for performing one iteration of full waveform inversion, per frequency group, for different source assembling strategies. Comparison of FWI results from different source assembling strategies for random phase encoded simultaneous sources illustrates that the close configuration could achieve the best velocity models. Even a reduced number of 225 sources with shot interval of 60m could obtain reliable velocity models. Also, comparison of required calculation time for different strategies shows that close configuration of 25 supershot gathers could achieve significant speed-up for the full waveform inversion.

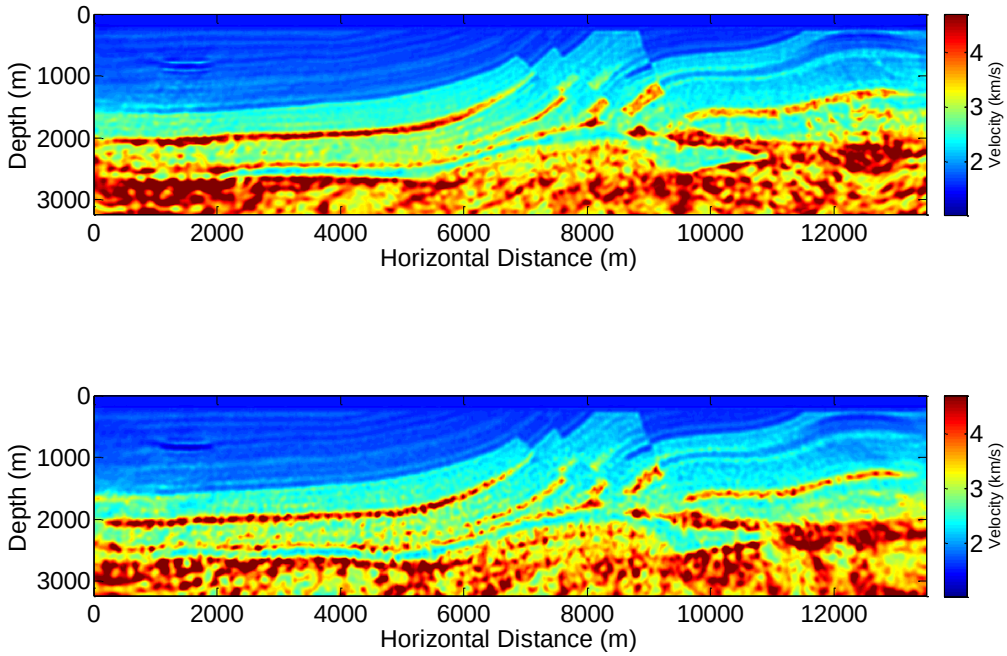

Figure 2.16 FWI results using full configuration of: 450 shots assembled in one supershot gather (top), and 225 shots assembled in one supershot gather (bottom)

Table 2.2 Required time(s) for one iteration of FWI using different source assembling strategies

	450 shots in 50 supershots	450 shots in 25 Supershots	225 shots in 25 Supershots
Close Configuration	227.22	135.07	134.73
Random Configuration	227.26	135.68	135.71
Full Configuration	49.05		48.56
450 Sequential Sources	1602.98		

2.10 Crosstalk Analysis

The analysis of crosstalk noise effect on the FWI results helps to distinguish between the possible levels of accuracy which could be obtained by random phase encodings and different spatial source configurations. **Figure 2.17** shows two FWI results using close configuration of 225 shot gathers assembled into 9 supershot gathers of 25 simultaneous sources. All the parameters for obtaining these two models are the same, except that in the top panel of **Figure 2.17** random phase encodings have been used while assembling shots into supershot gathers, but supershot gathers for the middle panel of **Figure 2.17** are formed without assigning any random phase encodings. It is obvious that the random phase encodings have a profound effect on reducing the crosstalk noise and improving the quality of the resulting model. The difference between these two models is shown in bottom panel of **Figure 2.17**. This residual velocity is the direct effect of the crosstalk noise which degrades the velocity model if no random phase encodings are used.

Although random phase encoding itself is the main tool to reduce the crosstalk effect, the spatial configurations of the individual sources in the supershot gathers are also very important. As results in the previous sections confirmed, the accuracy level of the models obtained using close, random, and full configurations are different. In order to evaluate the amount of crosstalk suppression using each of these shot selection strategies, I calculate the residual velocities by subtracting the FWI results using random phase encoded simultaneous sources and conventional sequential sources. Since the sequential sources produce no crosstalk in the FWI model, it could be used as a basis for the comparison of the resulting models from FWI using simultaneous sources. **Figure 2.18** shows the residual velocities for 225 individual shots assembled in 25 super shot gathers

using close configuration (top), random configuration (middle), and full configuration (bottom). As **Figure 2.18** illustrates, the difference between FWI result using close configuration and sequential FWI is negligible, however, random configuration and full configuration show a significant residual due to higher level of crosstalk.

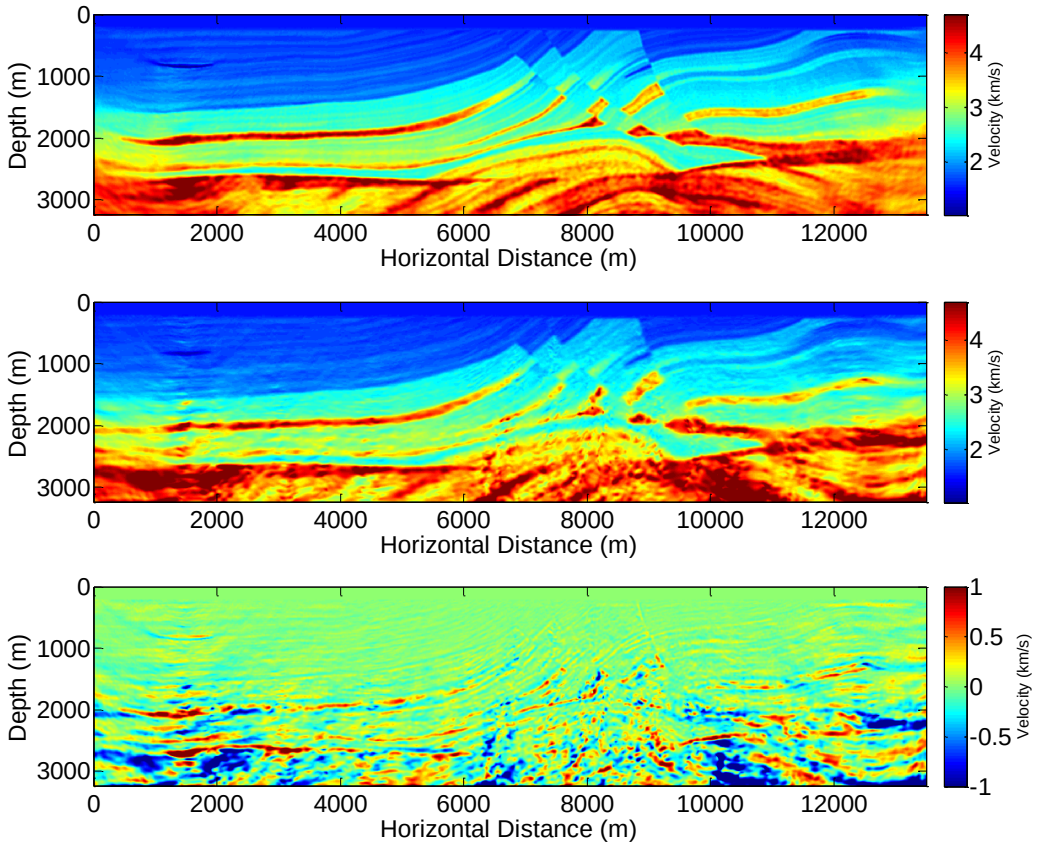

Figure 2.17 FWI result using simultaneous sources with random phase encodings (top) and without random phase encodings (middle). The difference which is caused by crosstalk noise is shown in the bottom.

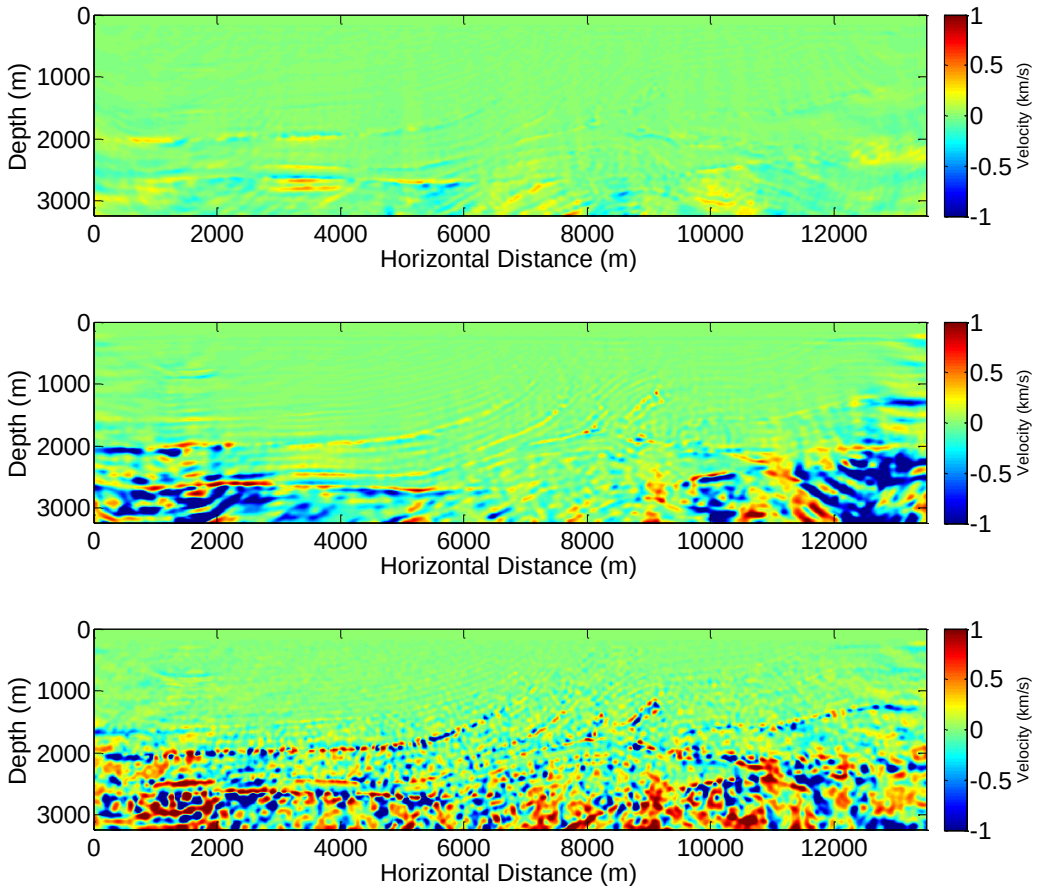

Figure 2.18 Residual velocities by subtracting resulting models of FWI using random phase encoded simultaneous sources from sequential FWI model, representing the crosstalk noise level for close configuration (top), random configuration (middle) and full configuration (bottom).

Anagaw and Sacchi (2014) evaluated the effect of frequency selection strategies on FWI results using random phase encoded simultaneous sources. They could confirm that a number of overlapping frequency groups can obtain reliable velocity models using different examples from Marmousi, Marmousi2, and BP/EAGE velocity models. One of the interesting conclusions they made is that the performance of the different frequency selection strategies depends on various factors including the quality of the initial model, acquisition geometry, level of the random noise in the data, the bandwidth of the seismic data, and the complexity of the subsurface unknown model. So far, I validated the developed simultaneous sources FWI engine for 2D acquisition geometry using noisy data with signal to noise ratio of 5 for the complex velocity model of Marmousi2. In the next chapters I will evaluate the effect of initial model and band-limited seismic data on FWI results and propose solution for the problems related to these issues.

Here I show one of the examples from Anagaw and Sacchi (2014) to demonstrate the possible improvement of FWI results using random phase encoded simultaneous sources. Although they did various tests using Marmousi2 model, the presented example here is just the closest model in terms of frequency bandwidth and frequency groups for FWI using four frequency groups with one overlapping value in the range of 2.93 to 20.02 Hz. This frequency range is very close to the frequency band which I used in the example of previous sections (2 – 20.66 Hz). **Figure 2.19** shows the true model, initial model and FWI result using noisy data with signal to noise ratio of 10 (after Anagaw and Sacchi, 2014). Although the part of Marmousi2 model which they used in their work is different from the model used in this thesis, it is still possible to make a comparison on the results. **Figure 2.20** shows the FWI result which has been obtained by frequency domain FWI of

Marmousi2 model using the developed code in the present research. It should be noted that acquisition parameters, number of supershots, and model dimensions are different and this comparison is just to demonstrate that the developed FWI code in this thesis achieves reliable velocity models for noisy data and complex subsurface model.

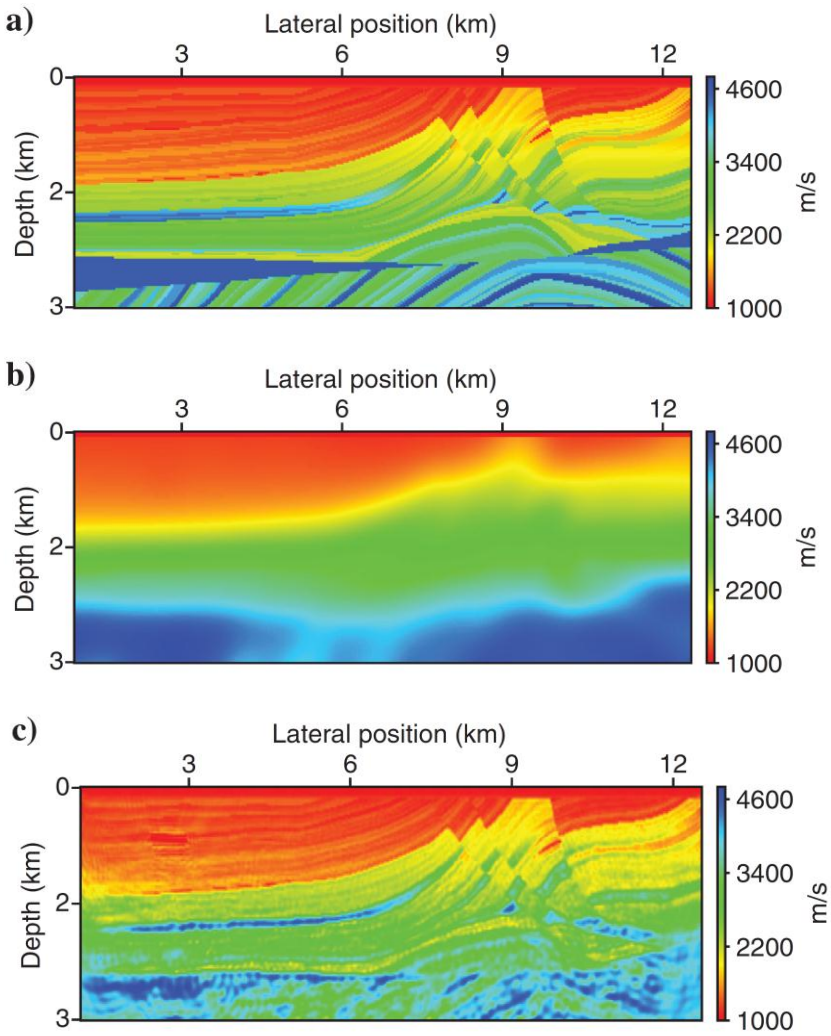

Figure 2.19 FWI result using simultaneous sources in Anagaw and Sacchi (2014). True velocity model (a), initial model (b), and FWI result using 3 supershots each including 40 simultaneous sources (c). (Panel (a) and (b) are the same as Figure 9 and panel (c) is the same as panel (c) of Figure 10 in Anagaw and Sacchi, 2014)

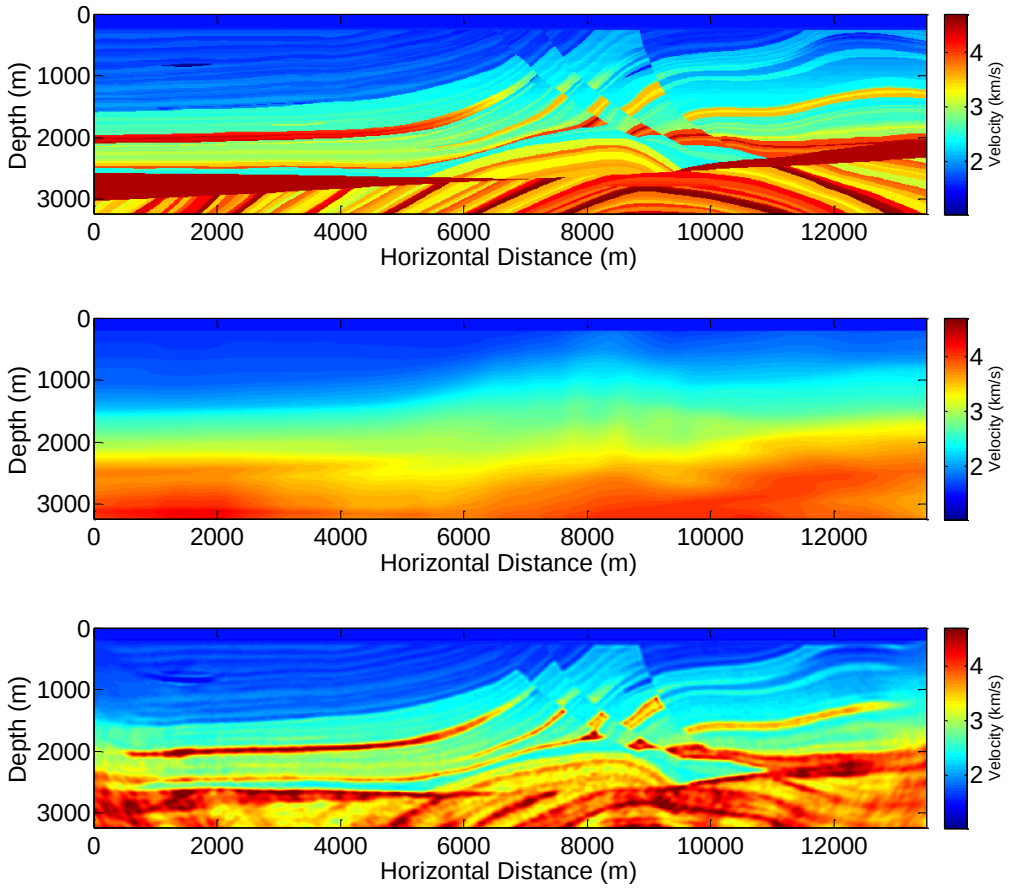

Figure 2.20 True velocity model (top), initial model (middle), and FWI result using 25 supershots of 9 simultaneous sources with Close Configuration for noisy data with S/N =5 (bottom) for the comparison purpose.

2.11 Discussion

Seismic full waveform inversion using random phase encoded simultaneous sources could be successfully applied to reduce the computation cost and time. Different examples from Marmousi2 complex model showed that accurate subsurface models could be obtained with effective suppression of crosstalk noise. Three geometrical shot selection strategies have been evaluated to achieve the best combination of time efficiency and model accuracy. A close configuration (CC) takes the neighboring individual sources from each segment of the survey area to assemble them in a supershot. This keeps the minimum distance between individual shots of a supershot and makes it possible to define an average offset from the center of the segment to all the receiver locations. This average offset is used in the form of a weighting matrix when calculating gradient to improve the deeper parts of the FWI results by using long-offset data. A random configuration (RC) selects the individual shots from a random distribution over survey area to assemble them into supershots. This method is supposed to increase the incoherence of crosstalk noise from iteration to iteration and help the random phase encodings to reduce the level of the noise. A full configuration (FC) takes all the sources in the survey and assembles them into one supershot gather.

Comparison of the FWI models using these three strategies and a crosstalk analysis showed that the close configuration could achieve the best velocity models using random phase encoded simultaneous sources. The random configuration could recover the subsurface structures with acceptable accuracy for shallow to medium depth. However, the results are degraded in the deeper parts of the model especially on the both sides of the model. One reason for this degraded FWI result is excluding the offset dependent

weighting matrix from gradient calculations. Since the individual sources in each supershot are from random locations of the survey area, it is not possible to define an average offset value for the receiver locations. The same problem happened when using full configuration, which has the highest level of crosstalk noise. Although the required processing time per FWI iteration using full configuration is significantly shorter than other configurations, the number of required iterations should increase for full configuration. Even with a large number of iterations, the level of crosstalk is still high and the FWI models are poor in the case of full configuration. It should be noted that the ideal speed-up in the simultaneous sources technique is assumed to be of the same order of number of individual shots assembled into one supershot gather. However, since the processing time is affected by other factors regardless of number of effective shots, the speed-up achieved by simultaneous sources is less that the ideal value.

2.12 Chapter Conclusions

I developed a full waveform inversion code using random phase encoded simultaneous sources to achieve high quality velocity models. By designing an algorithm for full waveform inversion in the frequency domain, I obtained computational efficiency and model accuracy through different examples from Marmousi2 model. In order to evaluate the effect of source selection strategies, I defined three different spatial configurations for shot selections prior to supershot gather formation. Close configuration, random configuration and full configuration of the seismic sources showed that the crosstalk noise level is directly related to the geometry of the shots assembling in one supershot gather. A crosstalk analysis on the results showed that the close configuration provides

the most reliable velocity model with negligible variations from conventional FWI result for the noisy data and complex subsurface model.

The random configuration could recover the subsurface structures with acceptable accuracy for shallow to medium depths, however, the results are degraded in the deeper parts of the model especially on the both sides of the model. This is evident in the crosstalk noise analysis, one reason for this inaccurate result is excluding offset dependent weighting matrix from gradient calculations for random configuration. Since the individual sources in each supershot are from random locations of the survey area, it is not possible to define a unique or average, offset value for the receiver locations. Consequently, offset dependent weightings are excluded from gradient calculations and deeper parts of the model are less accurate. The same problem happens when using full configuration, which has the highest level of crosstalk noise.

One interesting example showed that the number of required sources for full waveform inversion could be reduced by resampling the shot intervals from 30m to 60m. The same velocity models could be obtained by using 225, instead of 450, shot gathers in the close configuration of 25 supershot gathers. This helps to increase the shot interval in the future data acquisition plans, for the sake of a reduced acquisition cost and time. For all the full waveform inversion examples in the following chapters, I will use this optimized shot assembling strategy, i.e. close configuration of 225 shot gathers in 25 supershot gather of 9 random phase encoded simultaneous sources. The FWI engine developed in this chapter assures to achieve high resolution velocity models for complex media and noisy

data and makes the foundation for the next chapters. In the remaining of the thesis, I will focus on the initial velocity model building methods for band-limited seismic data.

CHAPTER III: SPARSE SPIKES REFLECTIVITY INVERSION, A PROCESSING STEP FOR FWI INITIAL MODEL BUILDING

3.1 Introduction

The reliability level of the information obtained from seismic reflection survey is restricted by the bandwidth of the seismic data. As Claerbout (1985) explains, estimated velocity from conventional seismic processing represents the low spatial frequency part of the subsurface model within the range of 0-2 Hz and reflectivity represents the high frequency part of the subsurface model within the range of 10-100 Hz and there is a gap between these two frequency ranges (see **Figure 1.3**). Since FWI is a data fitting problem which strictly relies on the low frequencies to build the low wavenumber component of the model, it is necessary to fill this information gap. In fact, the reflection data can cover only the higher spatial frequency part of the model spectrum and a considerable extent of lower frequency is not directly available.

It is possible to obtain the low frequency component of the model from well log data in the brownfield seismic cases, by using geologically constrained acoustic impedance inversion of the reflectivity section. Once the low frequency acoustic impedance values are estimated, the velocity model can be built using a known density model. I will show that the subsurface structures could be detected on the reflectivity section by interpreting geological horizons. These horizons will later be used to bridge between geological information from well log data at the well locations and seismic section by a horizon-guided well interpolation over the entire model. In order to do so, first I shall extract the reflectivity from seismic section in this chapter.

Velis (2008) introduced stochastic sparse spike deconvolution method for extracting the reflectivity series from seismic traces. He defined a least squares inverse problem to search for a number of spikes in the reflectivity series, which when convolved with the known seismic wavelet could match the input seismic data within a tolerance. I will develop a modified algorithm for sparse spikes reflectivity inversion to calculate the reflection coefficients of the seismic traces from time migrated section. The improvement in this algorithm compared to the work conducted by Velis (2008) is that there is no limit on the number of spikes in a reflectivity series and the algorithm automatically detects as many events as possible in the seismic section. Several synthetic examples and a real data example will be used to validate the method and a comparison with minimum entropy deconvolution (MED) will show that the reflectivity inversion results are much more reliable. In the following sections I will describe the theory and algorithm to apply reflectivity inversion.

3.2 Convolutional Model for the Seismic Data

Based on a convolutional model, any seismic trace can be reproduced by convolving a reflectivity series with a known wavelet. A noise component may be added to the data for a more realistic situation. Although the convolution of two signals to reproduce seismic data is simple, the reverse procedure is challenging because of the limited frequency band that is available. When the seismic record is the only known data in the deconvolution problem, it is difficult to extract the reflection coefficients at interfaces. Moreover, noise

component almost always contaminates data and makes the problem more complex. From a mathematical point of view, the convolutional model can be represented as

$$\mathbf{x}(t) = \mathbf{w}(t) * \mathbf{e}(t) + \mathbf{n}(t) \tag{3.1}$$

where $\mathbf{x}(t)$ is the recorded trace, $\mathbf{w}(t)$ is the seismic source wavelet, $\mathbf{e}(t)$ is the reflectivity series , and $\mathbf{n}(t)$ is the random noise. Assuming the Goupillaud model of the earth (Goupillaud, 1961), one could derive an equation in matrix form

$$\mathbf{x} = \mathbf{We} + \mathbf{n} \tag{3.2}$$

where $\mathbf{x}$, $\mathbf{e}$, and $\mathbf{n}$ are vectors of seismic trace, reflectivity series and random noise, respectively, each consisting of m samples. $\mathbf{W}$ is the $m \times m$ matrix of the convolution kernel whose elements are samples of the seismic wavelet. Equation (3.3) shows the convolution kernel under the zero-phase wavelet assumption, which results in a symmetric matrix; if one uses a minimum-phase wavelet the matrix $\mathbf{W}$ will be upper triangular. For the zero-phase case,

$$\begin{bmatrix} x_1 \\ x_2 \\ x_3 \\ \vdots \\ x_m \end{bmatrix} = \begin{bmatrix} w_1 & w_2 & w_3 & \cdots & w_m \\ w_2 & w_1 & w_2 & w_3 & \vdots \\ w_3 & w_2 & w_1 & w_2 & w_3 \\ \vdots & w_3 & w_2 & w_1 & w_2 \\ w_m & \cdots & w_3 & w_2 & w_1 \end{bmatrix} \begin{bmatrix} e_1 \\ e_2 \\ e_3 \\ \vdots \\ e_m \end{bmatrix} + \begin{bmatrix} n_1 \\ n_2 \\ n_3 \\ \vdots \\ n_m \end{bmatrix} \tag{3.3}$$

where w_1 is the peak sample of the zero-phase wavelet. In order to characterize reflecting boundaries adequately, one needs to extract the reflectivity series which is represented by **e** in equation (3.2).

3.3 Sparse Spikes Inversion as a Global Optimization Problem

Generally, inverse filtering is used in different deconvolution methods to develop a deconvolution operator to be applied on the seismic traces. A required assumption is minimum-phase wavelet, in order for the deconvolution operator to be stable. Moreover, there always is a possibility to increase the random noise level by conventional spiking deconvolution. While whitening the spectrum of input trace in the desired bandwidth, deconvolution operator inevitably boosts the higher frequencies which usually contain random noise. For this reason, conventional spiking deconvolution is usually followed by a band pass filtering to minimize the level of boosted random noise. Here I use a different method for extracting the reflectivity series without any of these problems. A least squares inverse problem is defined based on the method introduced by Velis (2008) as a stochastic spiking deconvolution. An objective function is defined as the misfit error

between input seismic trace and a synthetic trace which is built using convolutional model. The least number of sparse spikes which their convolution with known seismic wavelet minimizes the misfit error are searched within the reflectivity series. Arrival times of the best set of spikes for each trace is calculated using adaptive simulated annealing (Ingber, 1995) and the amplitudes are then calibrated for a minimal tolerance. Since the problem is solved for post-stack data and the number of expected spikes in a reflectivity series is small enough, global optimization algorithms could work with reasonable processing time. Distribution of the seismic reflections in a recorded trace is quite random and, as a result, one can search for reflection coefficients by using a random-search algorithm. For this purpose, I use the residual energy of the difference between the recorded seismic data and the synthetic trace from convolutional model as a misfit function, to be optimized using adaptive simulated annealing. The misfit value could be calculated by

$$F = \left\| \mathbf{x} - \mathbf{We} \right\|^2 \tag{3.4}$$

For normally distributed noise with mean zero and standard deviation σ the expected misfit is $m\sigma^2$, where m is the number of time samples. The threshold misfit related to the background random noise could be estimated and the expected misfit resulting from a synthetic trace based on different sets of spikes could be evaluated to reach the best number of spikes through the inversion (Velis, 2008). Although Velis (2008) considered

the number of spikes to be fixed for each seismic trace, here I use the threshold energy of residual to automatically control the inversion.

3.4 Optimization Using Adaptive Simulated Annealing

Adaptive Simulated Annealing (Ingber, 1995) is a robust global optimization tool for solving the inverse problems. The method, which is developed based on the physical phenomena of annealing, considers a system in an initial state with energy E_1, and then perturbs the system so that the energy becomes E_2. If $E_2 \leq E_1$ the system is always allowed to move to the second state, but if $E_2 > E_1$ the system is allowed to move to new state with probability P as

$$P = \exp\left(\frac{-\left(E_2 - E_1\right)}{T}\right) \tag{3.5}$$

where T refers to a parameter like physical temperature and is called the annealing schedule. This statement is known as Metropolis criterion (Metropolis et al., 1953). Ingber (1995) used an annealing schedule as

$$T_k = T_0 \exp\left(-ck^{\frac{1}{D}}\right) \tag{3.6}$$

where T_k is the annealing schedule, T_0 is a large-enough starting temperature, k is the time index of annealing, D is the parameter space dimension, and c is a constant for tuning the algorithm for various problems. The method performs a random walk over the parameter space and evaluates the misfit values randomly in order to achieve the stable state at the global minimum of the misfit function. Since there is always a probability of P that the sampler can move to a state with higher energy, as equation (3.5) shows, there are few chances of getting trapped in a local minimum of misfit functional, provided that the annealing rate is slow enough. One of the disadvantages could be excessive computation time in case of a model parameter space with large dimensions. However, in the sparse spikes reflectivity inversion the number of spikes to be extracted for each trace are small enough and the inversion is performed on the post-stack data, therefore, the computation time is negligible. In the following section, the inversion algorithm will be described in details.

3.5 Algorithm of Post-stack Sparse Spikes Inversion

The goal of sparse spikes reflectivity inversion is to extract the least number of spikes which their convolution with known seismic wavelet produces a synthetic trace which fits the input data within a tolerance. For this purpose, spikes are to be located one by one in the following way. Adaptive simulated annealing searches for the first spike whose tentative amplitude equals to the maximum absolute amplitude of the input trace, but has an unknown time lag. When ASA selects a trial random value for the time lag, the spike is convolved with a known seismic wavelet. The convolved trace is then subtracted from

the recorded seismic trace to produce a residual trace. The energy of the residual forms the misfit value for the optimization, as equation (3.4) shows. Several random estimations of misfit are performed by ASA to reach the global minimum of the misfit function. Once the best arrival time is detected by ASA, this spike with tentative amplitude but exact time lag is saved in the developing reflectivity series. The convolution of the seismic wavelet with this reflectivity series gives a synthetic seismic trace which is subtracted from the original recorded trace to produce a new input dataset to search for the next spike. This procedure continues locating the spikes one by one, until the energy of the residual reaches a predefined minimum criterion, e.g. the background noise energy, and the search scheme stops automatically. After achieving the best collection of time lags, the amplitudes of all spikes are calculated and finalized by using linear least squares fitting to the original recorded trace.

Figure 3.1 shows a flowchart of the algorithm that can be used to develop reflectivity series. Here I use the energy ratio of input signal to residual trace to automatically control the random search procedure. Therefore, there is no need to make any prior assumption about the number of spikes. The resulted reflectivity series can be compared with the output of spiking deconvolution algorithms. However, conventional spiking deconvolution operators are identical to a mathematical inverse of the seismic wavelet, and in those methods the wavelet must be minimum-phase in order to design stable operators. In the reflectivity inversion, the reflectivity series is constructed without computing any operator and the result is not sensitive to the phase of the seismic wavelet.

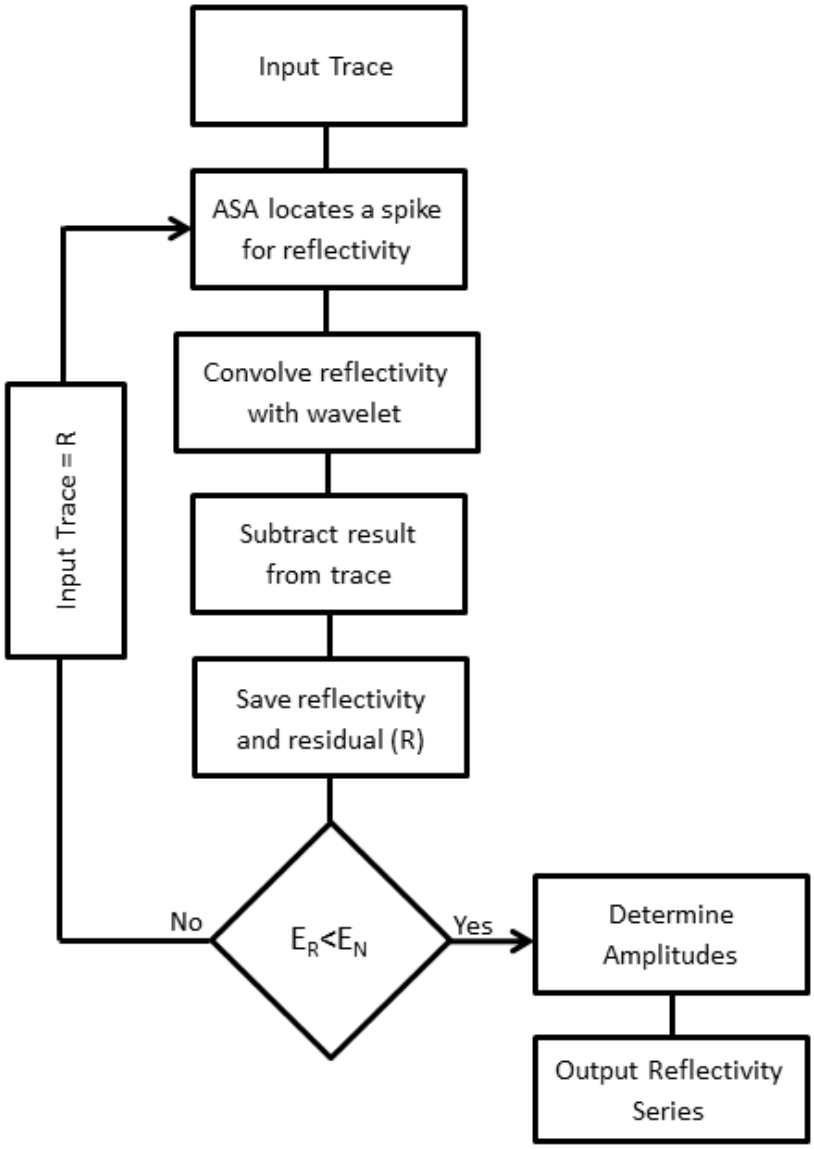

Figure 3.1 Algorithm of post-stack sparse spikes reflectivity inversion

3.6 Synthetic Examples

Different synthetic examples are used to validate the reflectivity inversion method. In this section, I will show the result of synthetic tests for minimum-phase and zero-phase wavelets, a single trace and a stacked section created using convolutional model, and a more complex example of Marmousi2 migrated section created using finite difference modeling and pre-stack time migration (PSTM).

3.6.1 Reflectivity Inversion on Minimum-phase and Zero-phase Wavelets

First, in the simplest case, I will show the results for estimating reflectivity series when the input trace is just a seismic wavelet. **Figure 3.2** shows two different types of input wavelets, i.e. Berlage wavelet (Aldridge, 1990) on the left side and Ricker wavelet on the right side, and the extracted spike using sparse spikes inversion method. The Berlage wavelet is minimum-phase and Ricker wavelet is zero-phase. Both wavelets have a dominant frequency of 30 Hz but are delayed by 50 and 100 time samples, respectively. As shown in the bottom panels of **Figure 3.2** both wavelets are correctly detected by the algorithm and a spike with accurate time lag and amplitude is estimated regardless of the phase characteristics of the wavelets.

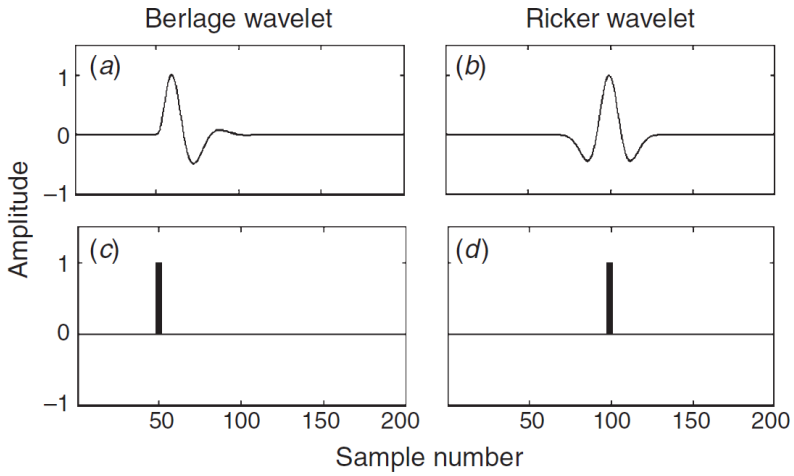

Figure 3.2 Two types of seismic wavelets and the resulting spikes from reflectivity inversion. Minimum-phase Berlage wavelet (a), Zero-phase Ricker wavelet (b), spike resulting from reflectivity inversion on Berlage wavelet (c), and Ricker wavelet (d).

3.6.2 Reflectivity Inversion on a Single Noisy Trace

A series of 12 spikes with random amplitude and arrival times have been used to generate a synthetic trace by convolving with a Ricker wavelet (with dominant frequency of 30Hz) to create an input trace for the reflectivity inversion. A normally distributed random noise with mean zero and standard deviation of 0.02 has been added to the trace to make a noisy trace with signal to noise ratio of 10. **Figure 3.3** shows the input noisy synthetic trace, the extracted reflectivity series, the modeled trace by convolving extracted reflectivity series and wavelet, and the residual of subtracting input and modeled traces. As is obvious in **Figure 3.3**, the method not only recovers the true reflectivity, but also removes remaining random noise from the original trace. The correlation coefficient between the input data and the resulting model is 0.9583. The final residual after

subtracting the developed model from original data is mostly the added noise, so this method can remove noise from the data as a by-product.

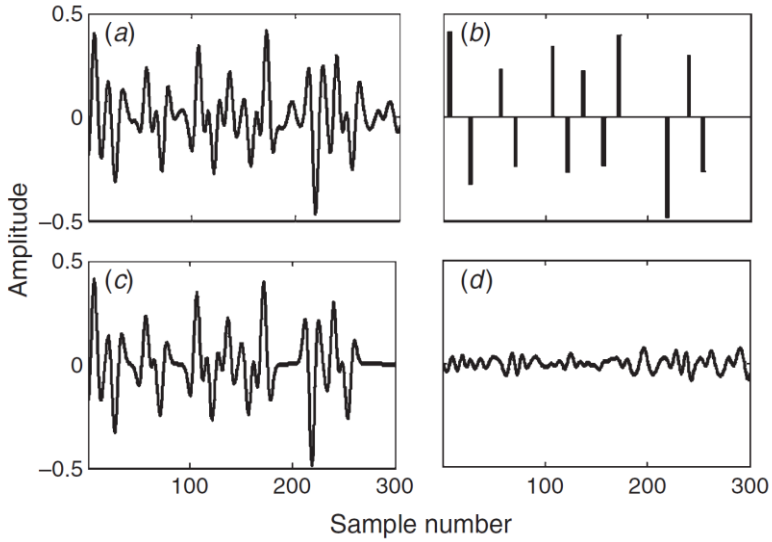

Figure 3.3 Input noisy trace (a), extracted reflectivity series (b), modeled trace by convolving known wavelet and resulting reflectivity (c), and the residual of subtracting modeled and input traces (d) which is almost the remaining random noise.

3.6.3 Reflectivity Inversion on a Stack Section

A portion of a stack section, generated using convolutional model, has been used as input to the reflectivity inversion algorithm. Again, random noise component has been added to the data to make the signal to noise ratio of 10. As **Figure 3.4** shows, the sedimentary layers could be modeled correctly and an accurate reflectivity section is extracted using the trace by trace algorithm. The correlation coefficient between input and modeled sections shows the reliability of the resulting reflectivity section. Although it is quite

difficult to distinguish between different reflection events of the input section, the high resolution reflectivity section clearly shows 12 distinct reflecting horizons.

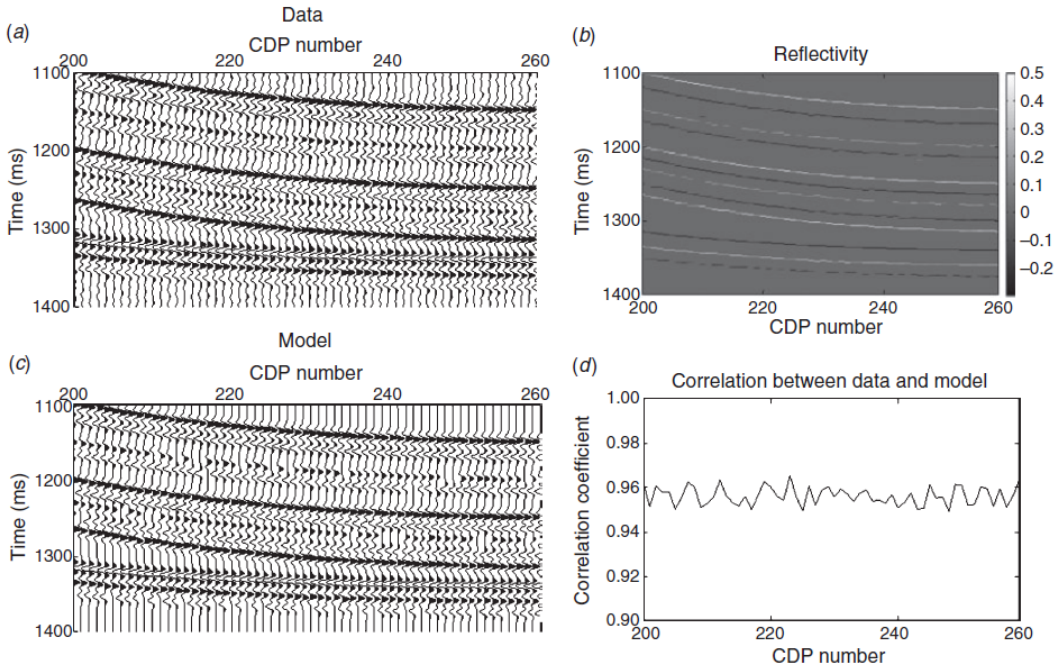

Figure 3.4 Input stacked section (a), extracted reflectivity section (b), modeled seismic section by convolving known wavelet and resulting reflectivity (c), and the correlation coefficient between input and modeled sections (d).

3.6.4 Reflectivity Inversion on Marmousi2 Time Migrated Section

The input seismic traces in all examples shown above have been generated based on convolutional model, i.e. by convolving a reflectivity series with seismic wavelet. This method of synthetic trace generation is valid under zero-offset assumption. However, in

order to check the validity of the method on a more complex and realistic dataset, it is necessary to generate the synthetic data using wave propagation techniques and develop the seismic section by data processing flows. Here I use the time domain shot gathers generated by finite difference modeling on Marmousi2 model, as in chapter II, to produce a pre-stack time migrated section using conventional data processing methods, including band-pass filtering, amplitude correction, velocity analysis, and migration. PML boundary condition has been applied on top of the modeling area to mitigate the multiple reflections from surface boundary. A number of 450 shot gathers have been simulated by 2D frequency domain finite difference wave propagation modeling and time domain gathers are generated using an inverse Fourier transform. Seismic sources are placed at a spatial distance of 30m and receivers are located on the surface at every 15m. The original shot gathers are exactly same as the ones used for frequency domain full waveform inversion in chapter II, because I will use the reflectivity inversion results later in chapter IV to build the initial model for FWI. **Figure 3.5** shows the pre-stack time migration (PSTM) section resulting from processing 450 shot gathers. The vertical dashed lines show the well locations in the survey area, which will be used in next chapter for horizon-guided well interpolation and FWI initial velocity model building. **Figure 3.6** shows the extracted reflectivity section resulting from sparse spikes inversion on the PSTM section. The high resolution reflectivity section clearly separates different horizons and makes it much easier to interpret the subsurface structures.

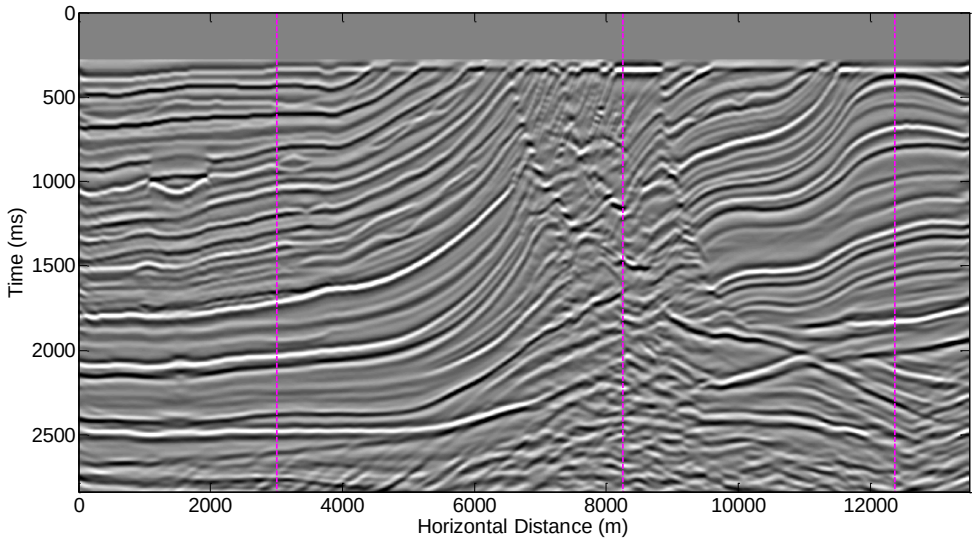

Figure 3.5 Pre-stack time migrated section of Marmousi2 dataset.

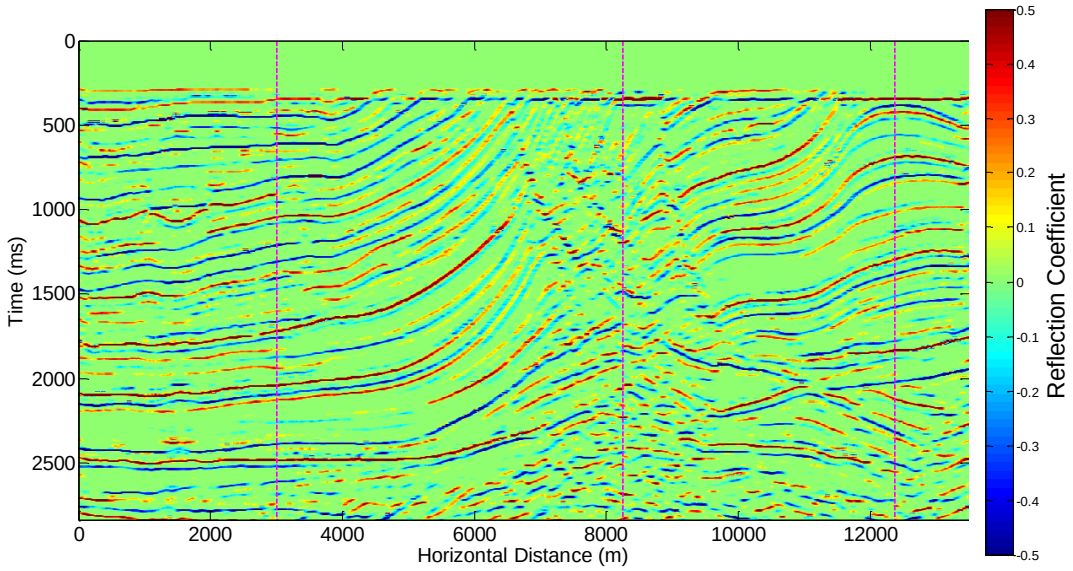

Figure 3.6 High resolution reflectivity section resulting from sparse spikes inversion on Marmousi2 PSTM section.

3.7 Real Data Example

To evaluate the results of sparse spikes reflectivity inversion on real data, a time window of post-stack seismic section has been selected and processed. **Figure 3.7** displays the input section of real data, the resulting reflectivity, the reconstructed seismic section, and the correlation coefficient between input and modeled data. As these results show, the method can handle real seismic sections with acceptable accuracy. ASA has located the spikes very well and their amplitudes have been calculated with acceptable accuracy. High correlation values between the input seismic section and the resulting model show that the modeled section based on the resulting reflectivity series fits the original data and the uncertainty of the solution is slight.

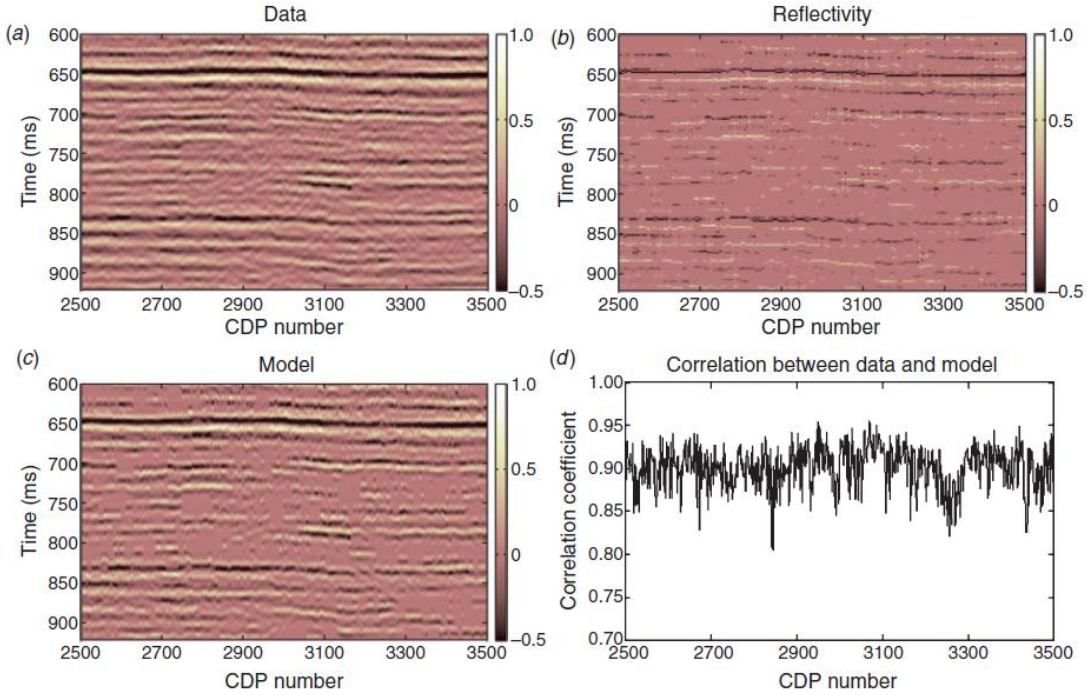

Figure 3.7 Input stacked section of field data (a), extracted reflectivity section (b), modeled seismic section by convolving known wavelet and resulting reflectivity (c), and the correlation coefficient between input and modeled sections (d).

3.8 Reflectivity Inversion vs. Minimum Entropy Deconvolution

Minimum Entropy Deconvolution (MED) was developed by Wiggins (1978) to enhance the resolution in seismic data when high amplitude reflections appear in the trace (e.g., bright spots). MED does not rely on assumptions about the phase of the wavelet or the reflectivity series spectrum. Moreover it tries to find the minimum number of spikes needed to represent the reflectivity just by using the recorded seismic trace. The details of the minimum entropy deconvolution process can be found in Wiggins (1978), Cabrelli (1984), and Sacchi et al. (1994). This method aims to maximize a norm V known as Varimax, which can represent some measure of simplicity in the data. The word Varimax comes from maximizing the normalized variance and can be represented in mathematical form as below

$$V = \sum_i \mathbf{V}_i \quad \text{and} \quad \mathbf{V}_i = \sum_i \frac{\mathbf{Y}_{ij}^4}{\left(\sum_j \mathbf{Y}_{ij}^2\right)} \tag{3.7}$$

where $\mathbf{Y}_{ij}$ is a matrix containing seismic traces filtered by the MED filter,

$$\mathbf{Y}_{ij} = \sum_{k=1}^{N_f} \mathbf{f}_k \mathbf{x}_{i,j-k} \tag{3.8}$$

where **x** and **f** are seismic trace and the MED filter operator, respectively. In order to calculate the MED filter, one can differentiate V with respect to the filter coefficients to maximize the Varimax (Wiggins, 1978). Here I make a simple comparison between the ASA sparse spikes inversion method and the MED method. Since these methods have much in common this comparison makes sense. Both methods make no restrictive assumption over the seismic wavelet or the reflectivity series. Also they try to extract reflectivity series by optimizing a norm of the data. ASA minimizes the l_2 norm of the difference between modeled and observed data to locate spikes, on the other hand, MED tries to maximize the Varimax. Furthermore, they represent models for the reflectivity of the earth that contain the least number of spikes that can reproduce the seismic trace. By using the MED method one tries to compress the wavelet to a spike. However, since the Varimax is unaffected by the spacing or polarity of the spikes (Wiggins, 1978) the MED method requires specific parameterization to locate the time lags of spikes. Also, the coefficients of the MED filter must be scaled accurately to achieve meaningful amplitudes. **Figure 3.8** shows a synthetic trace which has been processed by ASA and MED to extract reflectivity series. In MED some undesired spikes with small amplitude appear in output. Furthermore, the results of the MED process are highly dependent on the filter length. It is obvious in **Figure 3.8** that inappropriate filter length can lead to unrealistic series of spikes that weaken the accuracy. On the other hand, ASA detects the time locations of the spikes successfully, and there is no artificial spike in the resulting reflectivity series. Amplitudes are also well estimated and represent the true reflection coefficients that had been used in the original synthetic trace. Therefore, the results from

ASA reflectivity modelling are more accurate, and this method performs better than MED algorithms.

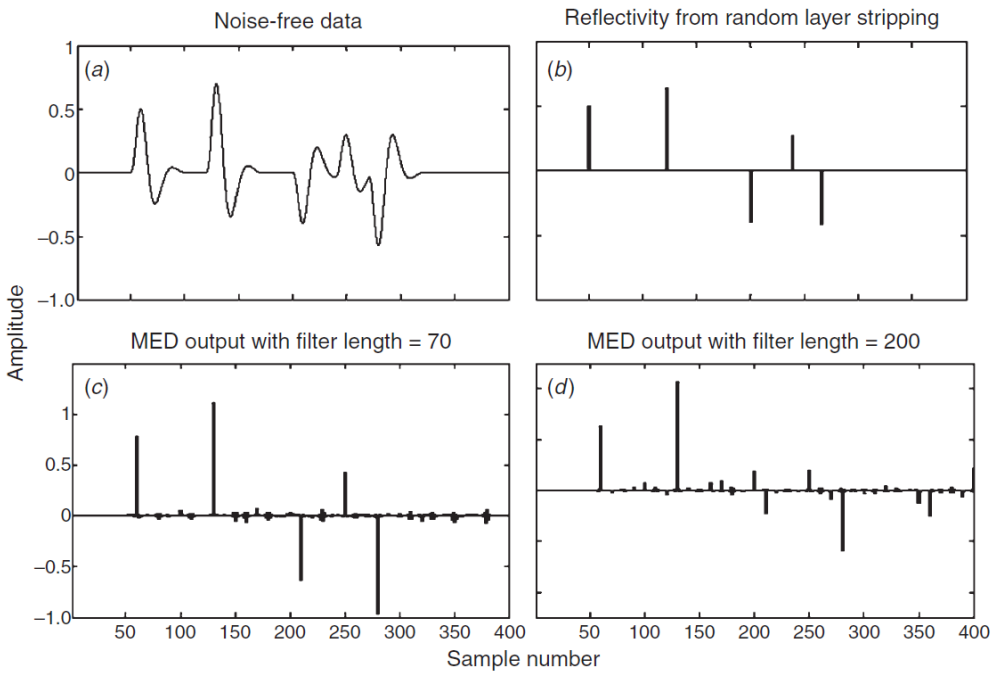

Figure 3.8 Noise-free input trace (a), reflectivity series resulting from sparse spikes inversion (b), reflectivity series resulting from MED with filter length of 70 (c), reflectivity series resulting from MED with filter length of 200 (d)

3.9 Discussion

Since reflectivity series of the seismic data can represent a quantitative measure of the subsurface structures, in terms of reflections coefficients, it is possible to estimate the acoustic impedance values from reflectivity section. The main objective of extracting reflectivity at this stage is to prepare geological constraints for a constrained acoustic impedance inversion which finally builds an initial velocity model for FWI in the next chapter. As **Figure 3.6** shows, the high resolution reflectivity section can be effectively used for the detailed interpretation of the subsurface structures. However, since FWI only requires the low spatial frequency components in the initial model, an interpretation of the major geological horizons will suffice and the fine structures will be developed using the high resolution FWI velocity models. This will be discussed in details in the next chapter.

The reflectivity sections developed here are based on the convolutional model with a stationary seismic wavelet which is known. As the real data example in **Figure 3.7** shows, this simplified assumption works well even for the field data. However, if the source wavelet is not stationary, i.e. varying from shot to shot and/or at different times at the seismic section, this varying behaviour of the source wavelet must be taken into the account. One solution to this problem is to justify the wavelet for the separate windows in the seismic section prior to reflectivity inversion. Also a reliable wavelet estimation method should be used to correct for the wavelet variations of the different seismic sources.

3.10 Chapter Conclusions

A least squares inverse problem has been defined based on the convolutional model to extract the reflectivity series from post-stack brownfield seismic. The goal of the sparse spikes reflectivity inversion is to find the least number of spikes which when convolved with known seismic wavelet produce a synthetic trace which matches the input data

within a tolerance. Adaptive simulated annealing could be effectively used to solve the inverse problem and build a high resolution reflectivity section from seismic traces. Different synthetic and real datasets confirmed validity of the method and a comparison with minimum entropy deconvolution showed that the reflectivity inversion provides a stable solution to the stochastic spiking deconvolution. The accurate information on reflection coefficients of the seismic waves and the arrival times of on the seismic time section show that the subsurface features are reconstructed using the convolutional model. The resulting reflectivity section from Marmousi2 model will be used in the next chapter as an accurate source of geological constraints to build an initial model for full waveform inversion. The accurate picking of horizons would strengthen lateral redundancy and help to develop the low frequency part of the model using these geological constraints.

CHAPTER IV: FWI INITIAL MODEL BUILDING USING SEISMIC DATA PROCESSING RESULTS

4.1 Introduction

Full waveform inversion is essentially a data fitting problem which is solved using local optimization methods. Since the problem is highly nonlinear with a large number of model parameters to be estimated, the misfit functional involves too many local minima. In other words, there are a large number of models which could falsely fit to the data, but there is only one exact solution which resides at the global minimum of the misfit function. Local optimization algorithms require an initial model in the vicinity of the true model in order to achieve a correct solution of the problem without getting trapped in any local minima. In fact, the initial model should be able to create modeled waveforms which are kinematically less than half a period away from recorded data. The background low wavenumber component of the model which satisfies this requirement could be built in the early stages of frequency domain multi-scale FWI, only if low enough frequencies exist in the observed data.

The problem is that the observed seismic data has a limited bandwidth and because of the restrictions in the data acquisition technologies the low frequency components are not practically observed. Therefore, it is not realistic to start FWI from frequencies lower than recording limits (≈5 Hz). Despite this fact, all the reported FWI applications using simultaneous sources consider the seismic data to have very low frequency content, an assumption which easily breaks in the real world. If one fails to provide the low wavenumber components in the initial model for FWI using band-limited data, the gradient updates will go to the wrong direction and cycle skipping will happen.

Tarantola (1986) suggests that the background initial model could be built from seismic data itself even when the low frequencies are not available. Traveltime tomography has been widely used as a method to build the initial velocity model for full waveform inversion (Kamei et al., 2012; Brenders and Pratt, 2007). Full waveform inversion in Laplace domain (Shin and Cha, 2008; Koo et al., 2011) and Laplace-Fourier domain (Shin and Cha, 2009) have been introduced as new methods to mitigate the sensitivity of the FWI problem to initial model by developing the long wavelength component of the background model in the early stages of FWI. Cooke and Schneider (1983) used geological constraints extracted from well logs to improve acoustic impedance inversion by importing low frequency component of the model from well data. Ferguson and Margrave (1996) used well logs to improve the impedance section from recursive inversion and could achieve reliable results.

I will propose two new methods for building FWI initial velocity models using seismic data processing products in the brownfield cases. First, I suggest a method to extract the low wavenumber component of the acoustic impedance from well logs and interpolate it along horizons interpreted using reflectivity section from previous chapter. The reflectivity section calculated using sparse spikes inversion is used for a horizon guided well interpolation and constrained acoustic impedance inversion. The role of reflectivity is to bridge between geological information from the well logs and seismic data from migrated section to provide the low wavenumber component of the model. A density model, which could be estimated from well interpolation or empirical relations (Gardner et al., 1974), converts the results of the constrained acoustic impedance inversion to P wave velocity, to be used as starting model for FWI.

I will also suggest a second solution to the initial model building problem for the case that no well data is provided. I will show that the seismic data itself is capable of providing low wavenumber components of the model through conventional data processing sequence. As Claerbout (1985) stated, the stacking velocities resulting from *apparent* velocity analysis can provide a very low spatial frequency component of the model (see **Figure 1.3**) and there is an information gap between the low and high frequency parts of the model. The main reason for this gap could be related to the complexities in the subsurface model which restricts the reliability of the stacking velocities. If the dip complexities could be handled properly, then velocity models from seismic data processing should be able to make a reliable background velocity model.

Wave equation migration velocity analysis (WEMVA) and differential semblance optimization (DSO) are among the initial velocity model building methods for FWI, however, these methods are relatively expensive due to the several rounds of pre-stack migration needed. Moreover these applications are only provided in a few number of industrial software and the application remains limited to those packages. Alternatively, I will show that dip move-out (DMO) correction is capable of relaxing the dip complexities in a much cheaper way. Acting as a *partial pre-stack migration*, DMO correction is able to solve the subsurface complexities related to steep dips and a velocity analysis after DMO correction can build the low wavenumber component of the model for FWI initialization. Examples from Marmousi2 model will demonstrate the reliability of the proposed new initial models for band-limited full waveform inversion using random phase encoded simultaneous sources.

4.2 The Importance of Initial Model

Multi-scale full waveform inversion in frequency domain can clearly illustrate the importance of initial model for a successful application of FWI. While starting from low frequencies, the long wavelength background model is built automatically in the early stages of FWI. **Figure 4.1** shows evolution of the velocity model through frequency domain multi-scale full waveform inversion. Six frequency groups, each including 3 individual frequencies same as in **Table 2.1**, are used for acoustic FWI. The group numbers on top of each panel indicate the frequencies which have been used for frequency domain FWI to achieve the velocity model shown in each panel. Starting from 2 Hz with a smooth version of true model, the result of FWI using each frequency group is used as initial model for the next group. As **Figure 4.1** shows, the lower frequencies build a low resolution background velocity model and pass it to higher frequencies to add more details into the model. If the lower frequencies are absent, a fact in real field data, the initial model should bear the missing part of the model.

It is clear that how important the low frequencies are to update the model. For example, if the frequencies lower than 4.3Hz are not available in the recorded data, one needs to have an initial model as accurate as panel **c** in **Figure 4.1** to obtain the same final result as panel **h**. This will assure proper fitting between observed data and simulated waveforms and prevents cycle skipping. If any additional source of data were available to build the low wavenumber component of the model, it should be used to start FWI from a reasonable frequency in accordance with the observed data from field. Since well logs are accurate sources of full-band data, the low frequency component of the model could be extracted from well data to solve the cycle skipping issue.

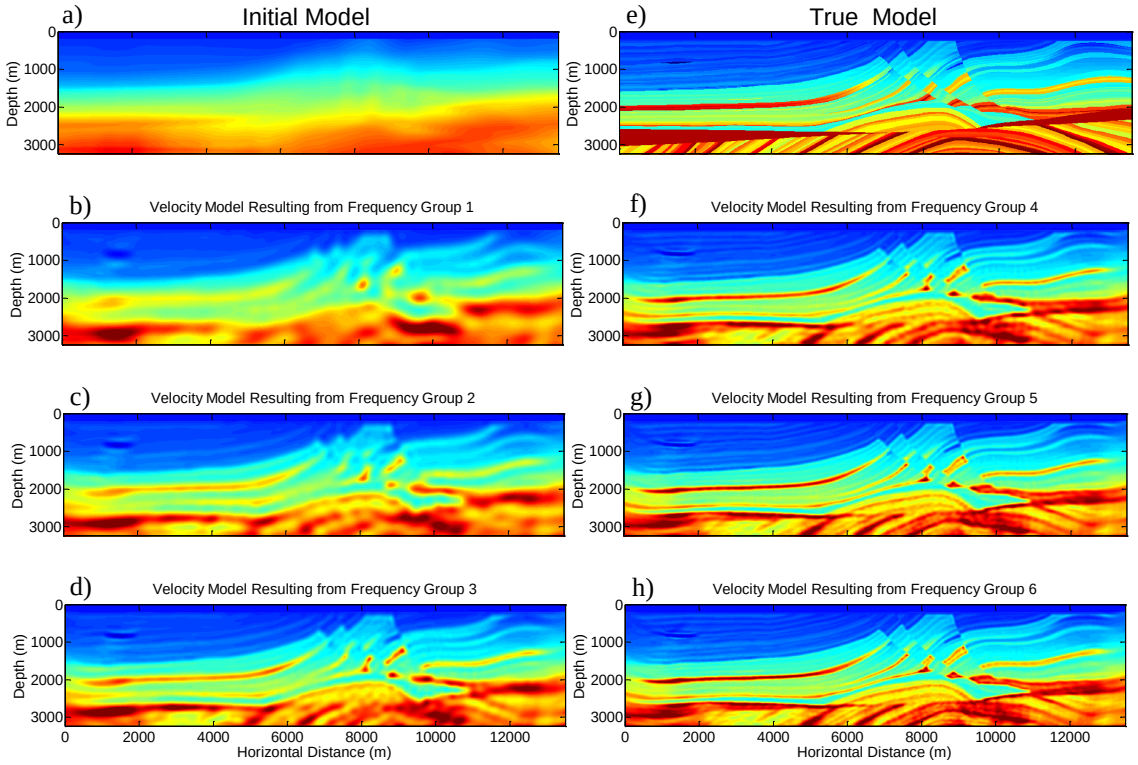

Figure 4.1 Multi-scale frequency domain FWI illustrates the importance of low frequencies and initial model. Starting model, true model, and FWI models resulting from each frequency group are shown.

4.3 Horizon-guided Initial Model Building Using Reflectivity Model and Well Log Data

In this section I shall describe the method for constructing a reliable initial velocity model for full waveform inversion by using the reflectivity section. The reflectivity section is used in two stages of initial model building. First, it is used as a high resolution reference of horizons to guide an interpolation of well log data. Later, it will be used again to perform constrained acoustic impedance inversion, which finally results in a velocity model by having a known density. Ferguson and Margrave (1996) introduced an algorithm for using well logs to improve seismic band-limited impedance inversion results by incorporating the low frequency part from well logs. Their algorithm, shown in **Figure 4.2** with some modifications for this thesis, could successfully compensate the limited frequency content of the seismic data. The acoustic impedance values are obtained from well logs and converted from depth to time, then tied to the seismic section. The linear trend of the impedance is removed for the convenience in the following frequency domain conversions. Fourier transform of the de-trended acoustic impedance provides the wide-band spectrum from well logs. On the other hand, sparse spikes reflectivity section is converted to acoustic impedance using a simple recursive inversion. The resulting impedance is converted to frequency domain by Fourier transform. Then a scalar is calculated to match the power spectrum of frequency domain impedance from well logs and reflectivity. This scalar is multiplied to impedance spectrum resulted from reflectivity. Then the low-pass filtered impedance spectrum from well logs is added to it. Finally the enhanced spectrum is converted to time domain using inverse Fourier transform and the linear trend is added to obtain the final result.

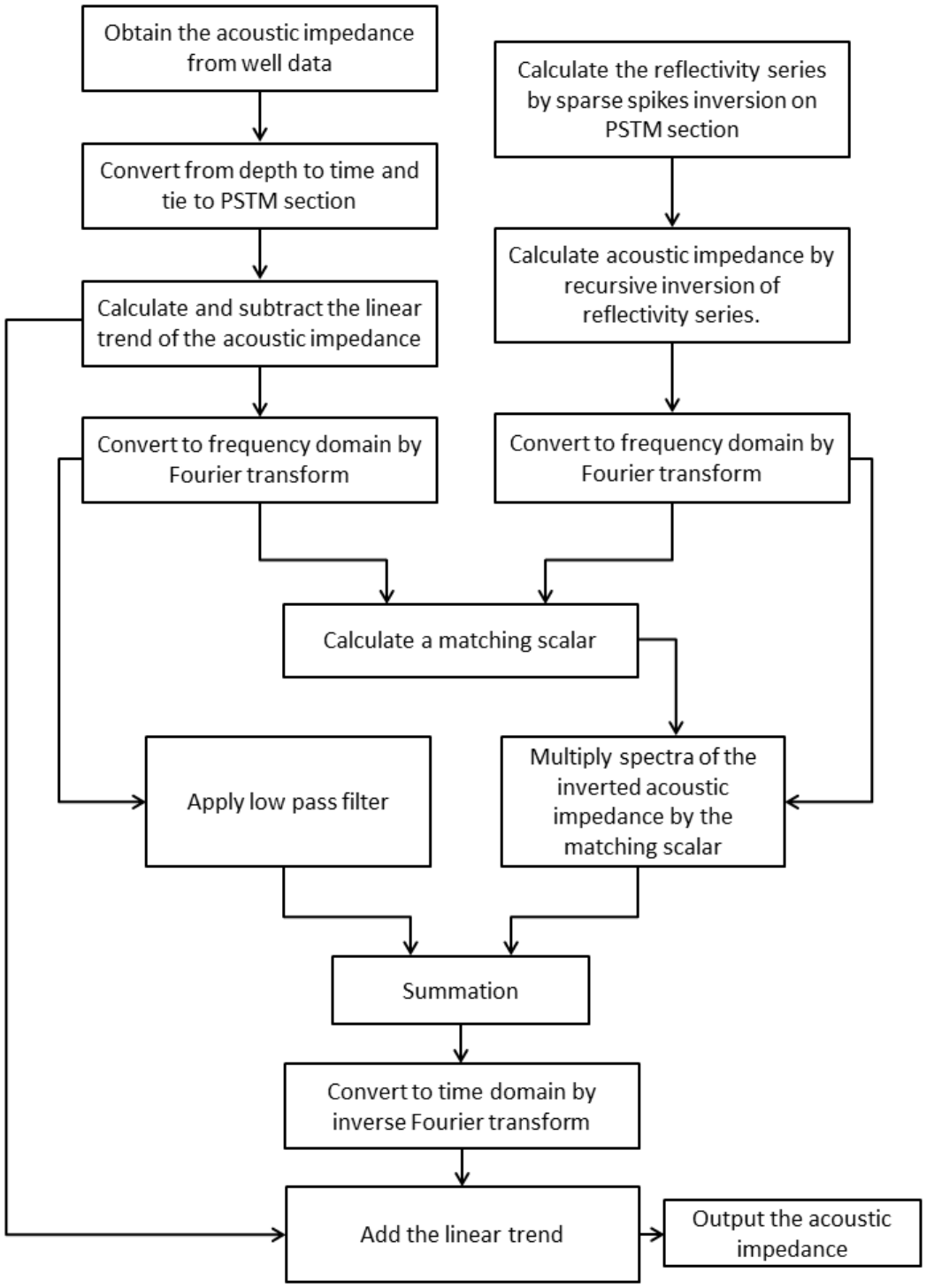

Figure 4.2 Flowchart of constrained acoustic impedance inversion using reflectivity series and well logs.

The difference between algorithm introduced here and the algorithm used by Ferguson and Margrave (1996) is that they estimated acoustic impedance values by integrating seismic traces and taking the exponential of integration result. Here I estimate the acoustic impedance values from reflectivity section by using a simple recursive inversion. Since the algorithm needs to be applied in a trace by trace order, it is necessary to have a good reference impedance from well logs. However, well log are only provided at three well locations in the survey area, as illustrated by vertical dashed lines on PSTM section in **Figure 4.3**. In order to obtain a reliable estimation of the acoustic impedances from well logs, I use the horizons from high resolution reflectivity section to interpolate the well logs along the horizons. The horizon-guided well interpolation expands the well data over the whole survey area, and then the algorithm of **Figure 4.2** could be used to add the low frequency part of the expanded model into acoustic impedances from reflectivity inversion. Finally a density model is used to convert the acoustic impedance to P wave velocity. The examples in this thesis use a constant density model, as mentioned in chapter II, for synthetic data generation and inversion. However, density model could be extracted from well logs and interpolated using the same horizon-guided interpolation method, or could be estimated using empirical relations (Gardner et al., 1974).

Figure 4.3 shows the pre-stack time migrated (PSTM) section of Marmousi2 dataset which has been produced using conventional data processing sequences. This section was used in the last chapter to extract the reflectivity section shown in **Figure 4.4**. Now I will use the extracted reflectivity section to estimate P wave velocities by using well interpolation and constrained impedance inversion, as described above. First, I shall display the resulting velocities at well locations, which use the exact well logs from three wells in the survey to constrain the acoustic impedance inversion and estimate P wave velocity. **Figure 4.5** shows the estimated velocities using the algorithm of band-limited impedance inversion for the exact well logs at three well locations. The inverted velocities are in good accordance with the original velocities from well logs. **Figure 4.6** shows the estimated velocity model using horizon guided interpolation and band-limited acoustic impedance inversion. It should be noted that a constant density model has been used here. This velocity model is converted from time to depth, in order to build the initial model for full waveform inversion (**Figure 4.7**).

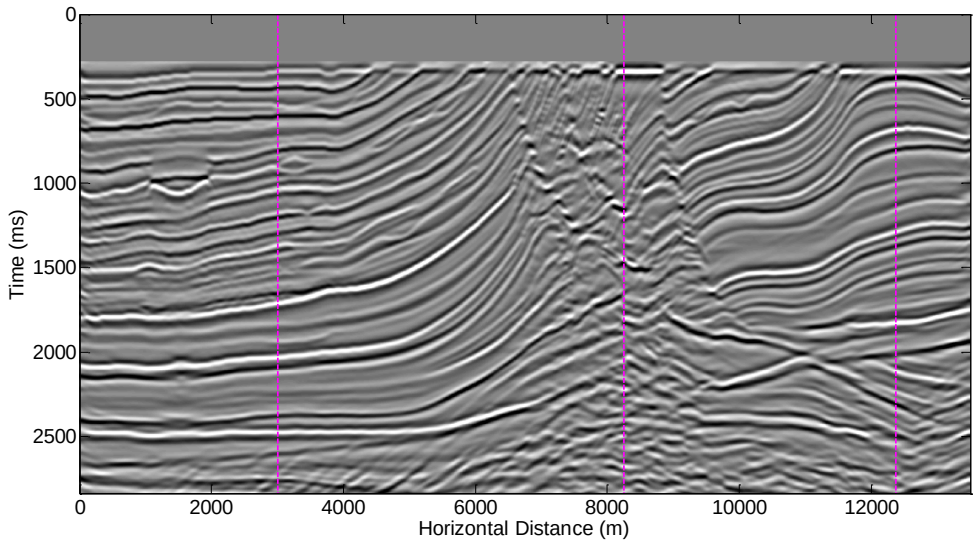

Figure 4.3 Pre-stack time migration (PSTM) section of Marmousi2 dataset. Vertical dashed lines show three well locations in the survey.

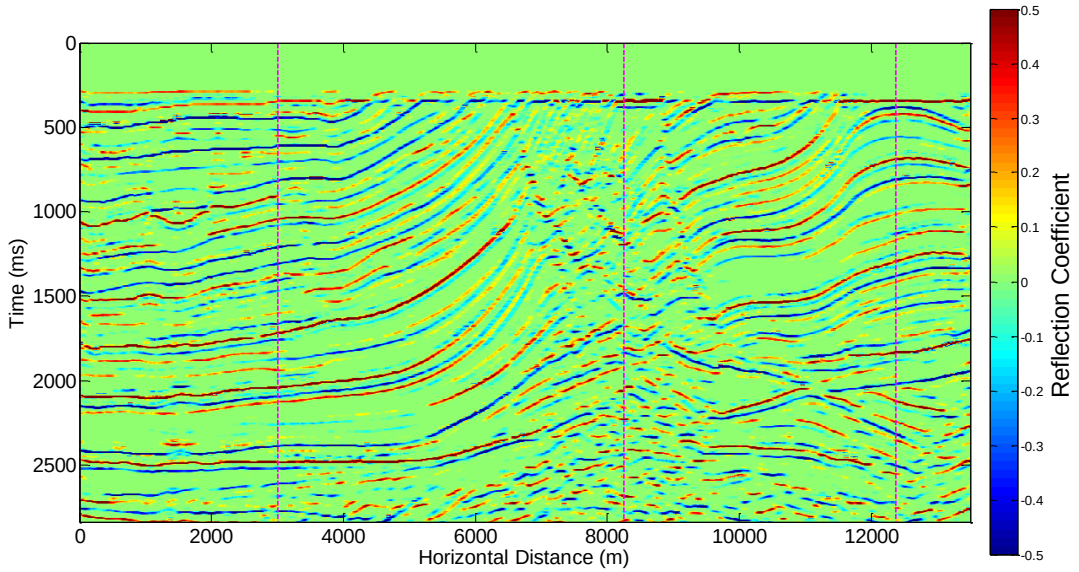

Figure 4.4 Reflectivity inversion resulted from sparse spikes inversion which will be used for horizon-guided well interpolation and acoustic impedance inversion.

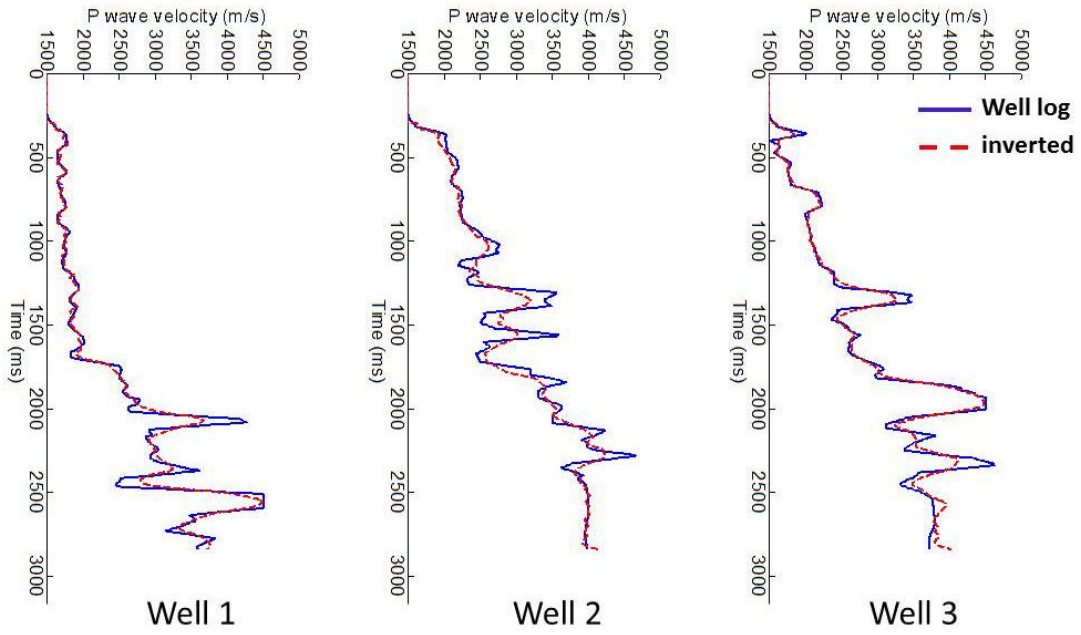

Figure 4.5 Estimated P wave velocities using band-limited impedance inversion algorithm at three well locations. Blue line shows the P wave velocity from well logs and dashed red line shows the post-stack inversion result with a constant density model.

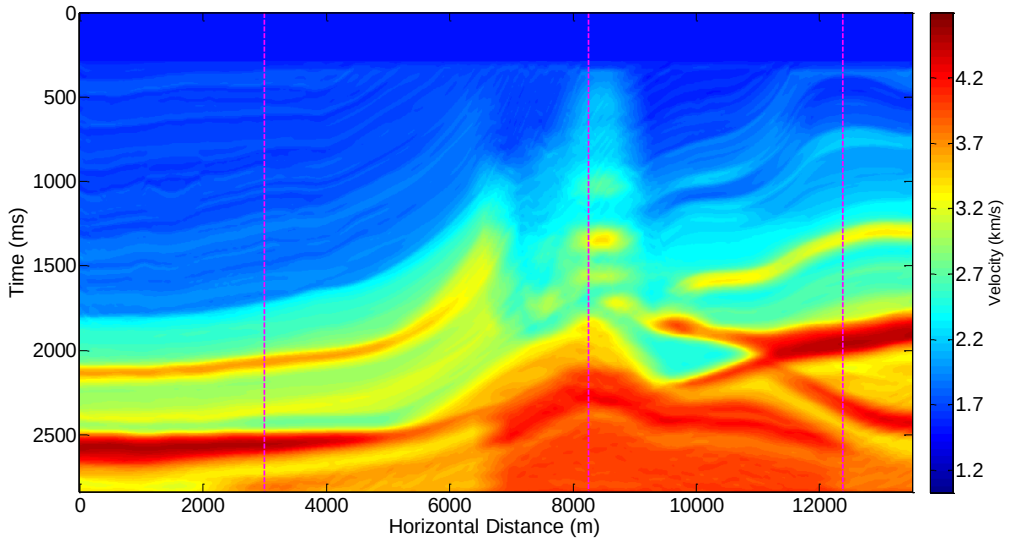

Figure 4.6 Estimated P wave velocity model using horizon-guided well interpolation and band-limited impedance inversion by the algorithm of constrained acoustic impedance inversion.

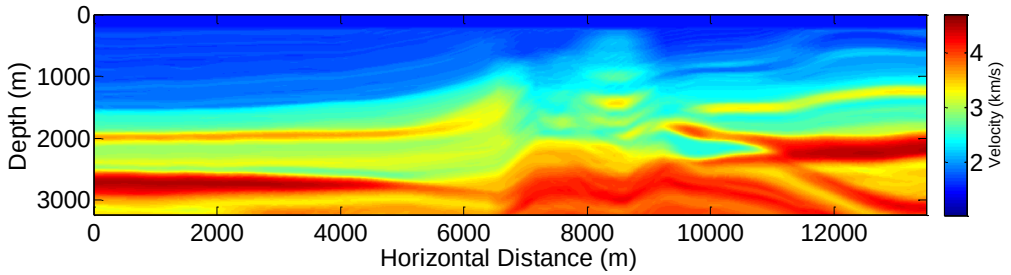

Figure 4.7 Horizon guided initial velocity model for FWI, built by depth conversion of velocity model shown in **Figure 4.6**.

4.4 FWI Results Using New Horizon-guided Initial Model

The importance of initial model for a successful application of full waveform inversion has been illustrated. Since the low frequency content of seismic data is usually missed during data acquisition, the new initial model which has been developed using horizon-guided well interpolation and acoustic impedance inversion must be evaluated for full waveform inversion using band-limited seismic data. In order to do this, two frequency sets are defined as **Table 4.1** shows. The first frequency set is the same as frequencies which had been used in chapter II for validating full waveform inversion code using random phase encoded simultaneous sources. The lowest frequency in this set is 2 Hz and frequencies are selected by the strategy suggested by Sirgue and Pratt (2004). Since this frequency set includes low enough frequencies I shall call it wide-band frequency set. The second frequency set which is shown in **Table 4.1** misses the first five frequencies and starts from 5.33 Hz. This frequency set is more realistic to be observed in the field datasets. I shall call this frequency set narrow-band set, due to the absence of low frequency components. Both frequency sets are arranged in 6 frequency groups and 30 iteration of FWI will be applied on each frequency group. I will use these two frequency sets in this chapter in order to evaluate the new initial velocity models.

Results of full waveform inversion using new horizon-guided initial model are shown in **Figure 4.8**. It should be noted that all the full waveform inversion examples in this chapter are performed using 225 individual shot gathers, at every 60 m, assembled in 25 supershot gathers of 9 simultaneous sources with close configuration (CC), to increase the efficiency of full waveform inversion by random phase encoded simultaneous sources. Panel **a** in **Figure 4.8** shows the initial velocity model which has been built

using horizon-guided interpolation and acoustic impedance inversion. Panel **b** shows the FWI results using wide-band dataset. It confirms that the FWI results are reliable by using this new initial model, when starting FWI from low frequencies. For a more realistic situation, narrow-band frequency set is used for FWI. Panel **c** shows that even when the low frequency components are absent in the seismic data, the new horizon guided initial model can recover the subsurface model with high accuracy. In fact, the low wavenumber component of the velocity model is borrowed from well logs, in the form of geological information interpolated by seismic reflectivity along the horizons. The same narrow-band frequency set is used to initialize FWI from smooth initial model which has been used in chapter II. As panel **d** shows, the narrow band FWI using smooth initial model fails to converge to the correct solution, because of the poor initial model and absence of low frequency components in the input seismic dataset, which results in cycle skipping issue. The normalized misfit values for wide-band and narrow-band FWI using the new initial are shown in **Figure 4.9**. Narrow-band FWI result by using new initial model and noisy input data with signal to noise ratio of 5 is shown in **Figure 4.10**. Even the noisy data obtains a good subsurface model which is comparable with wide-band FWI results.

Table 4.1 Two frequency sets (in Hz) for full waveform inversion

	group 1	group 2	group 3	group 4	group 5	group 6
wide-band	2.0, 2.5, 3.0	3.0, 3.5, 4.33	4.33, 5.33, 6.5	6.5, 7.83, 9.5	9.5, 11.5, 14.0	14.0, 17.16, 20.66
narrow-band	5.33, 6.5	6.5, 7.83	7.83, 9.5	9.5, 11.5	11.5, 14.0	14.0, 17.16

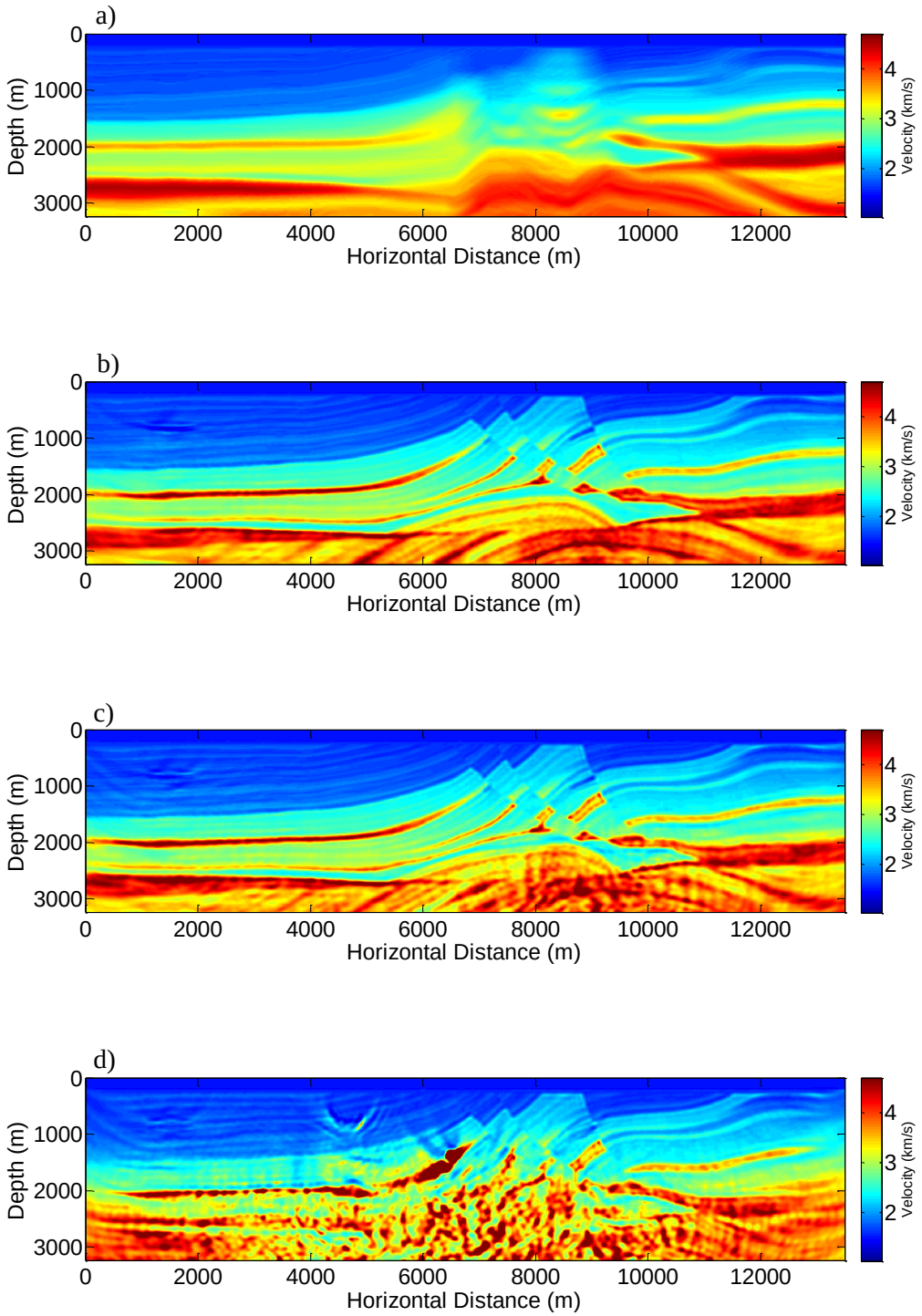

Figure 4.8 New initial model developed using horizon-guided well interpolation and acoustic impedance inversion (a), wide-band FWI (b), and narrow-band FWI (c) using this new initial model. Narrow-band FWI using the smooth initial model is shown in (d) for the comparison.

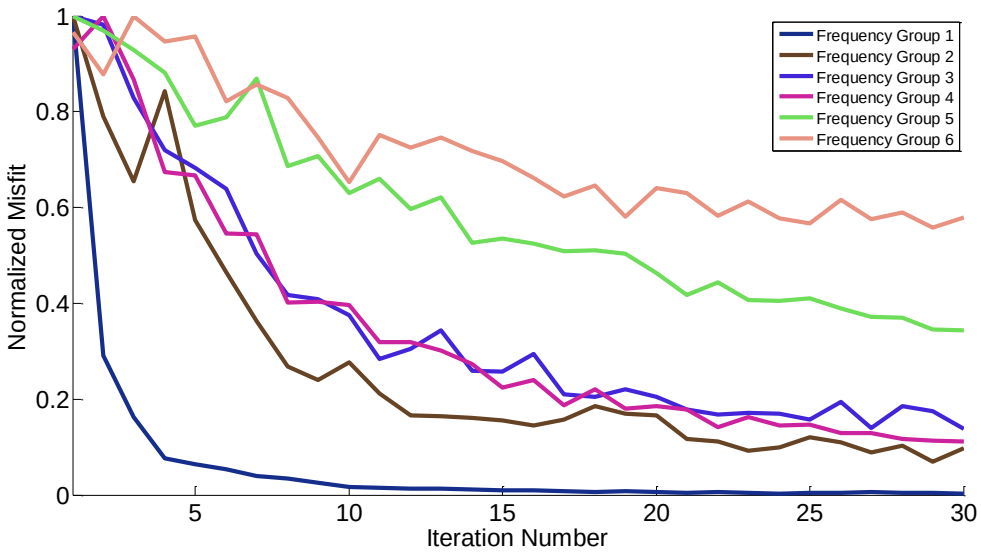

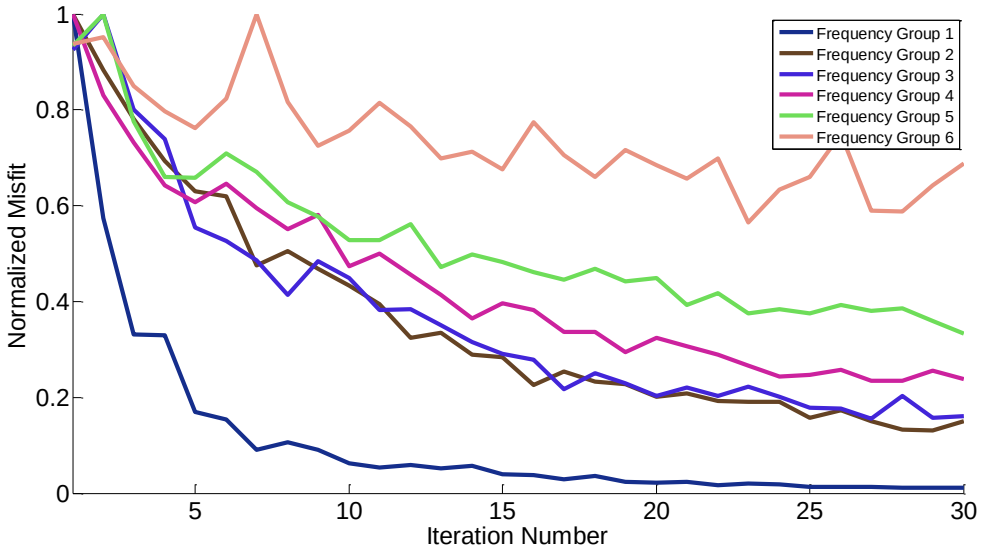

Figure 4.9 Normalized misfit values for wide-band FWI (top), and narrow-band FWI (bottom) using new horizon-guided initial model.

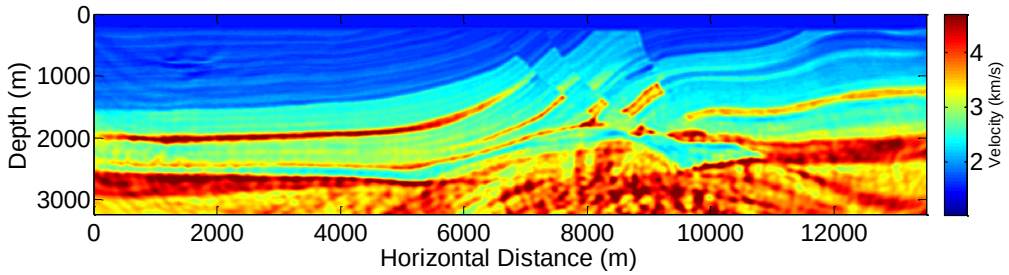

Figure 4.10 Narrow-band FWI result using new initial model and noisy input data with signal to noise ratio of 5.

Time domain sample shot gather generated using true velocity model and narrow-band FWI result using new initial model are shown in **Figure 4.11**, the time domain shot gather resulting from new initial model is also shown. As the waveforms show, the initial model is capable of producing the low frequency components which are necessary to avoid the cycle skipping problem in the waveform fitting.

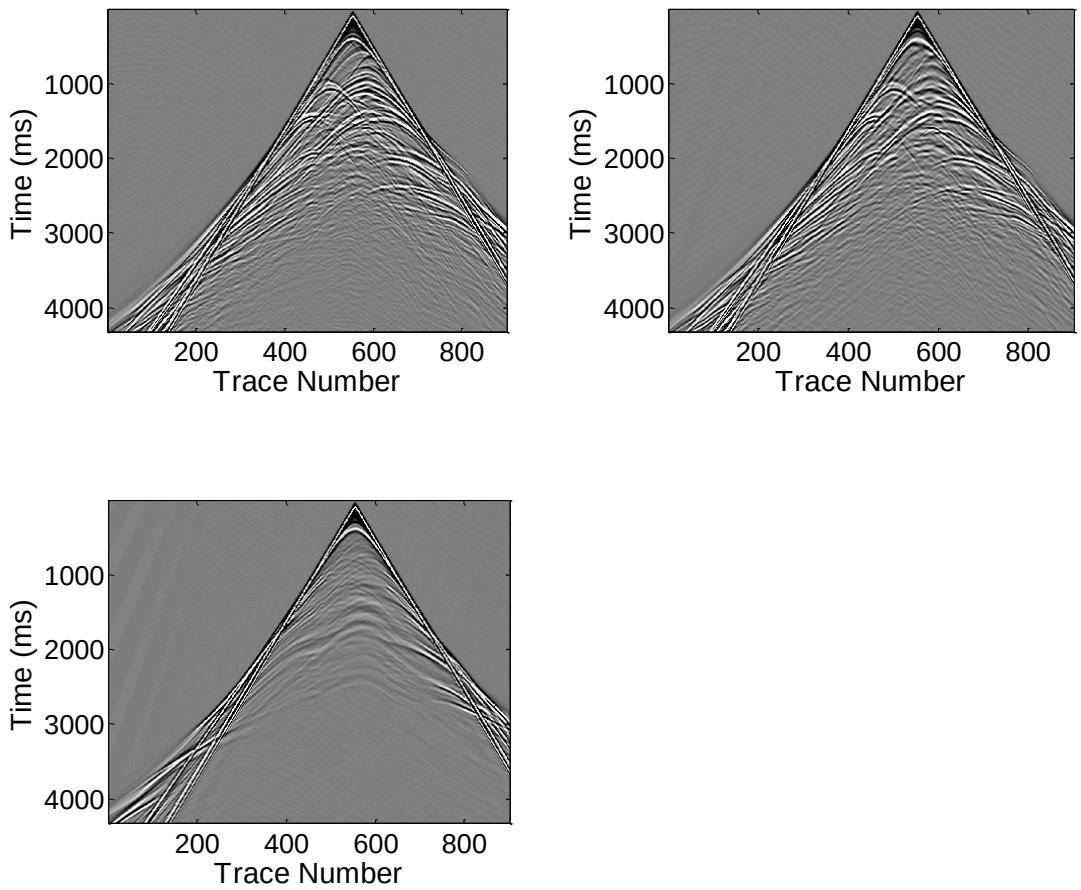

Figure 4.11 Time domain shot gathers generated using: true velocity model (top left), narrow-band FWI result using new initial model (top right), and new horizon-guided initial model (bottom).

4.5 Initial Model Building Using Dip Move-out Correction and Velocity Analysis

The initial model for full waveform inversion has been developed using horizon-guided well interpolation and acoustic impedance inversion, as I already described in details. However, it should be noted that one of the limitations of this method could be the dependency of the algorithm on well log data. It is necessary to consider a situation

where no well data appears in the survey area. In that case, alternative methods should be developed in order to build the initial model for FWI. Claerbout (1985) suggests that normal seismic data sets contain information on the long wavelengths of the model which is totally independent of the information on the short wavelengths (Tarantola, 1986). Here I propose the idea that the velocity analysis flows in seismic reflection data processing routines are capable to provide the long wavelength component of the model. RMS velocity field could be picked through stacking velocity analysis on coherence measures like semblance. The picked RMS velocities in time could be converted to interval velocities in depth to build the initial model for the full waveform inversion. However, one problem that may arise is that when subsurface structures include steeply dipping reflectors, the apparent RMS velocity which is interpreted using stacking velocity analysis is larger than true velocities with which the wavefields traveled in the earth (Levin, 1971). As a consequence, the dip effect should be handled properly in order to pick a reliable velocity. Migration velocity analysis (MVA) methods could solve this problem by combinations of several pre-stack depth migration and migration velocity update loops. However, the computational task of this method could be intensive due to several pre-stack migrations which are required. I will show that dip move-out (DMO) correction can properly handle the dips by applying a partial pre-stack migration operator with less computational cost. Since the DMO operator can correct even steeply dipping events in an efficient way, the apparent RMS velocity moves to the vicinity of the true velocity model and a velocity analysis after DMO correction will obtain the correct long wavelength component of the model which is required for FWI initial model.

4.5.1 The Effect of Dip Move-out Correction on Velocity Model

When seismic reflector is a dipping plane, the stacking velocity which is needed to flatten time CDP gathers is higher than the true velocity with which the energy traveled through the subsurface (Levin, 1971). Any process which deals with depth rather than time, e.g. pre-stack depth migration, full waveform inversion, etc. requires a velocity model close to the true velocity which energy traveled with. **Figure 4.12** shows a velocity analysis window near the horizontal location of 3000 m in the Marmousi2 model. Since the reflectors are almost horizontal in this area, the peaks of the semblance spectra fall in the neighborhood of the true RMS velocity trend. As a result, picking velocities on this trend will obtain a velocity field which is very close to the true velocity and can properly provide the long wavelength component of the model. As the figure shows, picked velocities (white line) are very close to true velocities (black line). However, this is not the case when there are significant numbers of steeply dipping layers in the subsurface structure.

Figure 4.13 shows the semblance on a CDP gather from horizontal location of 6700 m. This area includes a large number of steeply dipping reflectors which affect the apparent RMS velocity trend in the semblance panel. The left panel in **Figure 4.13** shows the semblance spectrum before applying any dip move-out correction, where the peaks of semblance spectrum are biased toward higher velocities and a reliable velocity model could not be picked based on this spectra. On the other hand, the right panel shows the semblance spectrum on the same CDP gather but after applying dip move-out correction. Here I used a DMO correction operator on common offset gathers in frequency-wavenumber domain (Liner 1990). The effect of DMO correction is evident, where the

peaks of the spectrum are relocated to the vicinity of the true velocity trend which is shown by black line. If one picks the velocities on the new semblance panel, an accurate RMS velocity field will be obtained and long wavelength velocity model for initializing FWI could be obtained by converting the RMS velocity to interval velocity in depth.

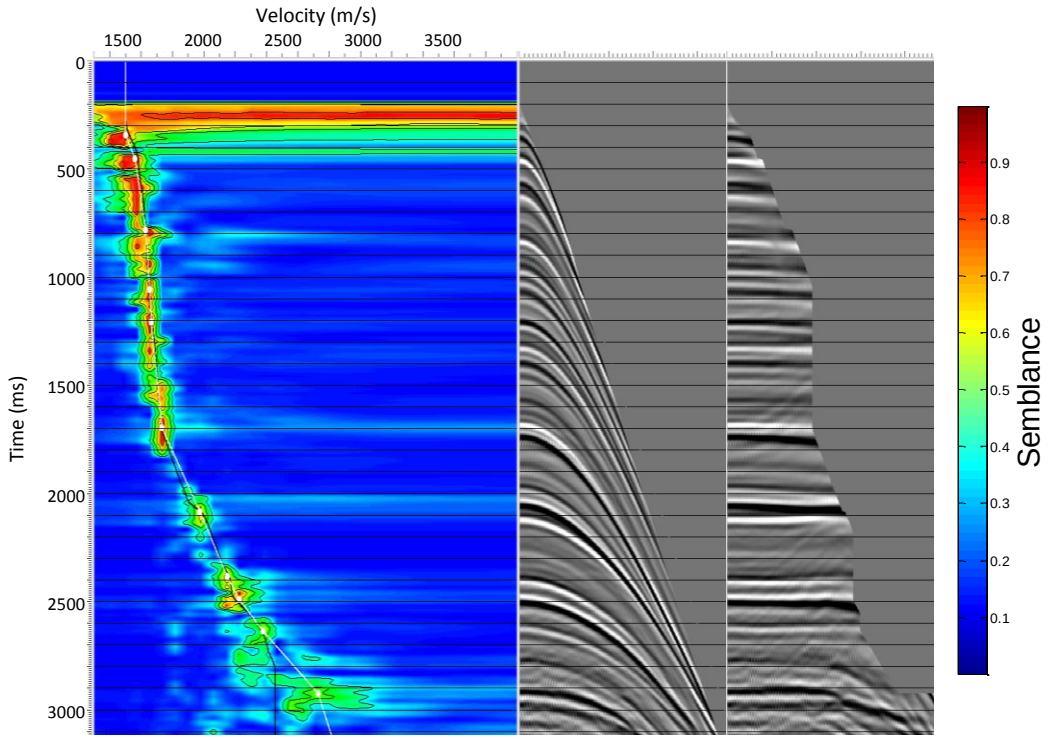

Figure 4.12 Semblance velocity analysis panel for a CDP gather near the horizontal location of 3000 m, where reflectors are almost horizontal. CDP gather before and after applying NMO correction is shown to check the normal move-out correction using picked velocities. True RMS velocity trend and picked RMS velocities are shown by black and white lines, respectively.

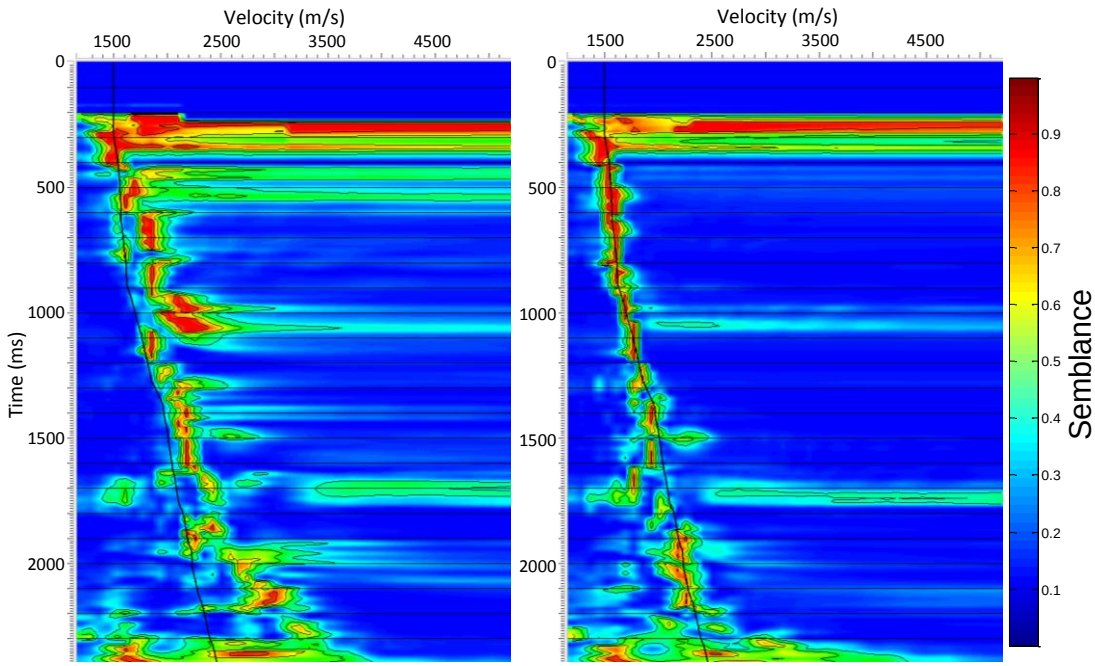

Figure 4.13 Semblance velocity analysis panel for a CDP gather near the horizontal location of 6700 m, where reflectors are steeply dipping. The apparent velocity trend is by far larger than true velocity trend. After applying DMO correction, the semblance peaks move to the vicinity of the true velocity trend.

4.6 FWI Results Using Initial Model from DMO Correction and Velocity Analysis

In order to illustrate the undesired effect of dipping layers on the velocity field, full waveform inversion has been applied on Marmousi2 dataset using narrow-band frequency set and an initial model which is converted from RMS stacking velocities picked without DMO correction. **Figure 4.14** shows this initial velocity model and the narrow-band FWI results. Since the low frequencies are absent in the seismic narrow-band dataset, the initial model should provide the long wavelength component of the background velocity model in order for FWI to converge toward the correct solution. However, because of steeply dipping layers, especially in the center of the model, the

initial velocity which is converted from stacking velocities without any dip correction could not help FWI and cycle skipping happens. It should be noted that on the both sides of the model, where reflectors are almost horizontal, the stacking velocity could provide the long wavelength component of the model. This is the origin of the idea that velocity analysis of reflection data should be capable of providing the background velocity model for FWI, provided that the dips are handled properly.

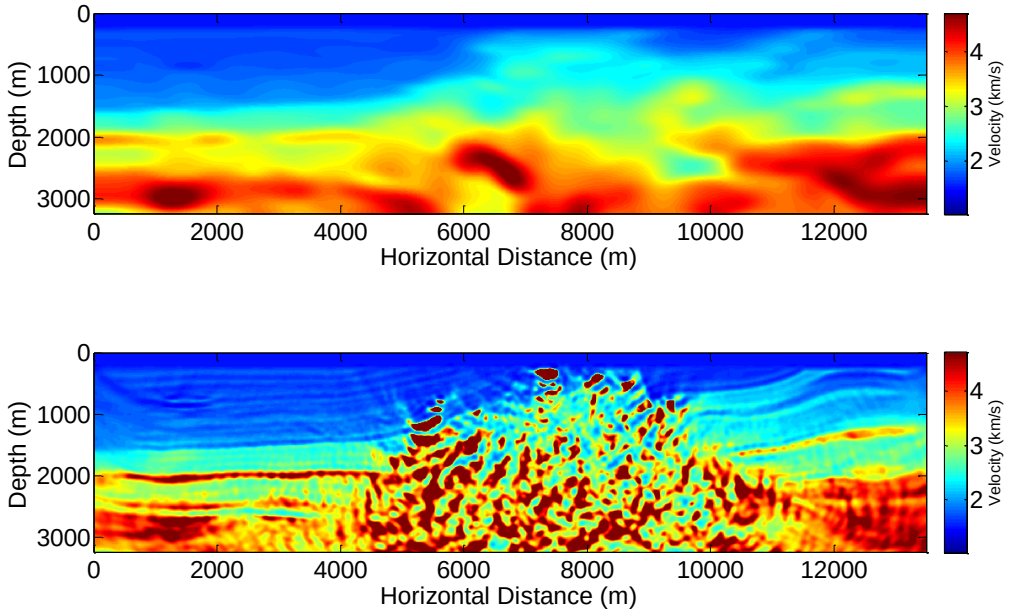

Figure 4.14 Initial velocity model converted from RMS stacking velocity without any dip correction (top), and failed narrow-band FWI result (bottom).

Now I shall use the new initial model which is developed by conventional velocity analysis after applying DMO correction. **Figure 4.15** shows the new initial model and

narrow-band full waveform inversion result. Although the low frequencies are absent in the input seismic data, the initial model is good enough to provide the long wavelength component of the model and FWI achieves a reliable result. Normalized misfit values for narrow-band FWI using the new initial model are shown in **Figure 4.16**. Time domain shot gather generated using the true model, the new initial model, and the narrow-band FWI result are shown in **Figure 4.17**.

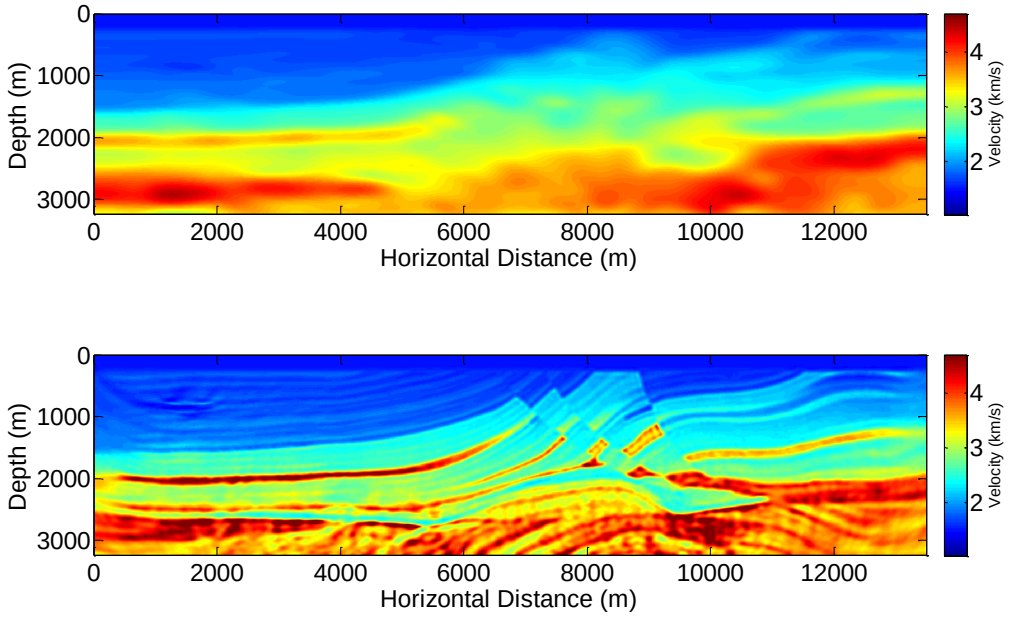

Figure 4.15 Initial velocity model converted from RMS stacking velocity analysis after DMO correction (top), and narrow-band FWI result (bottom).

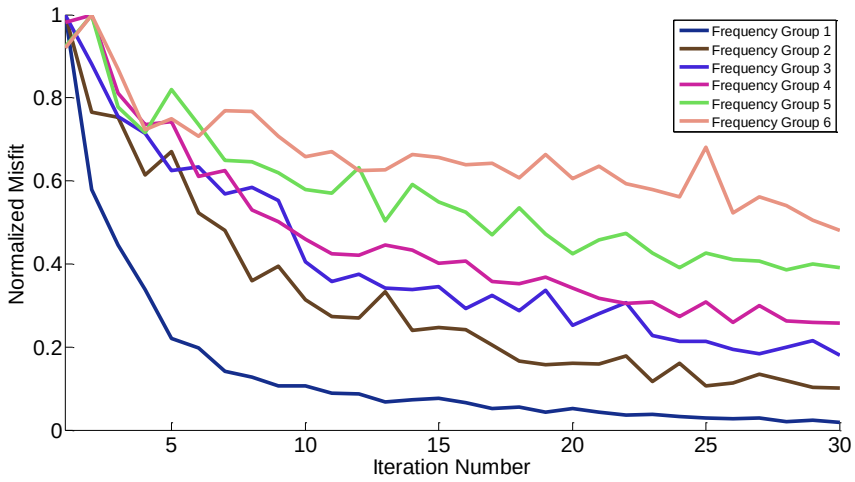

Figure 4.16 Normalized misfit values for narrow-band FWI using the new initial model from DMO correction and velocity analysis.

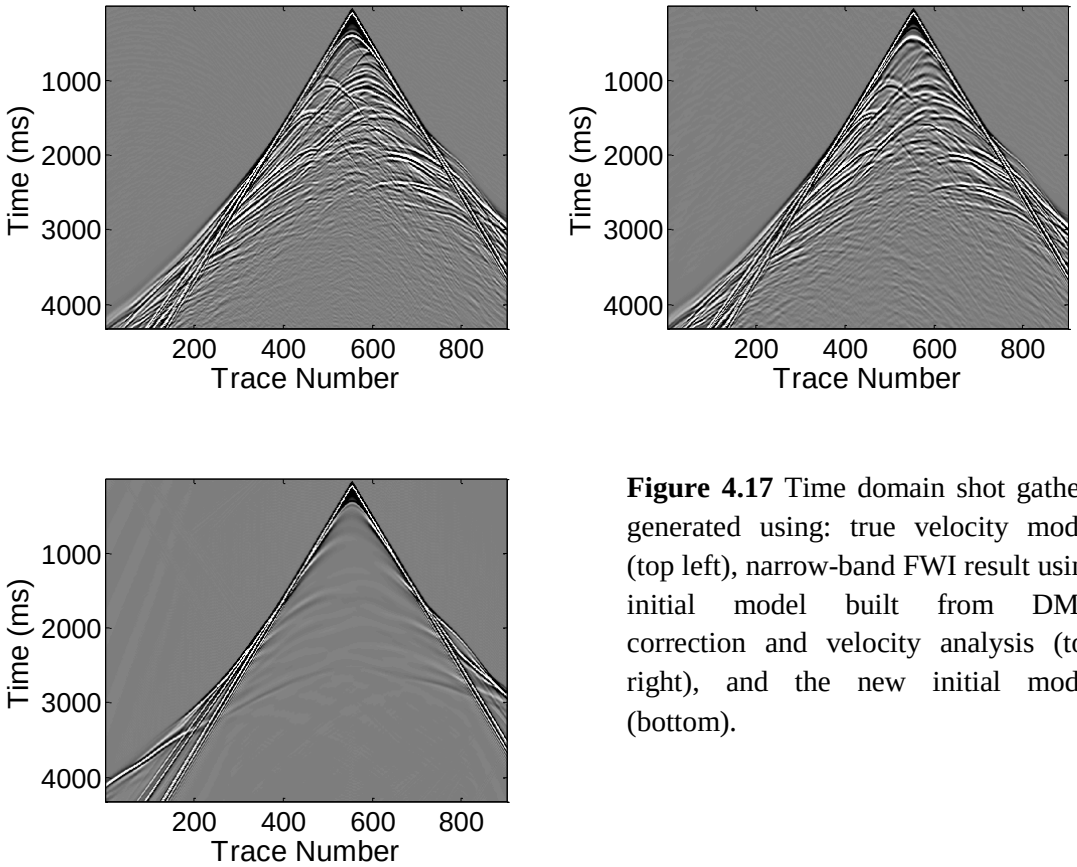

Figure 4.17 Time domain shot gathers generated using: true velocity model (top left), narrow-band FWI result using initial model built from DMO correction and velocity analysis (top right), and the new initial model (bottom).

Since the central part of the Marmousi2 model includes a combination of complex subsurface structures, it is worth to check the effect of dip correction on velocities for depth imaging results using pre-stack depth migration (PSDM). I used the initial velocity model which does not have any dip correction (**Figure 4.14**, top), the initial model after DMO correction and velocity analysis (**Figure 4.15**, top), and the narrow-band FWI result in **Figure 4.15** to apply a pre-stack depth migration on 450 time domain shot gathers of the observed dataset. Zoomed window of the central area in the PSDM images are shown in **Figure 4.18**. The initial velocity model which does not have any dip correction obtains an inaccurate depth section. The horizons are misplaced and the dips of the reflectors are not correct. On the other hand, the initial velocity model which has been created from velocity analysis after DMO correction achieves a much better depth section, but still the accuracy of the depth imaging is not satisfactory. Finally, performing PSDM using resulting velocity model from FWI achieves a reliable depth section which properly locates the subsurface structures.

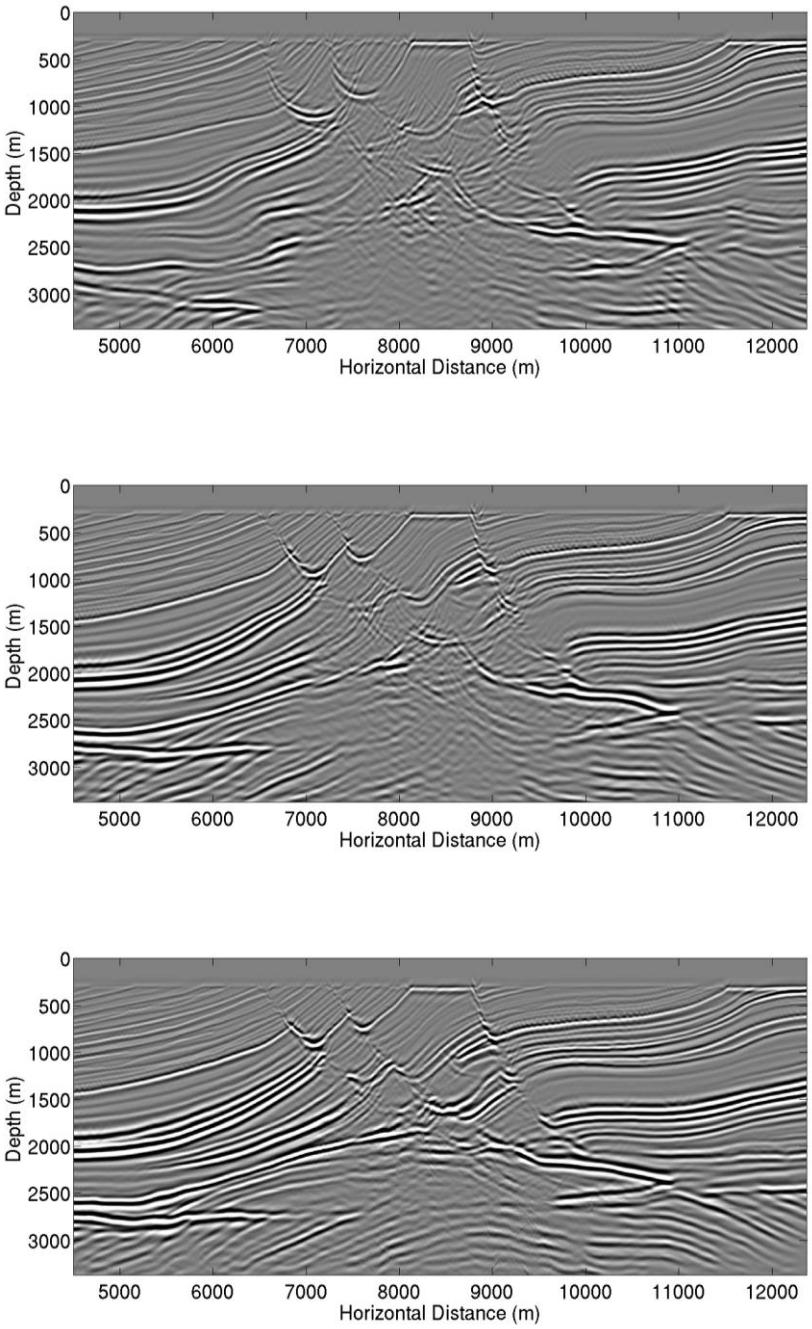

Figure 4.18 Pre-stack depth migration (PSDM) results of 450 time domain shot gathers from observed data using: initial velocity model without any dip correction (top), initial velocity model build by DMO correction and velocity analysis (middle), and narrow-band FWI resulting velocity model.

4.7 Velocity Profile Comparison

In order to compare the accuracy of full waveform inversion results using the two new initial velocity models, **Figure 4.19** shows the models from wide-band FWI with the smooth initial model (left), narrow-band FWI with the horizon-guided initial model (middle), and narrow-band FWI with the DMO corrected velocity model (right). The vertical dashed line shows a location where velocity profiles are extracted and compared in **Figure 4.20** for the evaluation of the models. This vertical line passes through a hydrocarbon reservoir which is characterized by the low velocity trap as indicated by the black oval. Both of the narrow-band FWI results using the new initial models can successfully recover the low velocity trap just same as the wide-band FWI result.

Although the velocity models illustrated in **Figure 4.19** are very similar, the vertical profiles show slightly different velocities in the deeper part (below 2.5 km) for the narrow-band FWI models. **Figure 4.20** illustrates the true, initial and FWI velocity profiles by green, dashed black, and blue curves, respectively. This vertical velocity profile has been selected from the very complex subsurface structure of Marmousi2 model, including faults, unconformity, and velocity reversals. As these profiles show, the new initial models are accurate enough to lead narrow-band FWI toward a final velocity model which precisely matched with the true model up to a depth of 2.5 km. However, since the geology is too complex in this area, the narrow-band FWI result is slightly different from wide-band FWI result at the depths below 2.5 km. Still, the results are reliable compared to the case of narrow-band FWI using poor smooth initial model which failed to converge toward the true model.

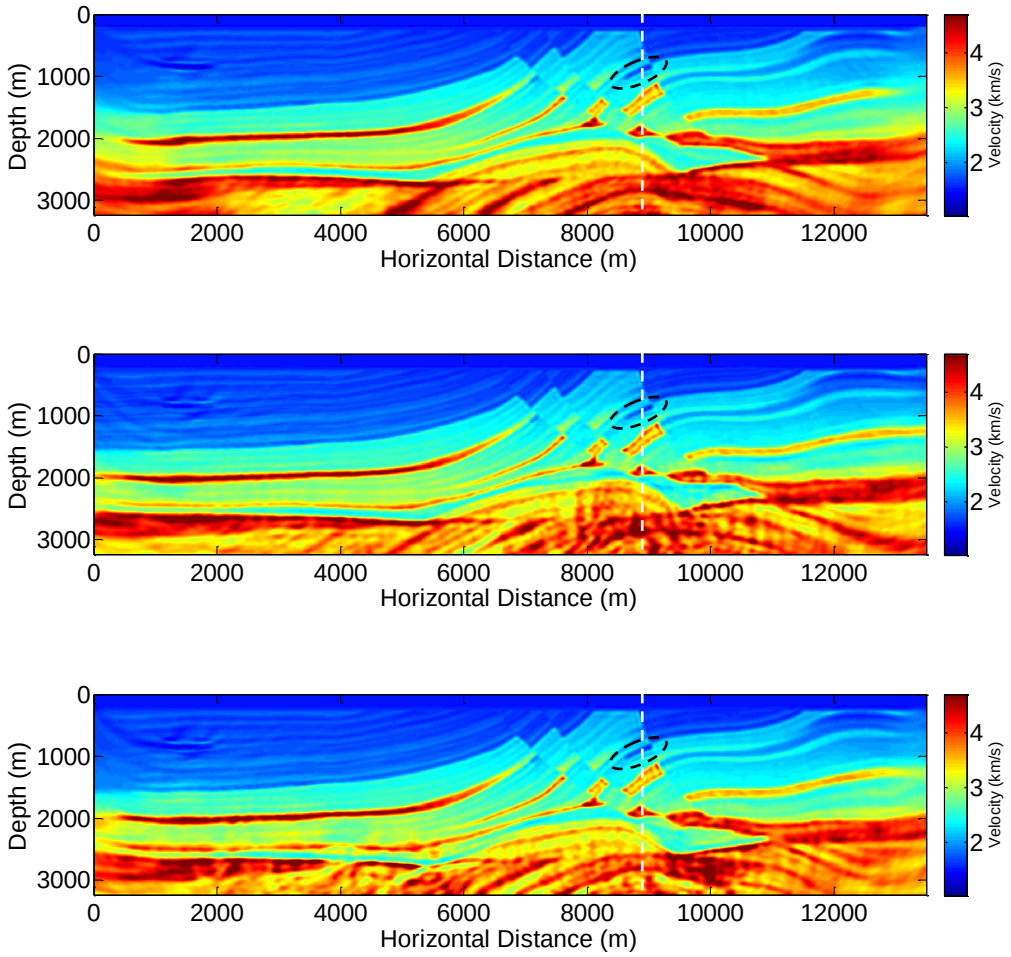

Figure 4.19 Resulting models from wide-band FWI with smooth initial model (top), narrow-band FWI with horizon guided initial model (middle), and narrow-band FWI with DMO corrected initial model (bottom). The dashed black oval shows a hydrocarbon reservoir in the model, which could be reconstructed perfectly by narrow-band FWI same as the wide-band FWI.

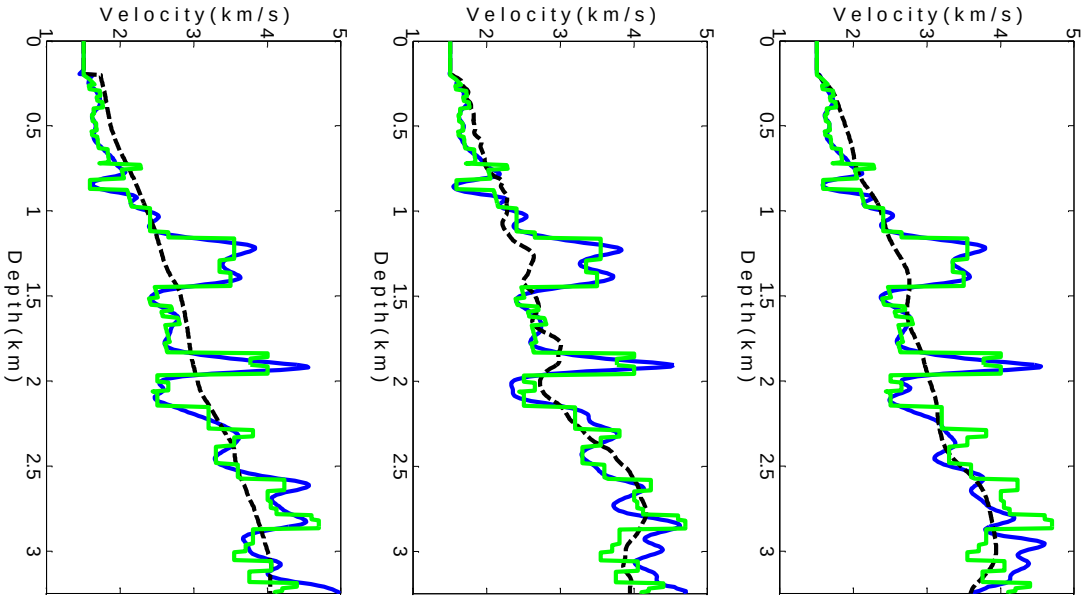

Figure 4.20 Vertical velocity profiles extracted from: wide-band FWI with smooth initial model (left), narrow-band FWI with horizon-guided initial model (middle), and narrow-band FWI with DMO corrected initial model (right). True, initial and FWI velocities are shown by green, dashed black, and blue curves, respectively.

4.8 Discussion

One of the problems for the successful application of full waveform inversion is the band-limited nature of the seismic data. The absence of the low frequencies due to the restrictions in data acquisition technologies is a crucial problem for FWI which strictly relies on these low frequencies to build the low wavenumber component of the velocity model. Although a number of FWI applications using random phase encoded simultaneous sources have been reported in the literature, all of them consider very low frequency components in the observed data. This is a weak assumption which easily breaks in the real world. In order to solve this problem, I suggested two new initial model building methods based on the data processing results and additional available data resources from well logs.

Two new methods were successfully developed for initial velocity model building using conventional data processing results in the brownfield situation. The low frequency component of the model could be extracted from these methods to help FWI achieve reliable results. The first method is to use a high resolution reflectivity section for horizon guided well log interpolation followed by geologically constrained acoustic impedance inversion to include the low frequency component of the model from well data. Geological constraints which are extracted by accurate picking of the horizons could bridge the low frequency gap in the velocity spectrum and fill the required part for the successful application of the band-limited FWI.

The second method for initial model building did not require any well data. Only a dip move-out correction is applied to relax the dip complexities of the subsurface structures

and a conventional velocity analysis helps to pick reliable RMS velocity field. The resulting RMS velocity is then converted to interval velocity in depth to be used as initial model for full waveform inversion. Both methods could successfully achieve acceptable velocity models using narrow-band full waveform inversion without requiring low frequency input data. Alternative methods for initial model building could be wave equation migration velocity analysis (WEMVA) and differential semblance optimization (DSO). Although these methods are among the robust techniques for velocity model building, the cost of them is much higher than the DMO correction and conventional velocity analysis. However, if the subsurface structure is too complex with severe lateral velocity variations DMO correction may not be able to resolve the geological complexity and it is necessary to use migration velocity analysis methods. Also, the current research focused on the initial model building methods for acoustic FWI as a guideline for more complex problems. Since the new initial models could successfully satisfy the requirements for the narrow-band acoustic FWI, the research is open to be extended to the elastic case.

4.9 Chapter Conclusions

Low frequency component of the velocity model could be extracted by two new methods using data processing results in the case of a brownfield situation. The first method uses the sparse spikes reflectivity section and available well logs to perform a horizon-guided well interpolation using the high resolution reflectivity section. Then a geologically constrained acoustic impedance inversion, improved with low frequencies from well logs, develops a reliable velocity model to initialize full waveform inversion iterations. The

new initial model could successfully achieve high resolution velocity models through a narrow-band FWI using the frequencies as low as 5.33 Hz, which is reasonably in accordance with the recording limits of the seismic data.

The second method for initial model building does not require any well data. A dip move-out correction is applied to relax the dip complexities and a conventional velocity analysis helps to pick a reliable RMS velocity field. The resulting RMS velocity is then converted to interval velocity in depth to be used as initial model for full waveform inversion. The second initial model could also achieve accurate velocity models using narrow-band FWI without requiring low frequency input data. Developing FWI initial model from seismic data processing products helps to efficiently use the available results of conventional processing routines. In fact, these new initial velocity models were able to fill the information gap between the very low frequency velocity and high frequency reflectivity by resolving the complexity of the subsurface structure. In the first method the missing low frequency part is borrowed from the well logs, and in the second method the missing low frequency part is recovered by relaxing the dip complexities using DMO correction and velocity analysis. Both models solve the cycle skipping issue and guide FWI toward the global solution of the problem.

CHAPTER V: Discussion

Two major problems occur in practice when simultaneous seismic sources are used for the full waveform inversion. First, the crosstalk noise which arises from interference between individual shots assembling in supershot gathers degrades the FWI models. Second, the underground seismic velocity estimation in a case of greenfield development is a challenging task.

In order to solve these problems a robust FWI algorithm using random phase encoded simultaneous seismic sources has been developed in this thesis. Different geometrical strategies for shot assembling have been evaluated and the best source configuration for supershot gather formation is suggested to effectively suppress the crosstalk noise. Two new initial model building methods are proposed to extract the low frequency component of the velocity model using help of geological constraints. It could be shown that an accurate velocity analysis after DMO correction is as effective as geological constraints to build the initial model for FWI.

Seismic full waveform inversion using random phase encoded simultaneous sources could be successfully applied to reduce the computation cost and time. Different examples from Marmousi2 complex model showed that accurate subsurface models could be obtained with effective suppression of crosstalk noise. Three geometrical shot selection strategies have been evaluated to achieve the best combination of time efficiency and model accuracy. A close configuration (CC) takes the neighboring

individual sources from each segment of the survey area to assemble them in a supershot. This keeps the minimum distance between individual shots of a supershot and makes it possible to define an average offset from the center of the segment to all the receiver locations. This average offset is used in the form of a weighting matrix when calculating gradient to improve the deeper parts of the FWI results by using long-offset data. A random configuration (RC) selects the individual shots from a random distribution over survey area to assemble them into supershots. This method is supposed to increase the incoherence of crosstalk noise from iteration to iteration and help the random phase encodings to reduce the level of the noise. A full configuration (FC) takes all the sources in the survey and assembles them into one supershot gather. Comparison of the FWI models using these three strategies and a crosstalk analysis showed that the close configuration could achieve the best velocity models using random phase encoded simultaneous sources.

In this thesis, two new methods were proposed for initial velocity model building using conventional data processing results in the brownfield situation. The first method is to use a high resolution reflectivity section for horizon guided well log interpolation followed by geologically constrained acoustic impedance inversion to include the low frequency component of the model from well data. The second method for initial model building does not require any well data. A dip move-out correction is applied to relax the dip complexities of the subsurface structures and a conventional velocity analysis helps to pick reliable RMS velocity field. The resulting RMS velocity is then converted to interval velocity in depth to be used as initial model for full waveform inversion. Both methods

could successfully achieve acceptable velocity models using narrow-band full waveform inversion without requiring low frequency input data.

Alternative methods for initial model building could be wave equation migration velocity analysis (WEMVA) and differential semblance optimization (DSO). Although these methods are among the robust techniques for velocity model building, the cost of them is much higher than the DMO correction and conventional velocity analysis. However, if the subsurface structure is too complex with severe lateral velocity variations DMO correction may not be able to resolve the geological complexity and it is necessary to use migration velocity analysis methods.

Future works could be open for the extension of the problem to the elastic case, where the FWI problem becomes more complex due to multiple parameters for inversion. Moreover, direct application of FWI to a greenfield case remains an open issue due to the difficulties in initial model building. It will be an interesting research topic to develop an algorithm for the application of FWI with simultaneous sources to the greenfield data. Also, the proposed methods for the brownfield case in this thesis showed reliable FWI results and it is worth to extend the work to the more complex situations including 4D applications such as Born-type approaches. By using the available data resources in the brownfield case, the thesis results proved that the suggested methods for FWI using simultaneous sources and initial model building provide a robust tool to revisit any available brownfield dataset for high resolution velocity model building.

CHAPTER VI: Conclusions

A robust full waveform inversion code using random phase encoded simultaneous seismic sources has been developed to address the two major FWI problems, i.e. crosstalk noise suppression in the simultaneous sources and low frequency initial model building in the case of a brownfield situation. The FWI code benefits from parallel processing capabilities and the quality of the models is assured with the accurate gradient and improved pseudo Hessian calculations. Using different examples from Marmousi2 model I could achieve a significant time efficiency using simultaneous sources FWI. Moreover, crosstalk analysis of three different shot assembling configurations confirmed that a close configuration of neighboring shots obtains the most accurate velocity model with the best time efficiency. The FWI models could be enhanced using this random phase encoding configuration by dramatically suppressing the crosstalk noise, which was one of the major problems for the application of FWI using simultaneous seismic sources.

Since well logs are accurate source of rock physics information, I proposed that it is possible to borrow this information to build a reliable initial velocity model for FWI. By extracting a reflectivity section and geological horizons from time migrated seismic data, I conducted a horizon-guided well interpolation on the acoustic impedance values from well logs. Then I used the interpolated model to perform a geologically constrained acoustic impedance inversion on the reflectivity section. After obtaining the acoustic impedance values, I used the density model to calculate P wave velocities. Finally, a depth conversion produced an accurate initial model for band-limited FWI using

simultaneous sources. The initial model could successfully lead the FWI toward the true Marmousi2 model and achieve a reliable velocity model.

I also proposed that if the dip complexities are handled properly, velocity models from conventional seismic data processing should be able to guide the band-limited FWI toward the correct solution. In order to relax the dip complexities prior to velocity analysis I used DMO correction, which works as a partial pre-stack migration and corrects the effect of even steep dips. It was successfully shown that an accurate velocity analysis after DMO correction is as effective as geological constraints to provide the low frequency components of the model for FWI application in the brownfield situation. Both new initial velocity models could obtain reliable results using random phase encoded simultaneous sources FWI by filling the information gap in the low spatial frequency part of the model.

The future work could be extended to solve the band-limited elastic FWI problem where the complexity of the multi-parameter inversion is more severe and elastic full waveform inversion using simultaneous sources has not been reported yet. Another open research topic will be to evaluate the possibility of direct processing of supershot data acquired under the greenfield situation. This could be a challenging work due to lack of any information on the velocity models in the greenfield case. Moreover, since brownfield FWI proved to be a promising method, it is worth to extend the research to the more complex situations such as multi-parameter waveform inversion and 4D Born-type problems.

REFERENCES

Anagaw, Amsalu Y., and Sacchi, Mauricio D., 2014, Comparison of multifrequency selection strategies for simultaneous-source full waveform inversion, Geophysics, **79**, P. R165–R181.

Askan, A., 2006, Full waveform inversion for seismic velocity and anelastic losses in heterogeneous structures: Ph.D. thesis, Carnegie Mellon University.

Beasley, C., Chambers, J., R. E., and Jiang, Z., 1998, A new look at simultaneous sources: 68th Annual International Meeting, SEG, Expanded Abstracts, 133–135, doi:10.1190/1.1820149.

Beasley, C., Moore, I., Monk, D., and Hansen, L., 2012, Simultaneous sources: The inaugural full-field, marine seismic case history. SEG Technical Program Expanded Abstracts: pp. 1-5, doi: 10.1190/segam2012-0834.1

Ben Hadj Ali, H., S. Operto, J. Virieux, 2011, An efficient frequency-domain full waveform inversion method using simultaneous encoded sources, Geophysics, **76**, P. R109–R124.

Berenger, J. P., 1994, A perfectly matched layer for absorption of electromagnetic waves. Journal of Computational Physics, **114**, 185–200.

Bleibinhaus, F., J. A. Hole, T. Ryberg, and G. S. Fuis, 2007, Structure of the California Coast Ranges and San Andreas fault at SAFOD from seismic waveform inversion and reflection imaging: Journal of Geophysical Research, doi: 10.1029/2006JB004611.

Boonyasiriwat, C., and G. T. Schuster, 2010, 3D multisource full-waveform inversion using dynamic random phase encoding: 80th Annual International Meeting, SEG, Expanded Abstracts, 29, 1044–1049.

Brossier, R., J.Virieux, and S. Operto, 2008, Parsimonious finite-volume frequency domain method for 2D P-SV wave modelling: Geophysical Journal International, **175**, 541–559.

Brossier, R., S. Operto, and J. Virieux, 2009, Seismic imaging of complex structures by 2D elastic frequency-domain full-waveform inversion: Geophysics, **74**, WCC1–WCC26.

Choi, Y., Min, D., and Shin, C., Frequency-Domain Elastic Full Waveform Inversion Using the New Pseudo-Hessian Matrix: Experience of Elastic Marmousi-2 Synthetic Data, Bulletin of the Seismological Society of America, Vol. **98**, No. 5, pp. 2402–2415

Claerbout, J. F., 1971, Toward a unified theory of reflector mapping: Geophysics, **36**, 467–481.

Claerbout, J. F., 1985, Imaging the Earth's Interior, Wiley-Blackwell, ISBN-10: 0865423040.

Cooke, Dennis A., and Schneider, William A., 1983, Generalized linear inversion of reflection seismic data, Geophysics, **48**, 665-676.

Drossaert, F. H. and Giannopoulos, A., 2007, A non-split complex frequency-shifted PML based on recursive integration for FDTD modeling of elastic waves. Geophysics, **72**, 2, T9–T17.

Ferguson, R.J, and Gary F. Margrave, 1996, A simple algorithm for band-limited impedance inversion, CREWES Research Report, Volume **8**, 21-1 – 21-10.

Gao, F., A. R. Levander, R. G. Pratt, C. A. Zelt, and G. L. Fradelizio, 2006a, Waveform tomography at a groundwater contamination site: Surface reflection data: Geophysics, **72**, no. 5, G45–G55.

Gardner, G. H. F., Gardner, L. W., and Gregory, A. R., 1974, Formation velocity and density: the diagnostic basics for stratigraphic traps: Geophysics, **39**, 770–780. doi:10.1190/1.1440465

Gauthier, O., J. Virieux, and A. Tarantola, 1986, Two-dimensional nonlinear inversion of seismic waveforms: Numerical results: Geophysics, **51**, 1387–1403.

Gelis, C., J.Virieux, and G. Grandjean, 2007, 2D elastic waveform inversion using Born and Rytov approximations in the frequency domain: Geophysical Journal International, **168**, 605–633.

Goupillaud, P. L., 1961, An approach to inverse filtering of near-surface layer effects from seismic records: Geophysics, **26**, 754–760. doi:10.1190/ 1.1438951

Graves, R., 1996, Simulating seismic wave propagation in 3D elastic media using staggered-grid finite differences: Bulletin of the Seismological Society of America, **86**, 1091–1106.

Hicks, G. J., and R. G. Pratt, 2001, Reflection waveform inversion using local descent methods: Estimating attenuation and velocity over a gas-sand deposit: Geophysics, **66**, 598–612

Howe, D., A. J. Allen, M. S. Foster, I. J. Jack, and B. Taylor, 2008, Independent simultaneous sweeping — A method to increase the productivity of land seismic

crews: 78th Annual International Meeting, SEG, Expanded Abstracts, 2826–2830, doi:10.1190/1.3063932.

Ingber, L., 1995, Adaptive simulated annealing (ASA): lessons learned: Control and Cybernetics, **25**, 33–54.

Jo, C. H., C. Shin, and J. H. Suh, 1996, An optimal 9-point, finite-difference, frequency-space 2D scalar extrapolator: Geophysics, **61**, 529–537.

Kamei, R., Pratt, R.G, and Tsuji, T., 2012, Waveform tomography imaging of a megasplay fault system in the seismogenic Nankai subduction zone, Earth and Planetary Science Letters, 343-353.

Koo, N., Shin, C., Min, D., Park, K., and Lee, H., 2011, Source estimation and direct wave reconstruction in Laplace-domain waveform inversion for deep-sea seismic data, Geophysical Journal International, **187,** 861–870.

Krebs, J., J. Anderson, D. Hinkley, R. Neelamani, S. Lee, A. Baumstein, and M. D. Lacasse, 2009, Fast full-wavefield seismic inversion using encoded sources: Geophysics, 74, no. 6, WCC177–WCC188, doi:10.1190/1.3230502.

Lailly, P., 1983, The seismic inverse problem as a sequence of before stack migrations: conference on Inverse Scattering, Theory and Application, Society for Industrial and Applied Mathematics, Expanded Abstracts, 206–220.

Levander, A. R., 1988, Fourth-order finite-difference P-SV seismograms: Geophysics, **53**, 1425–1436.

Levin, F.K., 1971, Apparent Velocity from Dipping Interface Reflections, Geophysics, **36**(3), 510-516.

Li, S., 2013, Wave-equation migration velocity analysis by non-stationary focusing, SEG Technical Program Expanded Abstracts: pp. 1110-1115, doi: 10.1190/segam2013-0252.1

Liner, C.L, 1990, General theory and comparative anatomy of dip moveout, Geophysics, **55**(5), 595-607.

Marfurt, K., 1984, Accuracy of finite-difference and finite-elements modeling of the scalar and elastic wave equation: Geophysics, **49**, 533–549.

Metropolis, N., Rosenbluth, A., Rosenbluth, M., Teller, A., and Teller, E., 1953, Equation of state calculations by fast computing machines: The Journal of Chemical Physics, **21**, 1087–1092. doi:10.1063/1.1699114

Min, D.-J., C. Shin, R. G. Pratt, and H. S. Yoo, 2003,Weighted-averaging finite-element method for 2D elastic wave equations in the frequency domain: Bulletin of the Seismological Society of America, **93**, 904–921.

Mora, P. R., 1987, Nonlinear two-dimensional elastic inversion of multi-offset seismic data: Geophysics, **52**, 1211–1228.

Mora, P. R., 1988, Elastic wavefield inversion of reflection and transmission data: Geophysics, **53**, 750–759.

Oh, J., and Min, D., 2012, Improved Pseudo-hessian for Frequency-domain Elastic Waveform Inversion, EAGE Annual Meeting Expanded Abstract, DOI**:** 10.3997/2214-4609.20148334.

Operto, S., J.Virieux, J. X. Dessa, and G. Pascal, 2006, Crustal imaging from multifold ocean bottom seismometers data by frequency-domain fullwaveform tomography: Application to the eastern Nankai trough: Journal of Geophysical Research, doi: 10.1029/2005JB003835.

Operto, S., J. Virieux, P. Amestoy, J. Y. L'Excellent, L. Giraud, and H. Ben-Hadj-Ali, 2007, 3D finite-difference frequency-domain modeling of viscoacoustic wave propagation using a massively parallel direct solver: A feasibility study: Geophysics, **72**, no. 5, SM195–SM211.

Pratt, R. G., and M. H. Worthington, 1990, Inverse theory applied to multisource cross-hole tomography, Part 1: Acoustic wave-equation method: Geophysical Prospecting, **38**, 287–310.

Pratt, R. G., Z. M. Song, P. R.Williamson, and M.Warner, 1996, Two-dimensional velocity model from wide-angle seismic data by wavefield inversion: Geophysical Journal International, **124**, 323–340.

Pratt, R. G., C. Shin, and G. J. Hicks, 1998, Gauss-Newton and full Newton methods in frequency-space seismic waveform inversion: Geophysical Journal International, **133**, 341–362.

Plessix, R.-E., 2006, Areview of the adjoint-state method for computing the gradient of a functional with geophysical applications: Geophysical Journal International, **167**, 495–503.

Ravaut, C., S. Operto, L. Improta, J. Virieux, A. Herrero, and P. Dell' Aversana, 2004, Multi-scale imaging of complex structures from multifold wide-aperture seismic data by frequency-domain full-wavefield inversions: Application to a thrust belt: Geophysical Journal International, **159**, 1032–1056.

Robertsson, J. O., B. Bednar, J. Blanch, C. Kostov, and D. J. van Manen, 2007, Introduction to the supplement on seismic modeling with applications to acquisition, processing and interpretation: Geophysics, **72**, no. 5, SM1–SM4.

Romero, L. A., D. C. Ghiglia, C. C. Ober, and S. A. Morton, 2000, Phase encoding of shot records in prestack migration: Geophysics, **65**, 426–436, doi:10.1190/1.1444737

Shin, C., Jang, J., and Min, D., 2001, Improved amplitude preservation for prestack depth migration by inverse scattering theory, Geophysical Prospecting, **49**, 592-606

Shin, C., and Y. H. Cha, 2008, Waveform inversion in the Laplace domain: Geophysical Journal International, **173**, 922–931.

Shin, C., and Y. H. Cha, 2009, Waveform inversion in the Laplace-Fourier domain: Geophysical Journal International, **177**, 1067–1079.

Stefani, J., G. Hampson, E. F. Herkenhoff, 2007, Acquisition using simultaneous sources: 69th Conference and Technical Exhibition, EAGE, Extended Abstracts.

Tarantola, A., 1984, Inversion of seismic reflection data in the acoustic approximation: Geophysics, **49**, 1259–1266.

Velis, D. R., 2008, Stochastic sparse spike deconvolution: Geophysics, **73**, R1–R9. doi:10.1190/1.2790584

Vigh, D., and E. W. Starr, 2008a, 3D plane-wave full-waveform inversion: Geophysics, **73**, no. 5, VE135–VE144.

Virieux, J., 1986, P-SV wave propagation in heterogeneous media, velocity stress finite difference method: Geophysics, **51**, 889–901.

Wiggins, R. A., 1978, Minimum entropy deconvolution: Geoexploration, **16**, 21–35. doi:10.1016/0016-7142(78)90005-4